Distribution Category:
Physics--Atomic and
Molecular (UC-34a)

ANL-84-90

ANL--84-90

DE85 018310

ARGONNE NATIONAL LABORATORY
9700 South Cass Avenue
Argonne, Illinois 60439

OPTICAL SPECTRA AND ELECTRONIC STRUCTURE OF ACTINIDE IONS IN COMPOUNDS AND IN SOLUTION

by

W. T. Carnall and H. M. Crosswhite

Chemistry Division

August 1985

TABLE OF CONTENTS

LIST OF FIGURES

LIST OF FIGURES

LIST OF FIGURES

LIST OF TABLES

LIST OF TABLES

LIST OF TABLES

OPTICAL SPECTRA AND ELECTRONIC STRUCTURE OF ACTINIDE IONS IN COMPOUNDS AND IN SOLUTION

by

W. T. Carnall and H. M. Crosswhite

Abstract

This report provides a summary of theoretical and experimental studies of actinide spectra in condensed phases. Much of the work was accomplished at Argonne National Laboratory, but references to related investigations by others are included. Spectroscopic studies of the trivlent actinides are emphasized, as is the use of energy level parameters, evaluated from experimental data, to investigate systematic trends in electronic structure and other properties. Some reference is made to correlations with atomic spectra, as well as with spectra of the (II), (IV), and higher valence states.

1.0. Introduction

This report serves several purposes. It provides a summary of experimental and theoretical analyses of trivalent actinide spectra in sufficient detail to constitute a useful reference as well as an indication of where additional work is needed. Frequent detailed comparisons with lanthanide spectra are included to support the analysis. In addition, it shows how well a model for extrapolating energy level parameters across a series reproduces the actual analyses of individual trivalent actinide-ion spectra. This model is also used to systematically predict energy level parameters for divalent and tetravalent actinide ions in cases where the experimental data are very limited. The predictions of energy level structure should be useful in suggesting and in helping to interpret new experiments. The basis is provided for extending the model to higher valence states of the actinides in binary or complex halide compounds. However, further analysis of experimental data is prerequisite to the development of meaningful extrapolated parameters in this range. This report does not address the analysis of actinyl-ion, i.e. AnO_2^{+}, AnO_2^{++}, etc., spectra.

One of the features that sets actinide and lanthanide spectra apart from those of other elements in the periodic table is that the f-orbitals can be considered both as containing the optically active electrons and as belonging to the core of filled shells. As a result of this dominant characteristic, the spectra of these elements, particularly of the trivalent

state, are moderately insensitive to changes in the ionic environment. This relative insensitivity of core electrons to external circumstances also means that for these elements there is a close connection between energy levels in compounds and those in gaseous free atoms and ions. Examples of this connection are discussed both for actinide and lanthanide spectra.

For the actinide valence states of most interest to chemists, 1+ through 7+, very few gaseous free-ion spectra have been sufficiently analyzed to provide a basis for guiding theoretical interpretation. With the experimental techniques used, highly-excited states belonging to many different overlapping configurations are produced simultaneously. This makes interpretation difficult and results in fragmentary analyses. The situation is further complicated by the fact that configuration interaction is more important in the actinides than in the lanthanides. As a result, most of our structural information for the f^N states comes from observation of forced-electric-dipole absorption and fluorescence transitions in optically clear crystals, and the best characterized spectra are those of the trivalent actinides and lanthanides. The analysis of actinide spectra in crystalline hosts is much simplified by the fact that except for divalent ions, the electronic transitions are restricted to those between nominal f^N levels in much of the accessible optical range. These transitions are normally forbidden by the parity selection rule, but, for example, for trivalent actinides doped into crystals such as $LaCl_3$, where there is no center of symmetry, enough of the character of opposite-parity configurations can be mixed in to induce such transitions, Dieke (1968). At the same time, the admixture (of the order of 0.1%) is small enough that the f-character of the levels is preserved and level calculations can be made on the assumption of a pure f^N configuration. Host single crystals such as $ThCl_4$ and $ThBr_4$ have also been successfully used in the study of some tetravalent actinide ion spectra. Theoretical analyses of higher valent (5+ and 6+) actinide spectra have been reported, but these experimental data are for the most part obtained in transmission through thin films of multicrystalline pure compounds or in single crystals of the pure binary or complex salts where detailed analysis is difficult.

The stability of f-orbitals against changes in the ionic environment in the trivalent state and in part in higher valence states results in energy levels of various compounds being closely correlated among themselves as well as with those of the free-ion where known. Ab initio free-ion calculations have therefore proven to be very useful for interpreting the crystal levels, and a parametric model based on these calculations has been developed. This model can be applied in a consistent way to ions of both the actinide and lanthanide series, Crosswhite and Crosswhite (1984a) and it is used here to help systematize our overall view of actinide spectra.

A major complicating factor in the theoretical interpretation of 5f-spectra is the extensive interconfiguration mixing, or configuration inter-

action, Wybourne (1965), Goldschmidt (1978), Hüfner (1978). This effect of mixing the character of other configurations into the $5f^N$-states involves not only competing configurations with large overlaps but also cumulative interactions with infinitely many distant electronic configurations. That this is a serious problem is demonstrated by analysis of isotope shifts and hyperfine-structure in actinide free-ion spectra, Fred (1967,1984). The parameters that describe the energy level structure for a configuration would show less variation if the independent-particle model were better justified. In the method of analysis described here the effects of configuration interaction are partially compensated by the use of effective operators in the atomic Hamiltonian for f^N-shells, Trees (1964), Wybourne (1965), Judd (1966), Judd et al. (1968), Goldschmidt (1978), Poon and Newman (1983) Judd and Crosswhite (1984), Judd and Suskin (1984).

2.0. The Relative Energies of Actinide Electronic Configurations

In order to emphasize the systematic correlations to be found in the energy level structure of actinide ions both as a function of atomic number, Z, and for configurations with the same number of f-electrons but different charge states, we begin by considering the types of interactions that have been used successfully to account for the structure. In the discussion of atomic spectra, attention is focused on identification of the ground (lowest energy) and excited electronic configurations of neutral as well as ionized species. The relative energies of the various electronic configurations thus established provide the basis for extending the interpretation of spectra (and thus electronic structure) to condensed media. In free neutral or ionic species, the energy level structure is attributed primarily to the interaction between electrons in unfilled shells. In condensed media there is superimposed the additional effect of the ligand field. Summaries of the actinide atomic spectra literature have been given by Carnall (1971) Crosswhite (1982), Blaise et al. (1983), and Fred (1984).

The progenitor of the actinide (5f) series is actinium; it is comparable to lanthanum in the corresponding lanthanide (4f) series. The electronic structure of zero-valent actinium, (Ac I)*, is represented as three electrons ($6d7s^2$) outside the radon core. This can be written [Rn]($6d7s^2$), but in the subsequent discussion the core symbol [Rn] will be omitted from

---

*The conventional spectroscopic notation for zero-valent actinium is Ac I. Similarly, the singly ionized species is Ac II, and the doubly charged, Ac III. The chemical notation for the latter is Ac^{2+} or Ac(II). When referring to free-ion spectra we will use the spectroscopic notation. When indicating the valence state of an ionic species in a condensed phase we will use the chemical notation. We use the symbol An to represent any actinide element, and Ln as the general symbol for the lanthanides.

the notation. All of the actinide atomic and ionic species are built on the radon core, but the nature of the electronic structure beyond the core is a function of excitation energy, atomic number Z, and state of ionization, Brewer (1971a,b, 1983). Thus within the energy range indicated in Figure 1, in addition to configurations involving 6d and 7s electrons, there are those containing 7p and 5f electrons.

Figure 1 is to be interpreted in the following manner. In Ac I the lowest-energy electron states result from the coupling of two 7s electrons and one 6d in a manner consistent with the Pauli Exclusion Principle. Further, an energy equivalent to ~9000 cm^{-1} is sufficient to promote a ground state 7s electron to the 6d shell, thus forming the lowest (ground) level of the excited configuration ($6d^27s$). Essentially the same energy is required to promote a ground state 6d electron to the 7p shell, giving the excited configuration ($7s^27p$). Only the lowest energy state (relative to the ground state) for each configuration is indicated in the figure. In many cases large numbers of excited states exist within each of the configurations so that the density of levels from overlapping configurations increases appreciably with excitation energy. However, since the coupling of two 7s electrons results in a filled subshell, we find that the ground configuration in Ac I ($6d7s^2$) is simple in structure, involving only the states of a single 6d electron, $^2D_{3/2}$ and $^2D_{5/2}$. Such states, written in terms of the quantum numbers S, L, and J, are subsequently referred to as free-ion states.

In Th II, the ground state belongs to $6d^27s$. Figure 1 indicates that the spectrum at lower energies is expected to be very complex because of the number of electronic configurations with nearly the same energy relative to the ground state. In Pa III, the three electrons beyond the Rn core in the ground state belong to the $5f^26d$ configuration. In U IV further stabilization of the 5f orbital has taken place and excited configurations occur at much higher energies relative to the ground state than was the case in Pa III, Th II, and Ac I. Thus in U IV, the electronic structure in the range up to ~30000 cm^{-1} is that characteristic of the $5f^3$ configuration. A recent extensive summary of systematic variations in the lowest-energy levels of configurations for An I and An II is given by Blaise et al. (1983).

Experimentally, free-ion spectra (both neutral and ionic species) are usually observed in emission, and the energy-level structure is deduced from coincidences of energy differences of pairs of spectrum lines, subject to verification by isotope-shift, hyperfine-structure and magnetic g-factor tests. In condensed phases, spectra are more commonly measured in absorption. Relative intensities associated with parity "allowed" and "forbidden" transitions are reflected in the nature of two processes: transitions in which the initial and final states belong to electronic configurations of opposite parity (parity-allowed transitions, e.g. $5f^3 \rightarrow 5f^26d$), and those in

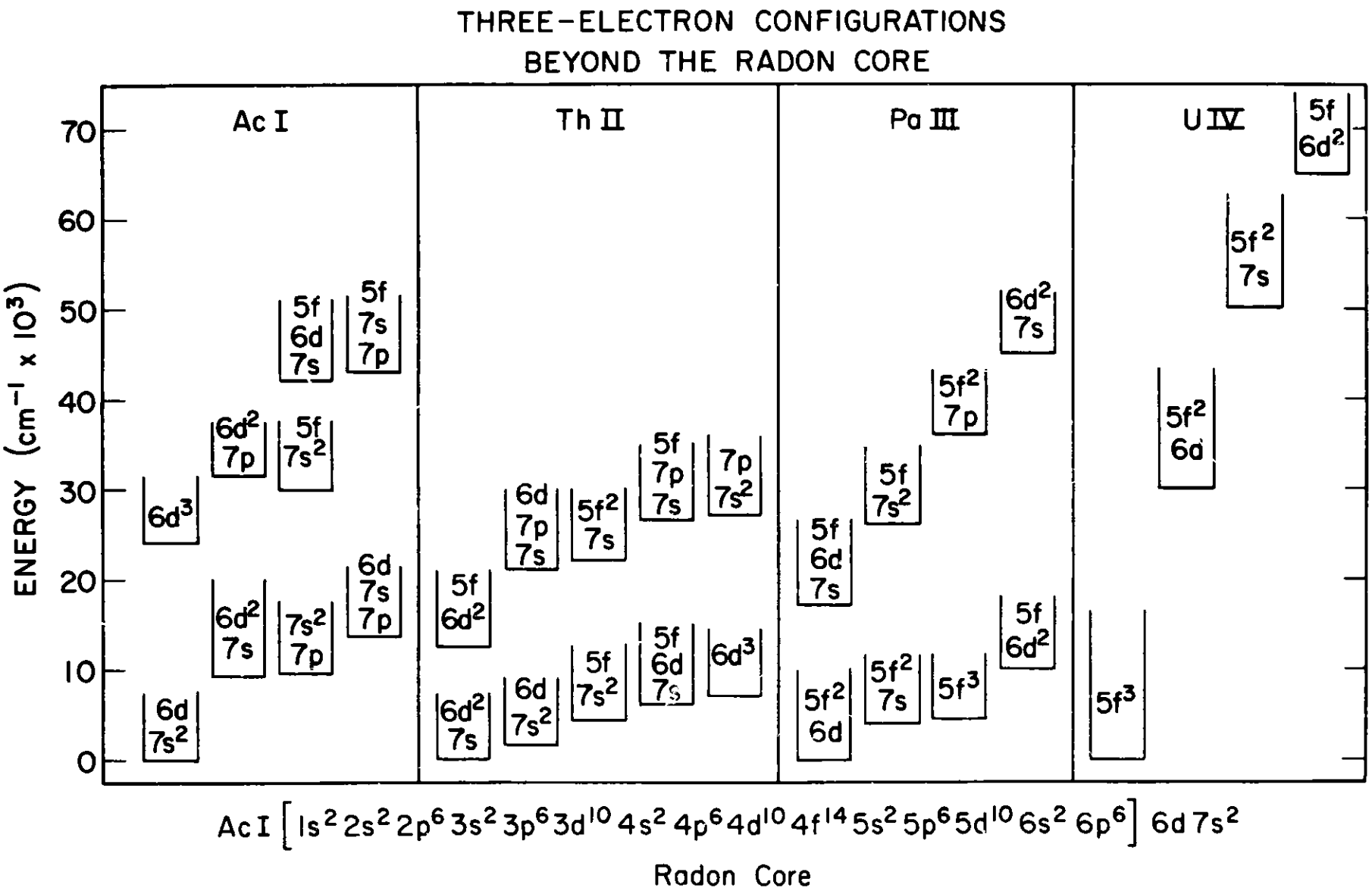

Fig. 1. Three-electron Configurations Beyond the Radon Core. From Brewer (1971a,b).

which both states belong to the same configuration (parity-forbidden transitions, e.g. $5f^3 \rightarrow 5f^3$). The latter are weak and sharp. The former are much more intense and are associated with broader absorption bands. Both types of transitions are apparent in Figures 2 and 3 which show the aqueous solution absorption spectra of the trivalent actinides. Relative intensities are discussed later.

2.1. "Free-Ion" $5f^N$-States in Condensed Media

For the trivalent actinides, as for the trivalent lanthanides, ligand-field (crystal-field) effects are small relative to the predominant electrostatic and spin-orbit interactions between the f-electrons which determine the electronic structure. In a number of instances, isolated bands in condensed phases such as in Figures 2 and 3 can be interpreted as envelopes which constitute a sum over transitions to the crystal-field components of individual SLJ-states within a particular $5f^N$-configuration. The effect of the environment is to remove the degeneracy of the free-ion state, but the resulting crystal-field components in, for example, the trivalent state, characteristically exhibit an energy spread of only 200-300 cm^{-1}. The center of gravity of such absorption bands is often referred to as the "free-ion state" energy in that particular medium. The energies of these so-called free-ion states shift from one medium to another; the total splitting of the crystal-field components that make up such states also varies with the medium for a given valence state. As the crystal-field splitting becomes larger, as observed particularly in higher valent actinides, approximate free-ion states can still be assigned to some isolated absorption features, but meaningful calculations must explicitly include the modifying effect that the crystal-field interaction has on the electrostatic and spin-orbit interactions.

2.2. Media Effects on the Free-Ion States in Excited Configurations

In Figure 1 the energy of the lowest state in the (excited) $5f^2 6d$-configuration of U IV relative to that of the ground state ($^4I_{9/2}$ of $5f^3$) is estimated to be 30000 cm^{-1} whereas in Figure 2 the onset of intense absorption features indicative of the lowest energy f d transitions in U^{3+}(aquo) is nearer to 24000 cm^{-1}. This energy difference (6000 cm^{-1}) is due to the influence of the solvation energy of U^{3+}(aquo) on the relative energies of the 6d and 5f electrons, Schaeffer and Jørgensen (1958), Jørgensen (1962). A similar E is found for the couple Np IV -Np^{3+}(aquo), but the energy of the lowest f d transition is greater in Np IV than in U IV. The magnitude of E can vary significantly depending on the nature of the ligand and the symmetry. Morrison (1980) attempted to compute approximate values for a host-dependent energy separation between the lowest-energy states in f^N and $f^{N-1}d$ configurations which in turn was dependent upon the energy level parameters of the host crystal. The model used focused on the contributions to the crystal-field arising from polarizable ligands. The resulting shifts

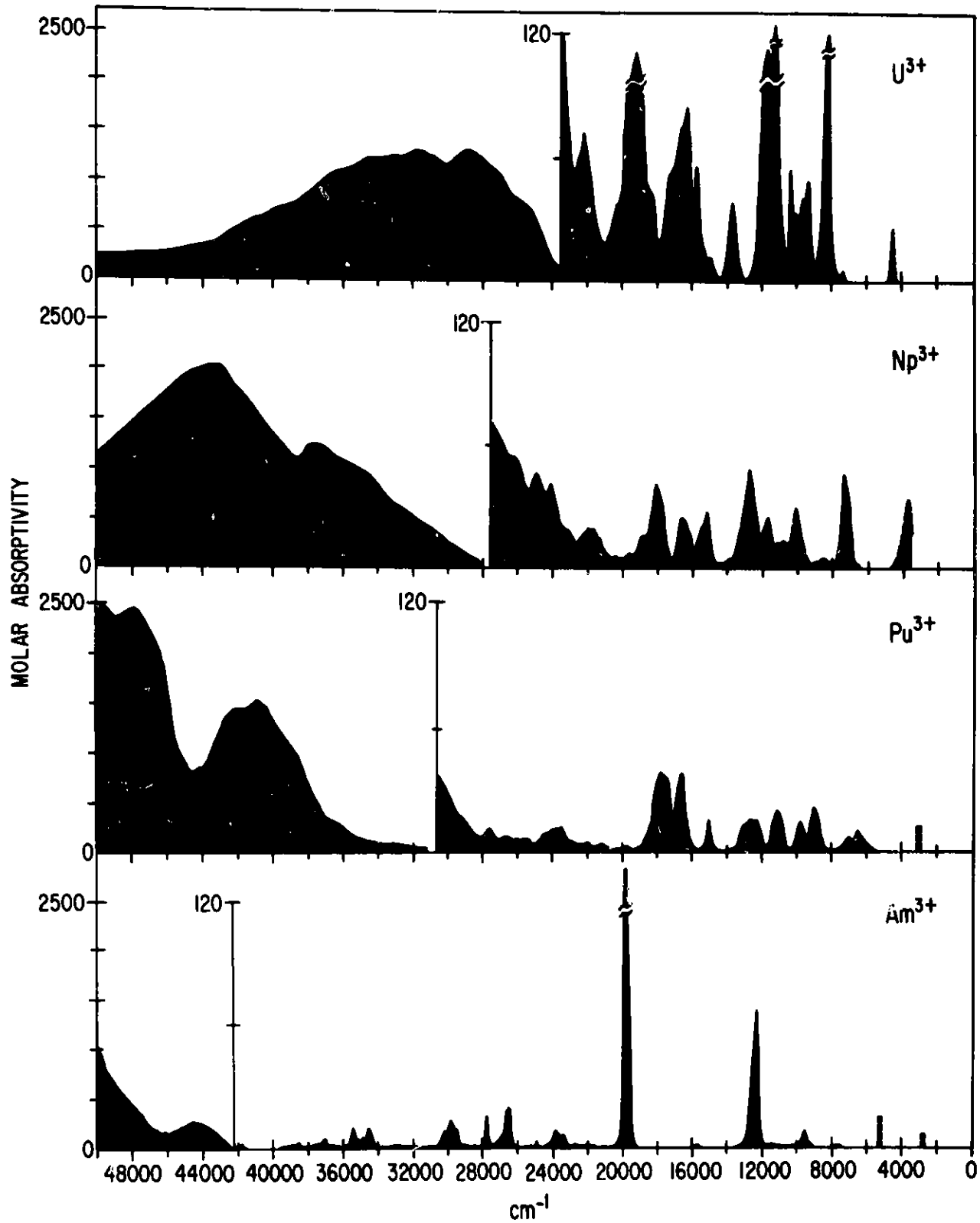

Fig. 2. Absorption Spectra of 3+ Actinide Ions in Dilute Acid Solutions.

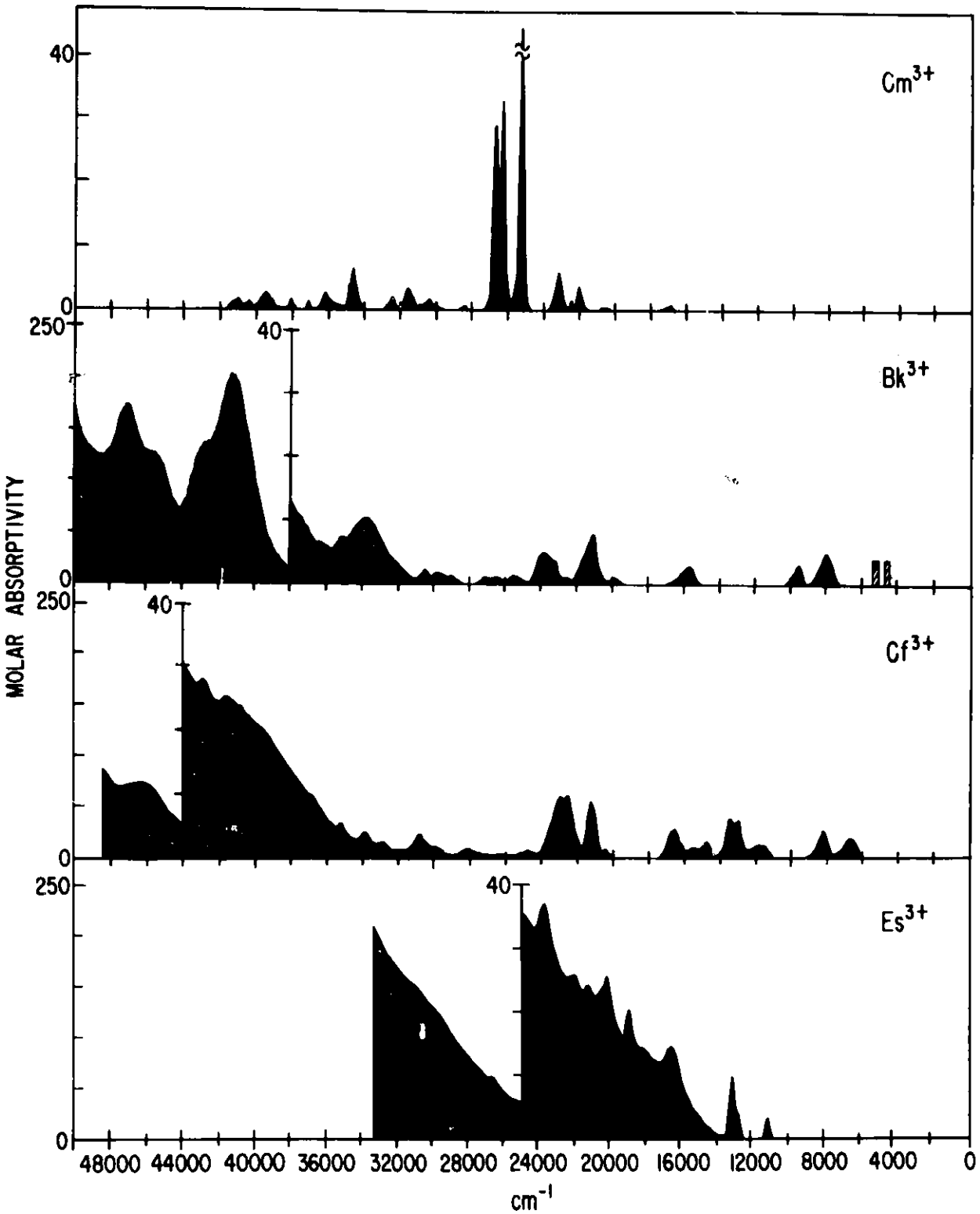

Fig. 3. Absorption Spectra of 3+ Actinide Ions in Dilute Acid Solutions.

were of the same order as those actually observed in Ln(III) spectra. However, it was subsequently pointed out that a second contribution, referred to as the ion-induced multipole contribution also gave contributions to the crystal-field that were comparable to the first and made the suggested approach unprofitable, Morrison et al. (1982).

From the regularities revealed in Figure 1 we can generalize. With increasing state of ionization beyond U IV, a concomitant increase in the energy gap between the ground states of the f^N and higher-lying configurations is expected. It is apparent from Figures 2 and 3 that this energy gap also increases with atomic number (Z) across a series of ions of the same charge state. However, there are half-filled-shell effects. Beyond Cm^{3+} ($5f^7$) the pattern of increasing energy of the f d transitions is seen to repeat. The actual correlations have been tabulated by Brewer (1971a,b). All free-ion energies recorded by Brewer for the various charge states must be corrected for medium effects for direct comparison with observed condensed phase spectra.

3.0. Interpretation of Observed Spectra of Trivalent Actinides

A great deal of progress had been made in interpreting condensed phase spectra of the trivalent lanthanide ions in terms of a physical model before much was known about the transuranium elements, Dieke (1968). Since, except for Th and Pa, each member of the actinide series exhibits a well characterized trivalent state, the model developed in treating lanthanide spectra has served as the basis for interpretation of trivalent actinide spectra as well, and extensive reference to lanthanide spectra is made here for comparison.

In what follows in this section, we summarize the results of modeling high-resolution spectra of An^{3+} in terms of the energy level structure for the An^{3+} ions. Regularities in the values of electronic-structure parameters that can be shown to exist for the 3+ actinides are then explored for other valence states. It should be emphasized that the modeling approach is independent of valence state, but the best data base for comparison is that developed for trivalent ions.

3.1. Free-Ion Models

There are two complementary aspects of theoretical modeling of atomic-electron systems, involving the radial parts of the atomic-electron wave functions on the one hand and angular parts on the other. Because the angular parts can be treated exactly, clear structural relationships can be demonstrated for various parts of the Hamiltonian. The work of B. R. Judd in particular has defined complete sets of generalized operators for several classes of Racah tensor operators which can be individually parametrized as needed to describe a particular atomic system. We have followed his lead in much of the modeling described in this report and we refer to this approach

as use of a parametric model. On the other hand, since by their nature these generalized parameters absorb a wide variety of distinct effects, the physical content of the parameters is not obvious. It is consequently useful to relate them to ab initio calculations of specific effects, as given by less exact but more physically meaningful integrals over the radial wave functions. We find that a single-configuration Hartree-Fock method gives valuable insight without undue computing requirements. The final parametric determination comes from a least-squares fitting of the more general parametric Hamiltonian variables to the experimental data.

The dominant interactions in the parametric model are (1) electrostatic repulsion between pairs of electrons and (2) the mutual interactions of the magnetic moments generated by the spin and orbital angular moments. We begin with the Schrödinger equation for the steady state of a many-electron atomic system.

$$H \Psi = E \Psi \tag{1}$$

The actual form of the Hamiltonian (H) assumes that the nucleus can be treated as a point charge. Since exact solutions, i.e. those based on an explicit form of the Coulomb interaction, are only known in the one-electron cases, some method of approximation must be utilized. This is usually the central-field approximation. Each electron is assumed to move independently in the field of the nucleus and an additional central field composed of the spherically averaged potential fields of each of the other electrons in the system. In other words, each electron is treated as if it moved independently in a spherically symmetric potential.

The Hartree-Fock (HF) approach seeks the evaluation of this potential using the variational principle, Hartree (1957), Slater (1960), Condon and Shortley (1963), March (1975), Fischer (1977), Cowan (1981). Computed values of the desired integrals can be obtained to varying degrees of approximation depending upon the sophistication of the computer codes used. The effects of configuration interaction, discussed later, can in principle be introduced. This is normally not done except for application to specific situations.

In the parametric model, each electron is assumed to move in a central field satisfying an equation, Eqn. 2, similar to the Schrodinger equation for the hydrogen atom, Wybourne (1965). However, the Coulomb potential $-\alpha^2/r$ is replaced by an implicit central-field potential U(r), which also includes the electrostatic mutual interactions of the electrons, averaged over their orbital motions:

$$\left[-\frac{\hbar^2}{2m} \nabla^2 + U(r) \right] \phi_i(a^i) = E(a^i)\phi_i(a^i) \tag{2}$$

Variables are separated as in the solution of the Schrödinger equation for the hydrogen atom, and the angular parts of the interaction are evaluated explicitly. The total Hamiltonian can be written:

$$H = H_o + H_e + H_{so} + H_{corr} \tag{3}$$

where H_o involves the kinetic energy of the electrons and their interaction with the nucleus, H_e is the electron-electron electrostatic term, H_{so} the sum of spin-orbit interactions, and H_{corr} represents higher-order interactions including configuration interactions and miscellaneous magnetic effects.

More specifically,

$$H_e = \sum_{k=0}^{6} F^k(nf,nf)\, f_k \quad (k \text{ even}) \tag{4}$$

and

$$H_{so} = \zeta_{nf} \sum_{\text{electrons}} (s \cdot l) \tag{5}$$

in which f_k and $(s \cdot \ell)$ are angular-momentum-dependent operators. The $F^k(nf,nf)$ are Slater radial integrals of electrostatic interaction, and ζ_{nf} is the spin-orbit interaction radial integral with n = 4 or 5 for cases of interest here.

If it is assumed that the difference in energy between the mean, E_p, of all levels of perturbing configurations and that of any level i of the f^N-configuration, $E_i(f^N)$, is very large such that $E_p - E_i(f^N)$ is effectively constant for all states i, then the closure theorem is valid and the effects of configuration interaction can be represented, Rajnak and Wybourne (1963), by

1) changes in F^k and ζ

2) additional 2,3---N body (effective) operators operating within the f^N-configuration.

Within the above context, the F^k integrals are not to be identified as the integrals of the Hartree-Fock model; as parameters they also absorb some of the effects of configuration interaction. This partially accounts for the large differences between the parametric and Hartree-Fock values of F^k and gives an estimate of the magnitudes of the required corrections to the basic model.

A model that is limited to the Slater integrals, $F^k(nf,nf)$ and the spin-orbit interaction, ζ_{nf}, results in correlations between observed and calculated free-ion states that are only approximate. The higher-order

correction terms must be added to achieve a good agreement with experiment. The nature of the corrections that refine the model suggests that the problem can be treated as if the f-electrons spent some time in higher-lying configurations where they move in larger orbits and interact less with each other, but in a manner related to the particular class of configurations occupied. These higher-order corrections to the simple model account in large part for the effects of configuration interaction, and are discussed in Section 3.3.

3.2. A Predictive Model for Trivalent f-Element Spectra

When the results of a Hartree-Fock calculation are compared to those of a parametric analysis of experimentally identified levels for a given element, the magnitudes of the computed energies, particularly those for F^k, are generally found to be too high. For a more realistic Hamiltonian, using the parametric approach, we show here that one can apply subtractive corrections to the estimates derived from ab initio calculations. These corrections turn out to be essentially constant over the series and in fact almost identical for both $4f^N$ and $5f^N$ shells. The significance of this is that mixing with high configurations can be taken as essentially a fixed contribution to a global parametric model, Crosswhite and Crosswhite (1984a).

Qualitatively, the radial wave functions for lanthanides and actinides are very similar in that the f-shell is inside filled s and p shells of one-higher principal quantum number, which partially shield it from external influences. A comparison of the Nd^{3+} and U^{3+} analogues is shown in Figure 4, where the f-electron radial functions are multiplied by an arbitrary factor for emphasis. Notice that for U^{3+} the f^N peak is considerably displaced toward greater values of the atomic radius (r) with respect to the shielding s and p shells, and the relative magnitude of the f-electron tail at large r with respect to the rest of the core function is larger and more exposed than for Nd^{3+}.

Because of the greater extension of the 5f radial wave functions with respect to those of the shielding 7s and 7p shells, they are more sensitive to changes in the valence-electron situation than for the corresponding lanthanide cores. Nevertheless, their rigidity is remarkable as compared to that for the valence electrons themselves. This can be seen quantitatively in the plots for the Slater electrostatic interaction integrals $F^k(5f,5f)$ and spin-orbit radial integral ζ_{5f}, which dominate the atomic Hamiltonian for all cases of interest to us here, Figures 5-8.

We have noted in Figure 1 that there is competition between 5f, 6d and 7s orbitals for occupancy of low actinide configurations for lower ionization states. However, if we confine our attention to the configurations of the elements beyond thorium we can limit the types to $5f^{Z-89}6d7s^2$ or $5f^{Z-88}7s^2$ for first spectra, $5f^{Z-89}7s^2$ or $5f^{Z-88}7s$ for second, $5f^{Z-89}6d$ or

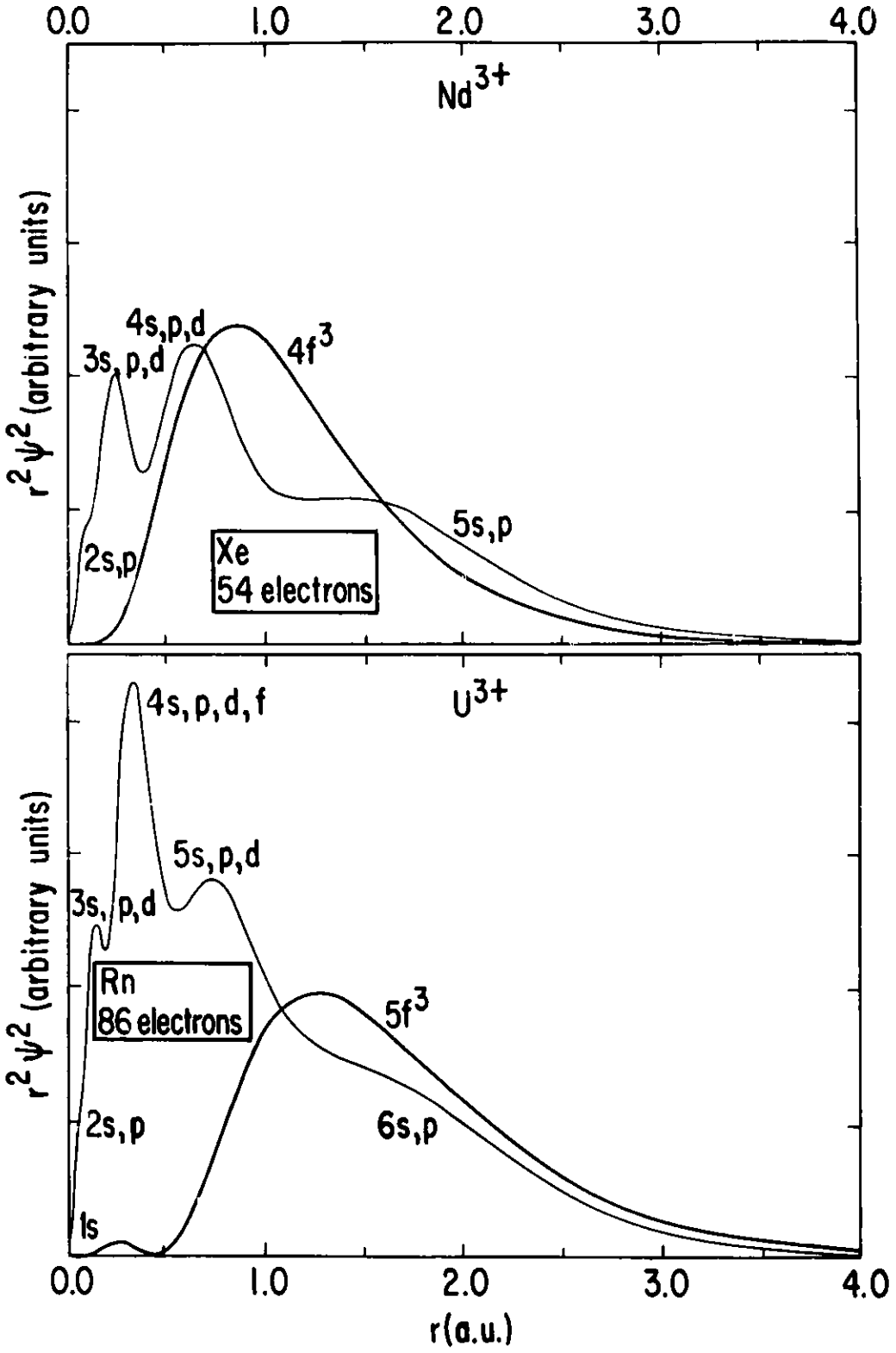

Fig. 4. Comparison of the Overlap of $4f^3$-5s,p Configurations for Nd^{3+} and $5f^3$-6s,p Configurations for U^{3+} as a Function of the Atomic Radius.

$5f^{Z-89}$ for third and $5f^N$ for fourth spectra and higher. Tables 1-4 show the results of ab initio calculations of the three $F^k(5f,5f)$ and the ζ_{5f} integrals for these types. Similar calculations were reported by Varga et al. (1970). The $F^k(5f,5f)$ and ζ_{5f} results are displayed in Figures 5-8. The heavy underlining in the tables and the filled circles in Figures 5-8 represent configurations that are lowest for those particular ions; open circles represent selected competing (next lowest) configurations. For instance, the ground configuration for neutral atoms is $5f^{Z-89}6d7s^2$ for Pa I through Np I; $5f^{Z-88}7s^2$ for Pu I and Am I, $5f^{Z-89}6d7s^2$ for Cm I, and $5f^{Z-88}7s^2$ again for Bk I through Fm I. These calculations were made using a version of a Hartree-Fock program written by Fischer (1969) and adapted for use at Argonne by M. Wilson to contain an approximate correction for relativistic contraction of s-electron orbitals, Cowan and Griffin (1976), Cowan (1981). We designate this version as HFR, Crosswhite and Crosswhite (1984a). For second spectra there is similar competition, this time between 5f and 7s orbitals, giving $5f^{Z-88}7s^2$ as the lowest configuration of Pa, U and the half-filled-shell case of Cm. Similarly, for the neutral atoms, the ground configuration can be $5f^{Z-89}6d7s^2$ for Pa, U, Np or Cm and $5f^{Z-88}7s^2$ for all the rest.

Inspection of Figures 5-7 shows that the addition of a valence-shell electron diminishes the Slater integrals for the $5f^N$ core slightly but not seriously, and that the effects are additive: $5f^{Z-88}$ III values are enhanced twice as much compared to $5f^{Z-88}7s^2$ I as compared to $5f^{Z-88}7s$ II (and nearly the same as the difference between $5f^{Z-89}$ IV and $5f^{Z-89}7s^2$ II). The $5f^{Z-89}$ IV - $5f^{Z-89}6d$ III difference is the same as that for $5f^{Z-89}7s^2$ II - $5f^{Z-89}6d7s^2$ I. Similiar results are found for the other Slater and spin-orbit interaction integrals which combine to dominate the atomic Hamiltonian. As a first approximation they can be taken to depend only on the population of the 5f shell itself and to be independent of the distribution over valence electron shells. When we compare these computed values with experimentally-determined parameters, it will be seen that the needed corrections correspond closely to the trends shown in Figures 5-8.

3.3. Effective Operators for the Free-Ion Interactions

The ab initio calculations are in error partly because of the assumption of a single-configuration model. Multiconfiguration calculations, which take configuration interactions into account, are more accurate, but they are much too time-consuming for general application to the many situations encountered in the analyses. However, a very useful result comes out of the calculations which have been made, namely that the energy-level shifts induced by these interactions can be mimicked by effective operators acting only within the f^N-configuration itself.

The angular momentum dependence of the conventional Slater electrostatic integrals is given by the expression, Wybourne (1965),

TABLE 1.

HFR Slater Integrals

$F^2(5f,5f)$

	Z =	91 Pa	92 U	93 Np	94 Pu	95 Am	96 Cm	97 Bk	98 Cf	99 Es	100 Fm
f^{Z-88}	s^2 I	57393	62891	67452	71461	75129	78531	81720	84766	87683	90499
	s II	58651	63691	68024	71900	75479	78821	81967	84975	87867	90662
	III	60122	64751	68843	72563	76031	79292	82379	85340	88193	90958
f^{Z-89}	ds^2 I	64137	68684	72662	76279	79660	82843	85865	88768	91592	94294
	s^2 II	65990	70110	73833	77274	80518	83596	86530	89361	92105	94774
	d III	65406	69573	73342	76820	80100	83211	86176	89034	91802	94494
	IV	67652	71442	74944	78223	81346	84331	87192	89964	92657	95284
f^{Z-90}	V	-	76724	79892	82908	85817	88625	91338	93984	96568	99099
f^{Z-91}	VI	-	-	84141	86982	89744	92428	95035	97590	100094	102555
f^{Z-92}	VII	-	-	-	90625	93280	95872	98402	100888	103331	105739

TABLE 2.

HFR Slater Integrals

F^4 (5f,5f)

Z =			91 Pa	92 U	93 Np	94 Pu	95 Am	96 Cm	97 Bk	98 Cf	99 Es	100 Fm
f^{Z-88}	s^2	I	36564	40290	43381	46094	48572	50868	53016	55065	57025	58194
	s	II	37429	40845	43779	46400	48818	51071	53190	55212	57154	59028
		III	38454	41587	44355	46868	49208	51405	53481	55471	57385	59238
f^{Z-89}	ds^2	I	41304	44396	47094	49543	51827	53975	56009	57961	59843	61668
	s^2	II	42621	45415	47935	50260	52447	54519	56491	58391	60230	62016
	d	III	42198	45024	47576	49926	52140	54235	56230	58150	60006	61809
		IV	43808	46370	48733	50942	53044	55049	56969	58826	60629	62385
f^{Z-90}		V	-	50199	52330	54356	56307	58188	60003	61772	63497	65185
f^{Z-91}		VI	-	-	55445	57347	59195	60988	62729	64432	66100	67739
f^{Z-92}		VII	-	-	-	60037	61810	63538	65222	66876	68501	70101

TABLE 3.

HFR Slater Integrals

F^6 (5f,5f)

Z =			91 Pa	92 U	93 Np	94 Pu	95 Am	96 Cm	97 Bk	98 Cf	99 Es	100 Fm
f^{Z-88}	s^2	I	26525	29304	31611	33638	35489	37204	38808	40338	41801	43210
	s	II	27170	29718	31909	33867	35674	37357	38939	40449	41897	43296
		III	27938	30276	32343	34220	35968	37609	39159	40644	42073	43455
f^{Z-89}	ds^2	I	30105	32417	34436	36268	37977	39583	41103	42561	43966	45328
	s^2	II	31101	33191	35076	36815	38450	39998	41471	42889	44262	45594
	d	III	30777	32892	34800	36558	38214	39780	41270	42704	44089	45435
		IV	32003	33918	35684	37335	38905	40403	41836	43222	44567	45877
f^{Z-90}		V	-	36860	38452	39965	41423	42827	44181	45500	46787	48045
f^{Z-91}		VI	-	-	40865	42285	43664	45002	46299	47569	48812	50032
f^{Z-92}		VII	-	-	-	44381	45702	46991	48246	49474	50687	51878

TABLE 4.

HFR Slater Integrals

ζ (spin-orbit)

Z =			91 Pa	92 U	93 Np	94 Pu	95 Am	96 Cm	97 Bk	98 Cf	99 Es	100 Fm
f^{Z-88}	s^2	I	1345	1636	1929	2230	2542	2869	3209	3566	3940	4333
	s	II	1367	1651	1941	2239	2551	2876	3215	3572	3945	4338
		III	1396	1674	1959	2255	2565	2889	3228	3583	3956	4348
f^{Z-89}	ds^2	I	1551	1826	2119	2412	2739	3070	3417	3781	4162	4562
	s^2	II	1583	1861	2149	2449	2764	3093	3438	3800	4180	4579
	d	III	1567	1846	2135	2436	2751	3082	3427	3790	4170	4570
		IV	1625	1898	2182	2479	2792	3119	3463	3824	4203	4601
f^{Z-90}		V	1835	2110	2397	2697	3014	3347	3697	4064	4450	4856
f^{Z-91}		VI	-	2316	2608	2914	3236	3575	3931	4306	4699	5112
f^{Z-92}		VII	-	-	2817	3130	3459	3805	4167	4549	4950	5371

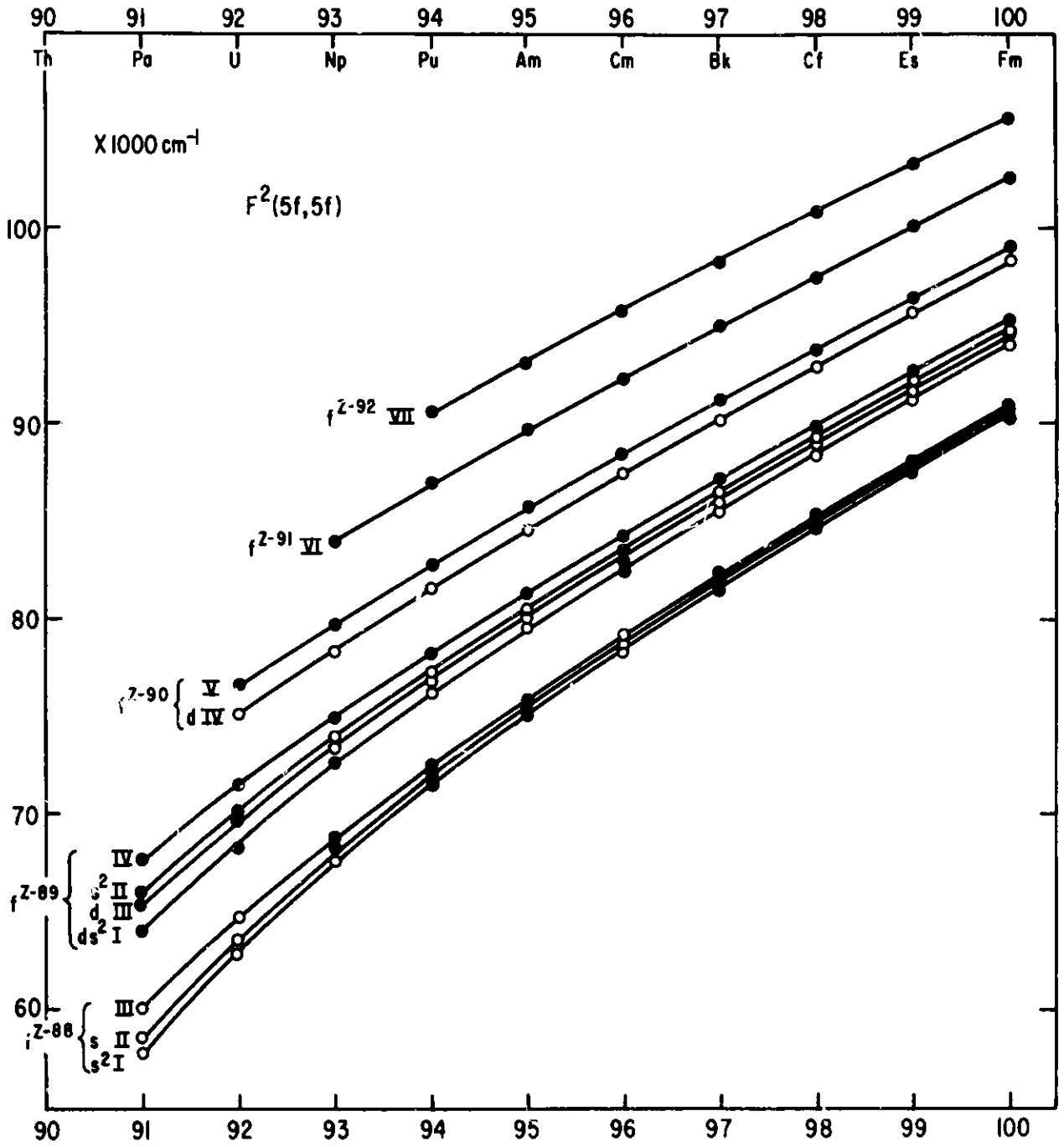

Fig. 5. Variation of Hartree-Fock (HFR) Computed Values of $F^2(nf,nf)$ with Atomic Number.

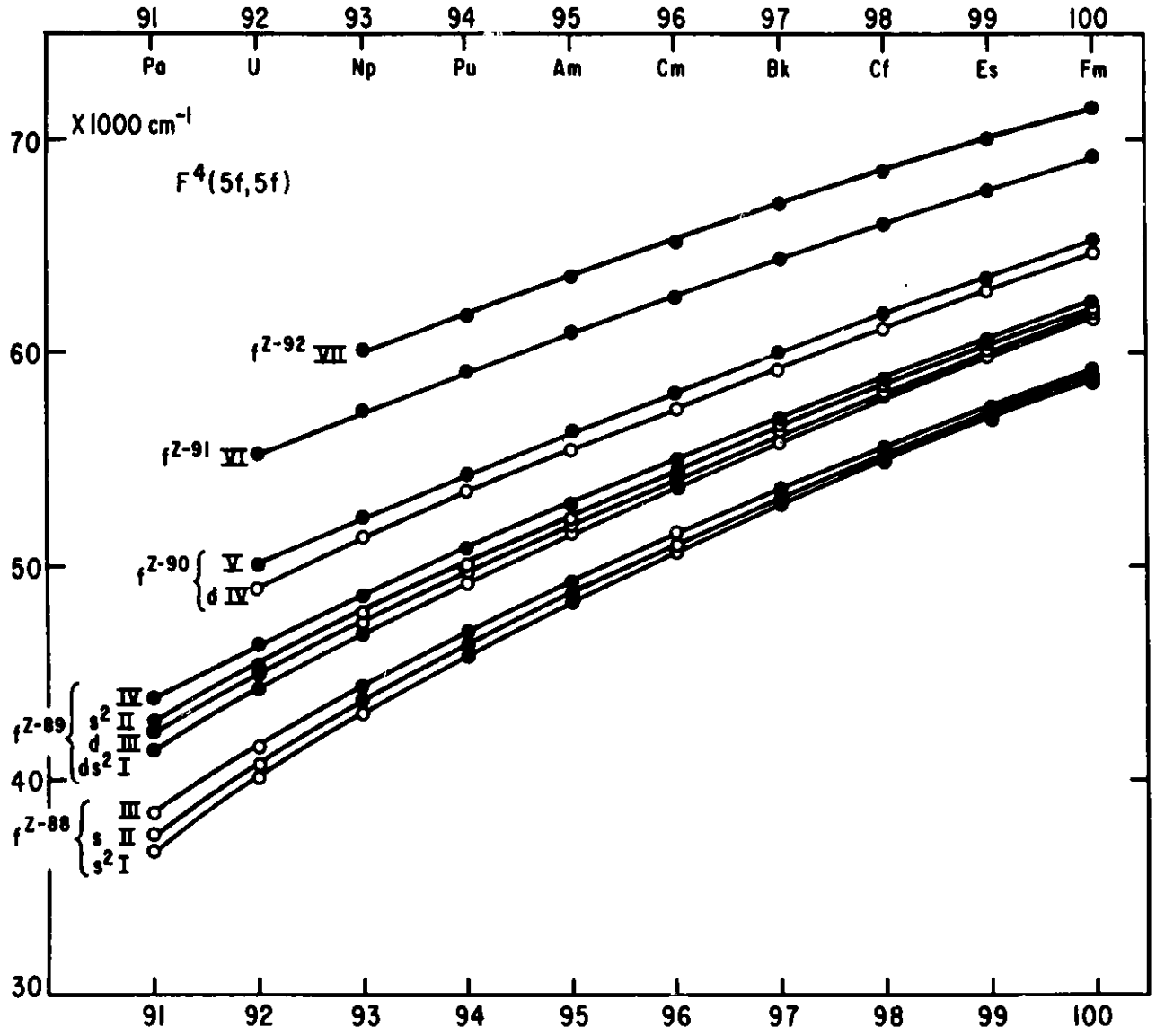

Fig. 6. Variation of Hartree-Fock (HFR) Computed Values of F^4(nf,nf) with Atomic Number.

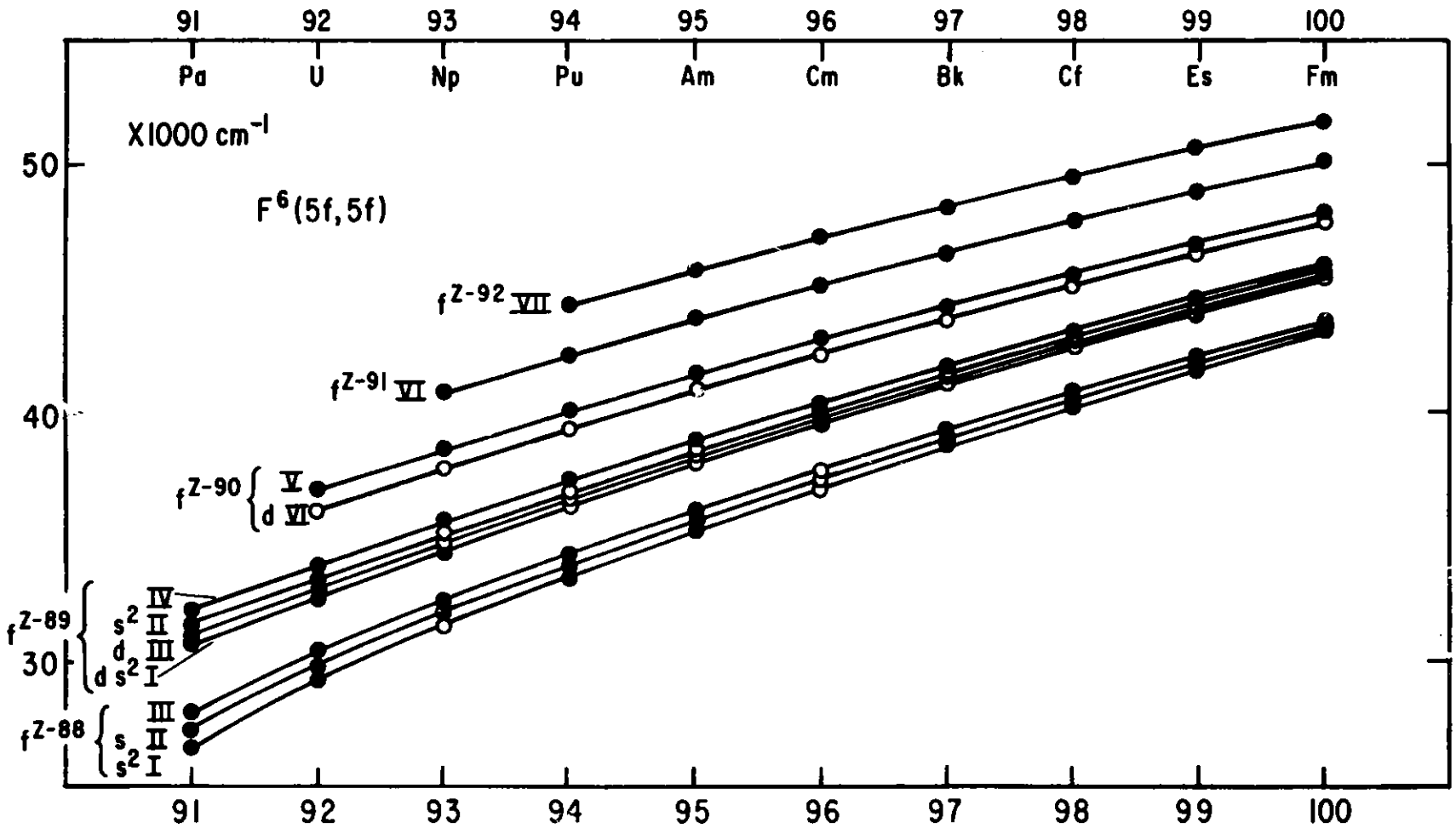

Fig. 7. Variation of Hartree-Fock (HFR) Computed Values of F^6(nf,nf) with Atomic Number.

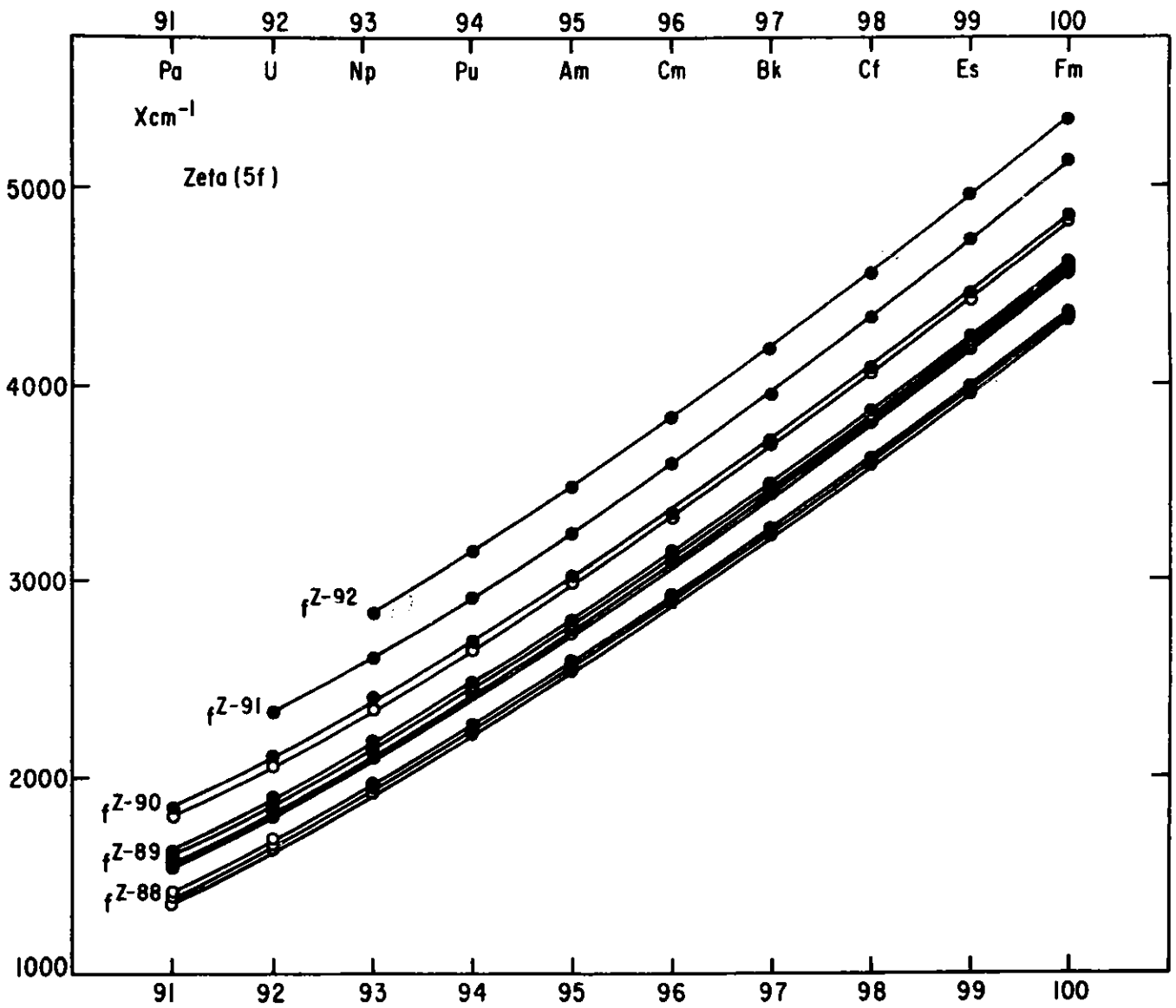

Fig. 8. Variation of Hartree-Fock (HFR) Computed Values of Zeta (5f) with Atomic Number.

$$f_k(\ell,\ell) = (-1)^L(\ell\|C^{(k)}\|\ell)^2 \begin{Bmatrix} \ell\ell k \\ \ell\ell L \end{Bmatrix} . \qquad (6)$$

A triangle (selection) rule on the indicated 6-j symbol limits the range to a maximum of $2\ell = 6$, in this case. A similar selection rule on a 3-j symbol which appears in the full expression for $(\ell\|C^{(k)}\|\ell)$ requires k to be even. The central-field approximation, therefore, limits the operative radial integrals, Racah (1949), Condon and Shortley (1963), Cowan (1981), to

$$F^k(nf,nf) = e^2 \iint \frac{r_<^k}{r_>^{k+1}} |R_{nf}(r_1)|^2 |R_{nf}(r_2)|^2 dr_1 dr_2 \quad n = 4 \text{ or } 5 \qquad (7)$$

(or adjustable parameters F^k, if parametric fitting is being considered) to the values k = 0,2,4,6. However, in the generalized description there arise much more complex radial integrals associated with angular momentum factors which also apply to the odd-k symbols, Crosswhite (1971). Because of the orthogonality properties of the 6-j symbols, and because the seven possible k values (0-6) are exactly equal to the number of electrostatic terms of the f^2 configuration, the three new effective operators defined in this way are just the number needed to complete the set of parameters required for the electrostatic description of the f^2 configuration.

However, this is not the only way to generate three effective operators independent of the four already in use. The most common convention for defining them uses the operators

$$\alpha\, L(L+1),\ \beta G(G_2) \text{ and } \gamma G(R_7) \qquad (8)$$

where $G(G_2)$ and $G(R_7)$ are Casimir operators, Casimir (1931), Wybourne (1965), and α, β, and γ are adjustable parameters.

Multiconfiguration calculations have shown that similar values of these effective-operator parameters are to be expected at both ends of the lanthanide sequence, Morrison (1972), and empirical evaluations are in agreement with this for both the lanthanides and actinides. The same mechanism will also generate corrections which project on the even-k operators. However these are automatically absorbed by their parameters, contributing to the nearly-constant correction discussed previously.

For three (or 11) electrons, similar arguments show the need for additional (three-body) operators in order to completely parametrize the electrostatic interactions. If consideration is limited to the interactions arising from second-order perturbation theory, only six new operators are needed, Judd (1966), and their experimental evaluation is consistent with results expected from first-principles calculations, Poon and Newman (1983).

Similar arguments hold for corrections to the spin-orbit interaction, as well as additional interactions of relativistic origin such as spin-other-orbit and spin-spin. Hartree-Fock calculations give good estimates of the Marvin radial integrals $M^{(k)}$ (k = 0,2,4) associated with spin-other-orbit and spin-spin interactions, Marvin (1947). Experimental investigations are needed for evaluation of the magnetic corrections associated with configuration interactions, but experience has shown that a single set of parameters P^k (k = 2,4,6, with $P^4 = 0.75\ P^2$ and $P^6 = 0.50\ P^2$) accounts for a large part of this class of corrections. Use of sets of all of the foregoing parameters has been explored in detail for all of the trivalent ions from U^{3+} through Es^{3+}, and values are given in Table 5 for An^{3+}:$LaCl_3$ and $AnCl_3$. Each case, except that for Am^{3+}, represents an independent fitting of parameters to experimental data.

3.4. The Crystal-Field Hamiltonian

When a lanthanide or actinide ion occurs in a condensed-phase medium, it retains a large part of its "free-ion" character, but energy levels are shifted to a greater or lesser degree, depending on the nature and strength of the interaction with the environment. A good part of this interaction can be absorbed by the nominal "free-ion" parameters themselves, and a measure of this contribution would give clues as to the nature of the interactions. Unfortunately, due mainly to the different methods by which the free-ion and condensed-phase levels are determined, there are very few cases in which both sets of parameters are known well enough for meaningful comparisons to be drawn. Some of the more useful of these and the means by which they can be incorporated into a predictive model will be discussed in Section 4.0.

In addition to modifications of the atomic parameters, there are medium-related effects which must be taken into account explicitly. The broken spherical symmetry that normally results when an isolated free gaseous ion is placed in a ligand field gives rise to a splitting of the free-ion level into a maximum of (2J+1) components. A single-particle crystal-field model has had remarkable success for lanthanides and somewhat more qualified, but nevertheless satisfactory, success for the trivalent actinides in providing an interpretation of the data, Dieke (1968), Crosswhite (1977), Hüfner (1978). The additional splitting induced by the crystal field can be described by the expression:

$$H_{CF} = \sum_{k,q,i} B_q^k \, (C_q^k)_i \qquad (9)$$

where the B_q^k are radial integrals treated as parameters, the C_q^k are tensor operators dependent on the symmetry of the crystal lattice and the sum over i represents the sum over the electrons.

The most extensive investigations of actinide spectra have been carried out for the +3 actinide ions doped into single-crystal $LaCl_3$, since $LaCl_3$ is a well-characterized crystalline matrix in which polarized spectra can be measured. Such investigations, supplemented by Zeeman-effect studies of the influence of applied magnetic fields on the energy levels, provide the basis for experimental characterization of the observed transitions in terms of the free-ion SLJ and crystal-field quantum numbers.

The relative energies of some of the low-lying states in U^{3+}:$LaCl_3$ are shown in Figure 9, Crosswhite et al. (1980). As indicated, each free-ion state is split by the crystal electric field. When viewed at the temperature of liquid He (~4K), only transitions from the lowest state (taken as the zero of energy and having a crystal field quantum number μ=5/2 in this case) are observed. Absorption bands, which are interpreted as arising from transitions between the $^4I_{9/2}$ (ground) and $^4I_{11/2}$ excited states are shown in Figure 10 as obtained at ~4K in moderate resolution. Most of the experimental results that have been reported were photographed using high-resolution grating spectrographs. Transitions to only three levels of $^4I_{11/2}$ were readily observed in absorption; that to a μ=1/2 state (found by other techniques near 4580 cm^{-1}) was too weak to be apparent. Electric-dipole selection rules in this case forbid transitions between the ground state (μ=5/2) and excited μ=5/2 states, so levels that would have corresponded to transitions at 4556 and 4608 cm^{-1} were established by fluorescence measurements.

As the energies of the components of various groups are established experimentally, the model free-ion and crystal-field parameters that reproduce the splitting can be computed by a suitable (least-squares) fitting procedure. The computed values are then used to predict the splitting patterns in other groups where not all the allowed components can be observed. Thus, in the analysis of such spectral data there is a continual interplay between theory and experiment. When large numbers of levels have been experimentally confirmed, most (in some cases all) of the parameters of the model can be varied simultaneously to establish the final values, Table 5. The differences between the F^k and ζ_{nf} integrals computed using Hartree-Fock methods and those evaluated (from Table 5) are shown in Table 6. The parameters for Bk^{3+} and Cf^{3+} were evaluated from data obtained from pure samples of $BkCl_3$ and $CfCl_3$, not doped $LaCl_3$. The consistency of the parameter differences over the series for each independently determined parameter is apparent.

In typical analyses of actinide and lanthanide spectra in condensed phases, the range of observation may extend well into the near ultraviolet to 30000-40000 cm^{-1}. The number of assignments made to different multiplets and states is usually sufficient to determine most of the energy level parameters. However, as indicated in Figures 11 and 12, the actual observations

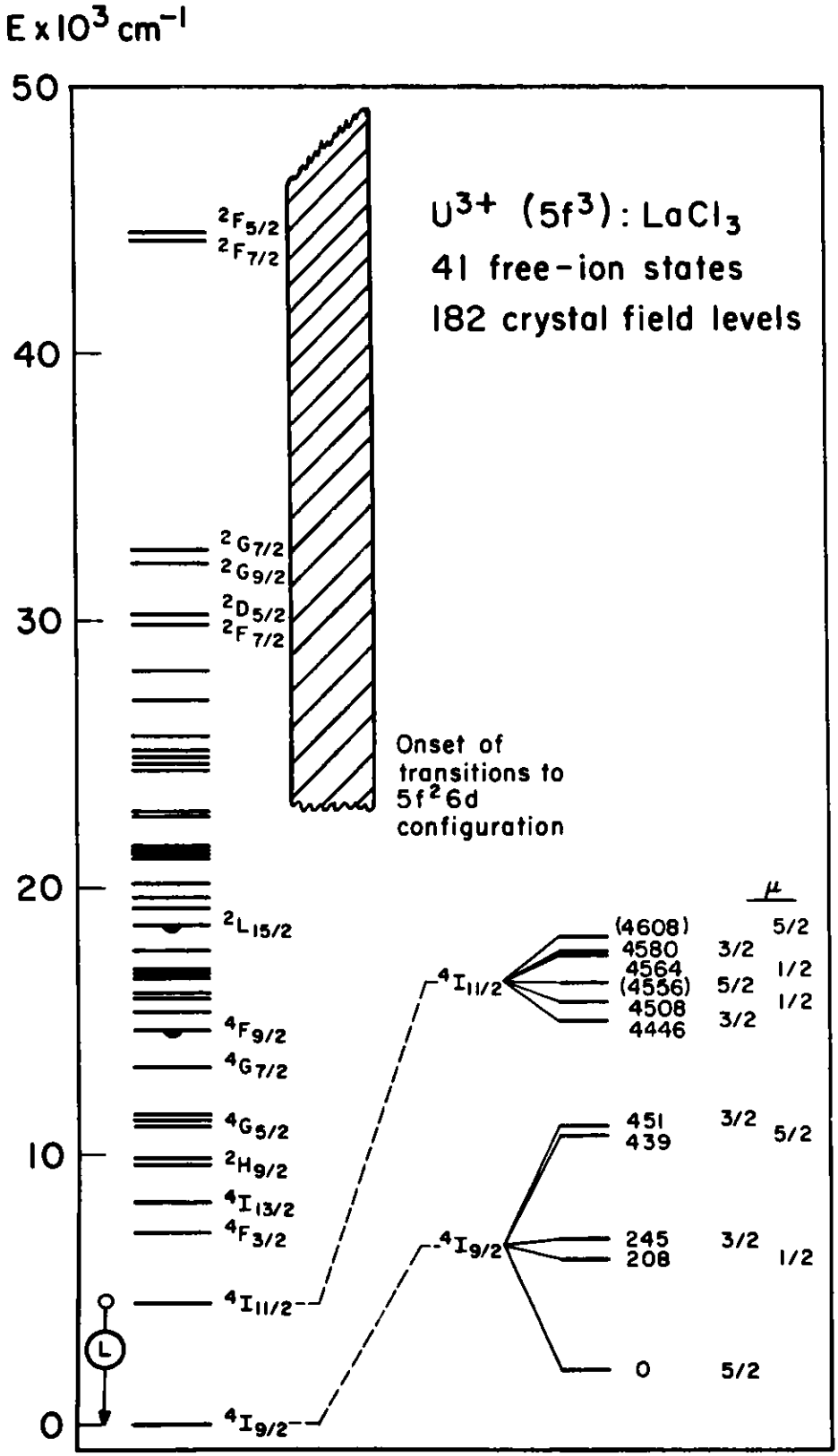

Fig. 9. Free-ion Energy Level Structure for U^{3+}:$LaCl_3$ Showing Crystal-Field Components for the $^4I_{9/2,11/2}$ States. The Laser Transition is Indicated by L, Crosswhite et al. (1980).

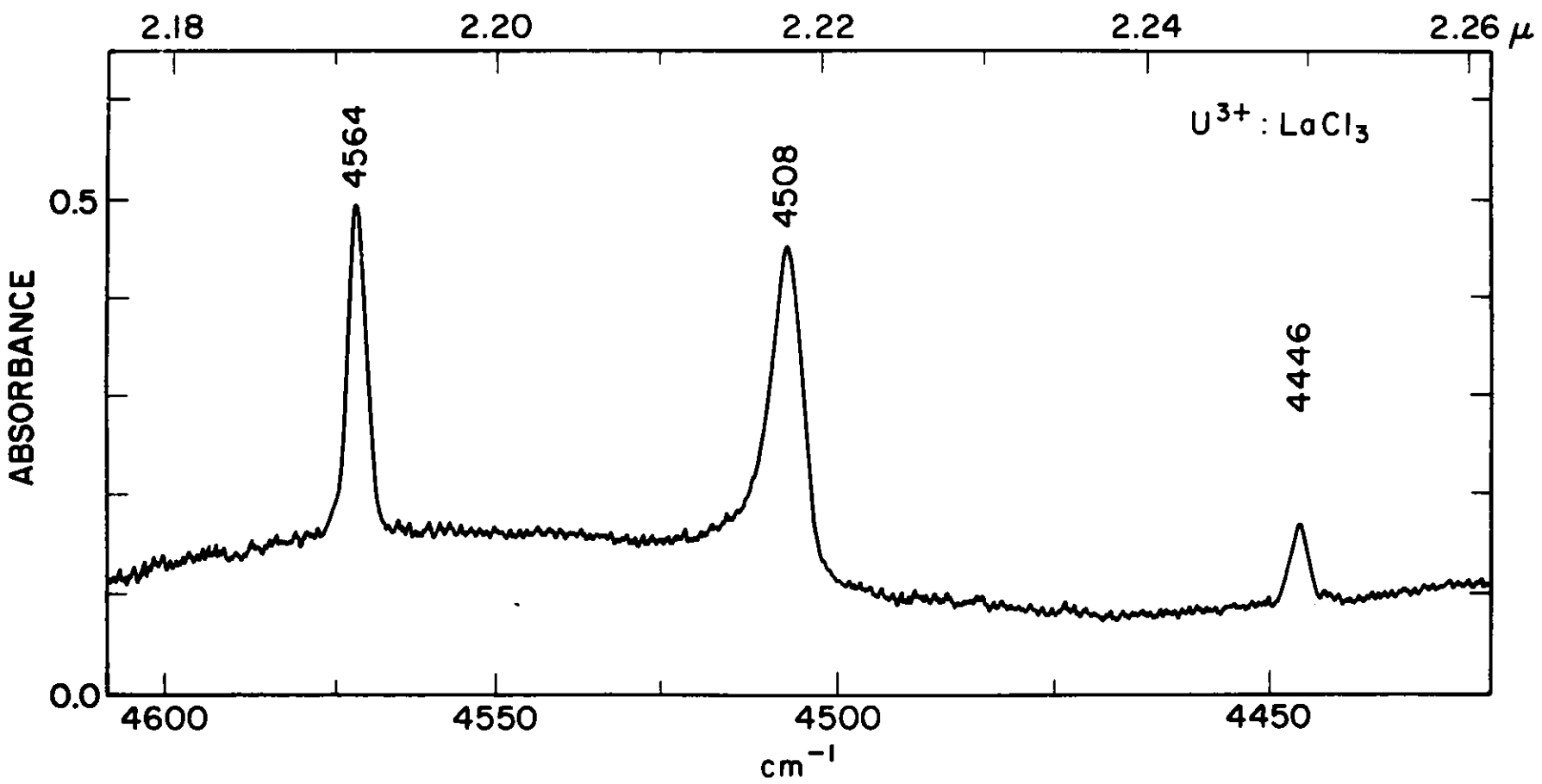

Fig. 10. Portion of the Absorption Spectrum of U^{3+}:$LaCl_3$ Recorded at 4K, Crosswhite et al. (1980).

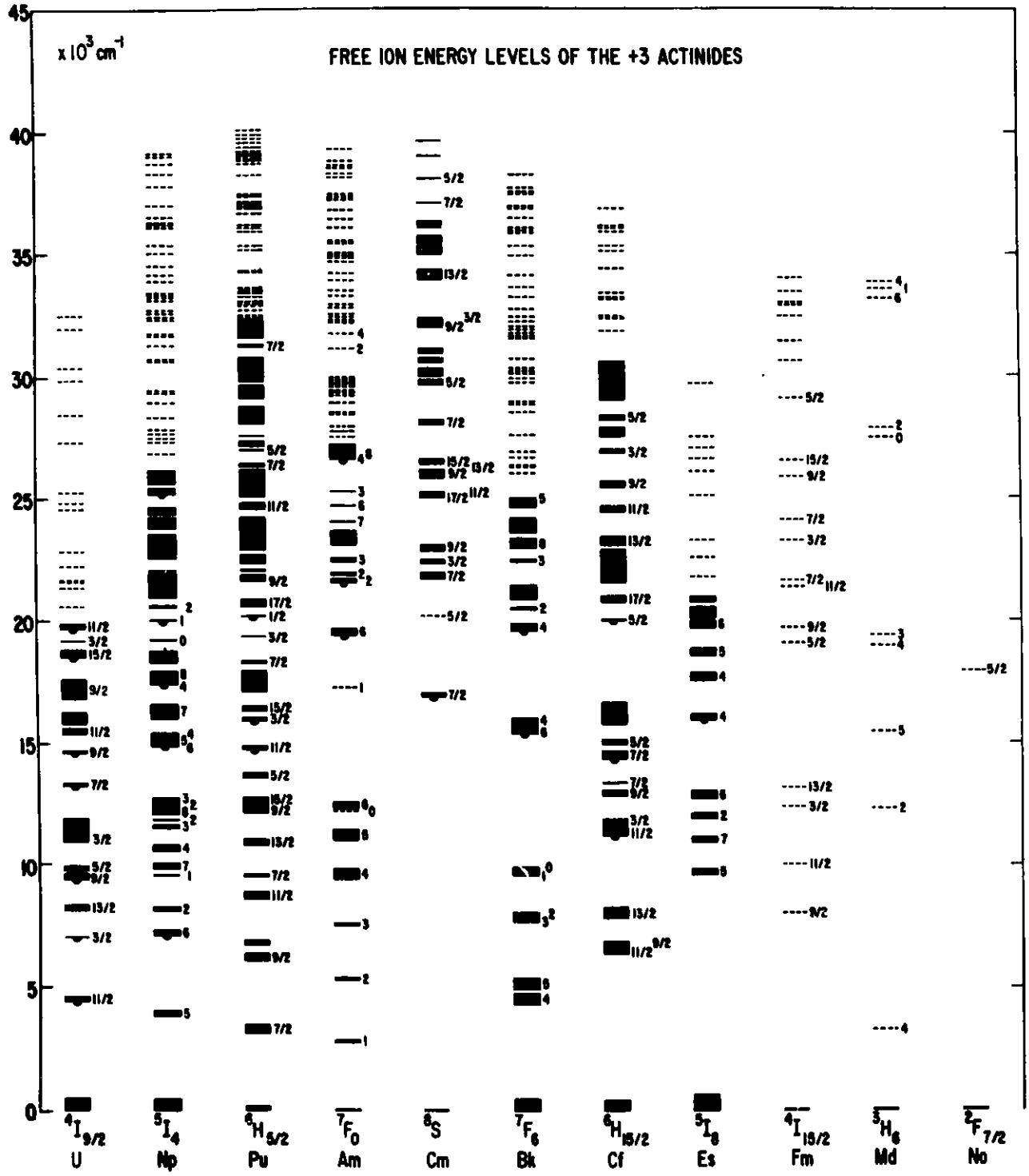

Fig. 11. Free-ion Energy Level Structures for An^{3+}. Energy Level Parameters and References Given in Table 5.

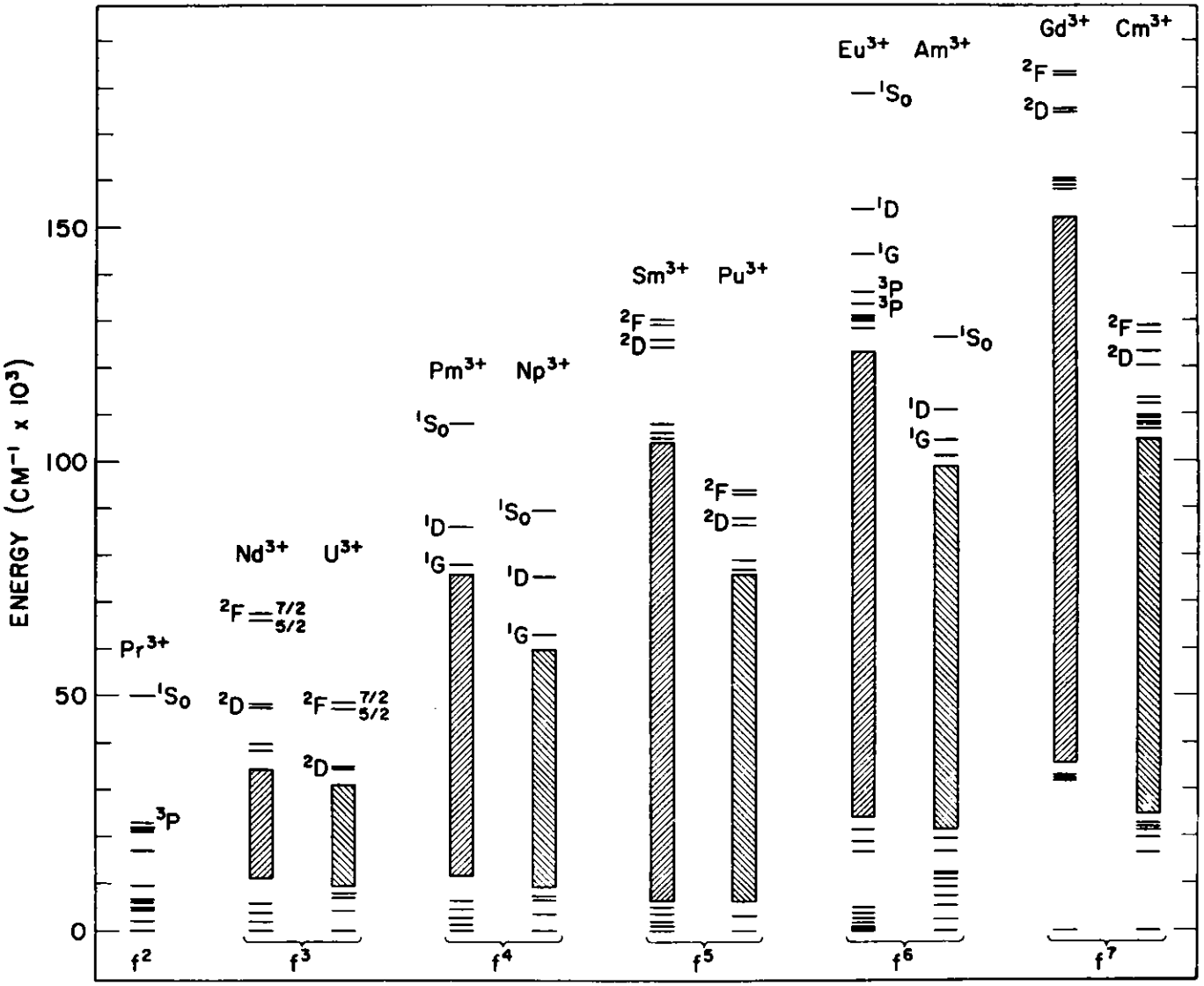

Fig. 12. Energy Spanned by the Complete $4f^N$- and $5f^N$-Configurations, N = 2-7. Cross-hatched Areas Indicate a High Density of Levels.

TABLE 5.

Energy Level Parameters for $An^{3+}:LaCl_3$[a,b]

	$U^{3+}LaCl_3$[c]	$Np^{3+}:LaCl_3$[d]	$Pu^{3+}:LaCl_3$[e,f]	$Am^{3+}:LaCl_3$[f,g]	$Cm^{3+}:LaCl_3$[f,h]	$BkCl_3$[i]	$CfCl_3$[j]	$Es^{3+}:LaCl_3$[k]
E_{ave}	19544	29989	39631	53667	64125	54953	49530	44709
F^2	39715(218)	44907(161)	48670(154)	51800	55109(129)	57015(120)	61014(223)	62766(273)
F^4	33537(302)	36918(245)	39188(294)	41440	43803(328)	45698(165)	44483(517)	48003(200)
F^6	23670(211)	25766(221)	27493(153)	30050	32610(168)	33552(154)	36168(323)	35309(326)
ζ	1623(4)	1938(2)	2241(2)	2580	2903(4)	3216(6)	3568(3)	3962(6)
α	27.6(0.9)	31.5(0.3)	29.7(0.4)	29.0	28.4(0.8)	29.9(0.4)	27.7(0.8)	[20.9]
β	-722(33)	-740(18)	-671(15)	-660	[-650]	[-674]	-681(41)	[-500]
γ	[1000]	899(70)	1067(79)	1000	935(107)	[913]	1082(137)	[700]
T^2	217(90)	278(22)	186(11)	200	200	200	[300]	[200]
T^3	63(13)	44(7)	48(13)	50	50	40	86(23)	[50]
T^4	255(23)	65(7)	38(21)	40	40	65(63)	54(32)	[50]
T^6	-107(49)	-361(18)	-364(22)	-360	-360	-326(50)	-350(57)	[-360]
T^7	617(78)	434(22)	364(15)	390	390	442(40)	281(40)	[400]
T^8	[350]	353(17)	332(18)	340	340	380	364(27)	[340]
$M(0)^1$	[0.67]	0.68(0.17)	0.95(0.21)	0.99	1.09	1.19	1.3	[1.0]
$P(2)^m$	1276(104)	894(14)	822(44)	850	922(37)	523(73)	578(60)	825(184)
B_0^2	260(64)	163(26)	226(25)	230	244(42)	[250]	476(36)	363(101)
B_0^4	-532(139)	-632(48)	-543(48)	-610	-710(84)	-922(82)	-1108(73)	-1264(249)
B_0^6	-1438(113)	-1625(52)	-1695(45)	-1590	-1383(113)	-1324(76)	-1367(79)	-1466(167)
B_6^6	1025(88)	1028(35)	1000(40)	980	929(77)	910(44)	963(63)	749(124)

Table 5. (continued)

	$U^{3+}:LaCl_3$	$Np^{3+}:LaCl_3$	$Pu^{3+}:LaCl_3$	$Am^{3+}:LaCl_3$	$Cm^{3+}:LaCl_3$	$BkCl_3$	$CfCl_3$	$Es^{3+}:LaCl_3$
No Levels	51	150	155	-	88	60	90	36
σ	26	20	18	-	27	22	28	33

a. The data for U^{3+} through Cm^{3+} were obtained in absorption and fluorescence using doped single crystals of $LaCl_3$; while spectra for Bk^{3+} and Cf^{3+} were measured in absorption with thin films of the pure halide. Preliminary data for Es^{3+} were obtained from excitation spectra of Es^{3+} doped into single crystal $LaCl_3$.

b. Values in brackets were assigned and were not varied; the values in parentheses are the r.m.s. errors. Values for α were divided by 1000.

c. Crosswhite et al. (1980).

d. Carnall et al. (1980).

e. Lämmermann and Conway (1963), Conway and Rajnak (1966), Carnall et al. (1970).

f. Hessler and Carnall (1980).

g. Values of parameters obtained by extrapolation. Experimental data given by Pappalardo et al. (1969), Conway (1964b).

h. Gruber et al. (1966), Carnall and Rajnak (1975).

i. Carnall et al. (1973a).

j. Carnall et al. (1973b).

k. Paszek (1978), Hessler et al. (1978), Hessler (1984).

l. In establishing values for M(0), M(2), and M(4), the following ratios were maintained, M(2)/M(0) = 0.56, M(4)/M(0) = 0.38. When M(0) was varied, the established ratios were maintained constant.

m. The procedure for establishing values of $P^{(K)}$, K = 2,4,6, was identical to that cited above: P(4)/P(2) = 0.75, P(6)/P(2) = 0.5.

TABLE 6.

Comparison of Energy Level Parameters Computed Using Hartree-Fock Methods and those Evaluated from Fitting Experimental Data for An^{3+}.

	U	Np	Pu	Am	Cm	Bk	Cf	Es
F^2(HFR)[a]	71442	74944	78223	81346	84331	87192	89964	92657
F^2(FIT)[b]	39715	44907	48670	51800	55109	57015	61014	62766
ΔP	31727	30037	29553	29546	29222	30177	28950	29891
F^4(HFR)	46370	48733	50942	53044	55049	56969	58826	60629
F^4(FIT)	33537	36918	39188	41440	43803	45698	44483	48003
ΔP	12833	11815	11754	11604	11246	11271	14343	12626
F^6(HFR)	33918	35684	37335	38905	40403	41826	43222	44567
F^6(FIT)	23670	25766	27493	30050	32610	33552	36168	35309
ΔP	10248	9918	9842	8855	7793	8274	7054	9258
ζ(HFR)	1898	2182	2479	2792	3119	3463	3824	4203
ζ(FIT)	1623	1938	2241	2580	2903	3216	3568	3962
ΔP	275	244	238	212	216	247	256	241

a. Computed using Hartree-Fock methods and including an approximate relativistic correction, (HFR), Cowan and Griffin (1976), Crosswhite and Crosswhite (1984a).

b. Computed by fitting to experimental data, Table 5.

may be limited to less than 50% of the total extent of the f^N configuration. The accuracy of predicted level energies in the ultraviolet range clearly remains to be thoroughly tested; however, it was possible to show for $Gd^{3+}:CaF_2$ that parameters determined based on assignments at <50000 cm^{-1} very adequately predicted the levels later observed in the vacuum ultraviolet range at >50000 cm^{-1}, Crosswhite et al. (1969).

The reduction in the overall range of energy for transitions characteristic of the $5f^N$-configurations compared to the $4f^N$-configurations in An^{3+} and Ln^{3+} is also indicated in Figure 12. The Slater electrostatic parameters in An^{3+} are typically only two-thirds as large as those of the Ln^{3+}, but ζ_{5f} is a factor of two larger than ζ_{4f}[1] so in comparison to the 4f case, the energy range of the $5f^N$-configurations is reduced, and the states are significantly more mixed in character because of the increased spin-orbit interaction.

In discussing Figure 9 it was pointed out that each free-ion state is split by crystal-field interactions into some number of components. Assigning energies corresponding to the centers of gravity of these components, thus defining the "free-ion" levels for the ion in a particular medium, yields the energy level scheme indicated at the left in Figure 9. While the levels are shifted to somewhat lower energies than those of the true gaseous free-ion states, the basic structure appears to be preserved and is usually only moderately changed from medium to medium for trivalent lanthanides and actinides. For example, the center of gravity of the $^4I_{11/2}$ state in $U^{3+}:LaCl_3$ in Figure 10 is ~4544 cm^{-1}. An isolated band in U^{3+}(aquo), Figure 2, near this same energy can be similarly identified. The "free-ion" states deduced for the 3+ actinides in $LaCl_3$ are shown in Figure 11 with the extent of the observed crystal-field splitting indicated where experimental measurements have been made.

While the spectra of several organometallic 3+ actinides (and lanthanides), such as plutonium tricyclopentadienide, have been measured, the analysis of data is still quite incomplete. Nevertheless, it seems apparent that the energy level parameters in this case, and indeed for most other matrices can at least be approximated by those characteristic of the actinides in the $LaCl_3$ host, Carnall (1979a).

3.5.1. Luminescence Spectra

Several excited states from which luminescence can be observed at low temperatures can be found in most crystal lattices into which the 3+ actinides have been doped. Prominent emitting states for $An^{3+}:LaCl_3$ are indicated in Figure 11 by pendant semi-circles. The crystal-field structures of the ground state and most of the excited states which occur in the far infrared range are usually defined via fluorescence measurements. For specific references see Table 5 and Hessler et al. (1978).

3.5.2. Actinide Lasers

Laser action from an actinide ion, U^{3+}, was reported in 1960, the same year that the first ruby (Cr^{3+} in Al_2O_3) laser was described. Stimulated emission from U^{3+}:CaF_2 at 4016 cm^{-1} could be detected even at 25°C, Sorokin and Stevenson (1960). The corresponding transition is indicated in Figure 9. Since that time, a huge literature describing different lasing ions and media has grown up. In the area of solid-state lasers, the rare earths are the dominant activators used; no further successful experiments with actinide ions have been reported. Nevertheless, the similarities in electronic structure of the 3+ lanthanides and actinides suggests that analogies to the demonstrated lasing properties of U^{3+} can probably be found.

The f→d transitions in the 3+ actinides occur at lower energies than in the lanthanides and the 6d appreciably overlaps the 5f configuration. In principle this should make it possible to pump the intense f→d band with the expectation of rapid non-radiative transfer of energy to the 5f-states. However the presence of strong absorption bands in the ultraviolet range, and in some cases low-lying charge transfer bands, increases the probability that intense excited-state absorption with non-radiative relaxation may occur. The net effect is the probable restriction of potential lasing transitions in the +3 actinides to the infrared region of the spectrum, Weber (1980).

3.6. Intensity Calculations for Trivalent Actinide Spectra in Solution

A systematic understanding of the energy level structure for An^{3+} serves as a foundation upon which to base the interpretation of other physical measurements. Considerable success has now been achieved in developing a parametrized model of f→f transition intensities.

The intensity of an absorption band can be defined as the area under the band envelope as normalized for concentration of the absorbing ion and the path length of light in the absorbing medium. A proportional quantity, oscillator strength P, has been tabulated for trivalent actinide ion absorption bands in aqueous solution. The experimentally determined oscillator strengths of transitions can in turn be related to the mechanisms by which light is absorbed, Condon and Shortley (1963);

$$P = \frac{8\pi^2 mc\sigma}{3he^2(2J+1)} \left[\chi \bar{F}^2 + n\bar{M}^2 \right] \qquad (10)$$

where $\bar{F}$ and $\bar{M}$ are respectively the electric-dipole and magnetic-dipole operators joining the initial state J to a final state J', $\chi = (n^2 + 2)^2/9n$ and n is the refractive index, σ is the energy of the transition (cm^{-1}), and the other symbols have their usual meaning.

Only a few transitions observed for the 3+ actinides have any significant magnetic-dipole character; however, the matrix elements of $\overline{M}^2$ can be evaluated directly from the knowledge of the eigenvectors of the initial (ψJ) and final ($\psi' J'$) states. The Judd-Ofelt theory, Judd (1962), Ofelt (1962), has successfully addressed the problem of computing the matrix elements of $\overline{F}^2$, and can be written in the form:

$$\overline{F}^2 = e^2 \sum_{k=2,4,6} \Omega_k \, (\psi J \| \underset{\sim}{U}^{(k)} \| \psi' J')^2 \qquad (11)$$

where $\underset{\sim}{U}^{(k)}$ is a unit tensor operator of rank k, the sum running over the three values k = 2,4,6 and Ω_k are three parameters which in practice are evaluated from measured band intensities. These parameters involve the radial parts of the f^N wave functions, the wave functions of perturbing configurations such as $5f^{N-1}6d$, and the interaction between the central ion and the immediate environment.

Judd was able to show both that the theory could successfully reproduce the observed intensities of bands throughout the optical range for Nd^{3+}(aquo) and Er^{3+}(aquo), and that intensity parameters, Ω_k, computed from first principles, were consistent with those derived in fitting experimental data, Judd (1962). A later systematic treatment of the intensities observed in the spectra of all Ln^{3+}(aquo) ions confirmed and extended the original correlation, Carnall *et al.* (1968), Carnall (1979b), Carnall *et al* (1983). Recently it was shown that a similar, systematic treatment of band intensities for An^{3+}(aquo) spectra could be successfully carried out with only Ω_4 and Ω_6 treated as variables, Table 7. The emphasis on aquo-ion spectra stems from the ability to identify many relatively isolated bands with single or very limited numbers of SLJ-states, the corresponding unambiguous quantitative nature of the oscillator strength calculation, and the wide range of data available; i.e. most members of the 4f- and 5f-series can be readily obtained as trivalent aquo ions in dilute acid solution. Intensity correlations for Ln^{3+} in a great many different host crystals, as well as in vapor complexes, have been developed. For the actinides, systematic and quantitative examination of transition intensities is presently restricted to An^{3+}(aquo) data.

Examination of Figures 2 and 11 shows that, particularly for U^{3+}, Np^{3+}, and Pu^{3+}, the density of states is high and few of the observed aquo-ion bands can be uniquely identified. Both the relative intensities of observed transitions and the density of states decreases in magnitude with increasing atomic number. Starting with Cm^{3+}(aquo), the heavy actinide aquo ion spectra, Figure 3, are all amenable to intensity analysis with excellent correlation found between observed oscillator strengths and intensities computed using the Judd parametrization, Carnall *et al.* (1985). While the oscillator strengths of An^{3+}(aquo) bands tend to be a factor of 10-100 greater than those observed for the lanthanides, one of the most striking

TABLE 7.

Intensity Parameters for An^{3+}(aquo) (in cm^2).[a]

	$\Omega_4 \times 10^{20}$	$\Omega_6 \times 10^{20}$	Number of transitions fit
U^{3+}	19 (13)	165 (37)	6
Np^{3+}	79 (60)	145 (47)	5
Pu^{3+}	12 (9)	67 (4)	6
Am^{3+}	7.6[b]	48[b]	
Cm^{3+}	17.9 (.6)	38.6 (2)	17
Bk^{3+}	18.8 (1)	18.3 (2)	14
Cf^{3+}	16.3 (1)	16.5 (1)	15
Es^{3+}	15.8[b]	18.5[b]	

[a]The value of Ω_2 was fixed at 1×10^{-20} cm^2 and only Ω_4 and Ω_6 were freely varied; errors indicated in parentheses. See Carnall *et al.* (1985).

[b]Estimated values.

features in Figures 2 and 3 is the change in intensity across the actinide series. With Bk^{3+}(aquo), Cf^{3+}(aquo), and Es^{3+}(aquo) there is an apparent transition to a heavy lanthanide-like character in the spectra with no bands being disproportionately intense, Carnall et al. (1984). Analysis reveals that the trends in the intensity parameter values over the series can be correlated with the extent to which higher-lying opposite-parity configurations like $f^{N-1}d$ are mixed into the f^N-configuration. There is much less mixing of $f^{N-1}d$ states into $5f^8$ (Bk^{3+}) than in $5f^3$ (U^{3+}) even though the proximity of the $f^{N-1}d$ to the f^N configuration is very similar in these two cases. An example of the type of correlation obtained between experiment and theory for An^{3+}(aquo) is given for Cm^{3+}(aquo) in Figure 13, Carnall and Rajnak (1975). The intensity parameters for the series are given in Table 7.

3.7. Fluorescence Lifetimes

One reason for the interest in computing intensity correlations in absorption is that once the parameters of the Judd-Ofelt theory are evaluated, they can in turn be used to compute the radiative lifetime of any excited state of interest via the Einstein expression

$$A(\psi J,\ \psi' J') = \frac{64\pi^2\sigma^3}{3h(2J+1)}\ (\chi'\overline{F}^2 + n^3\overline{M}^2) \qquad (12)$$

where $|\psi J\rangle$ and $|\psi' J'\rangle$ are the initial and final states, A is the rate of relaxation of ψJ by radiative processes, and $\overline{F}^2$ and $\overline{M}^2$ are the terms defined in Eqn. (10). The observed lifetime of a particular excited state, τ_T, is usually determined by non-radiative rather than radiative relaxation mechanisms. Thus we write

$$(\tau_T)^{-1} = A_T(\psi J) + W(\psi J) \qquad (13)$$

where $A_T(\psi J)$ is the total radiative relaxation rate from state $|\psi J\rangle$, that is, the sum of the rates of radiative decay to all states with energy less than that of $|\psi J\rangle$. If τ_R(calc) is the (computed) total radiative lifetime of $|\psi J\rangle$, then $\tau_R(\text{calc}) = [A(\psi J)]^{-1}$. Similarly, $W_T(\psi J)$ is a total rate summed over all non-radiative relaxation processes. The magnitude of the energy gap between a fluorescing state and the next lower energy state appears to play a major role in determining the non-radiative lifetime of that state; shorter lifetimes are correlated with narrower gaps.

On the basis of the existence of relatively large energy gaps in the spectra of some of the heavier actinides, Figure 11, experiments were initiated and fluorescence lifetimes were successfully measured in solution for excited states in Bk^{3+} and Es^{3+}, Beitz et al. (1981), as well as Cm^{3+}(aquo), Beitz and Hessler (1980). As indicated in Figure 14, which shows the lower

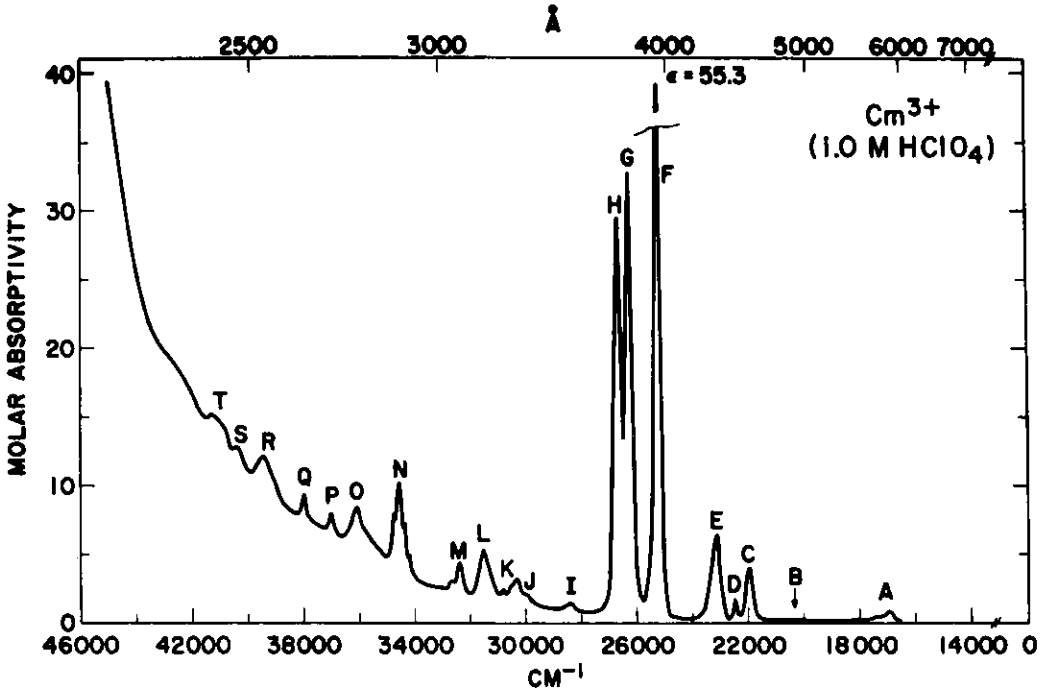

Band	2J	E(cm^{-1}) Center	Px10^6 Obs'd	Px10^6 Calc'd
A	7	17095	1.6	{2.0 E.D. 0.2 M.D.
B	5	20350	0.4	{0.6 E.D. 0.2 M.D.
C	7	21955	5.7	4.7
D	3	22435	0.7	0.01
E	9	23120	11	10
F	{17, 11}	25250	49	52
G	{9, 13}	26225	40	37
H	15	26630	35	34
I	7	28370	1.0	2.0
J	5	30030	1.1	1.1
K	{7, 5, 3}	30550	3.6	4.3
L	11	31500	8.2	9.5
M	{9, 3}	32500	3.2	5.3
N	13	34540	12	8.4
O	{17, 7, 11, 9, 13, 1}	35800	4.0	6.0
P	7	37010	1.2	0.3
Q	5	37995	2.0	0.6
R	{15, 3, 13, 5, 9}	39400	~10	5.1
S	{11, 7}	40300	~ 1.6	.44
T	{5, 9, 15, 11}	41100	~10	1.8

R.M.S. Deviation = 1.9 x 10^{-6}

Fig. 13. Absorption Spectrum and Intensity Analysis for Cm^{3+}(aquo), Carnall and Rajnak (1975). See Section 3.6.

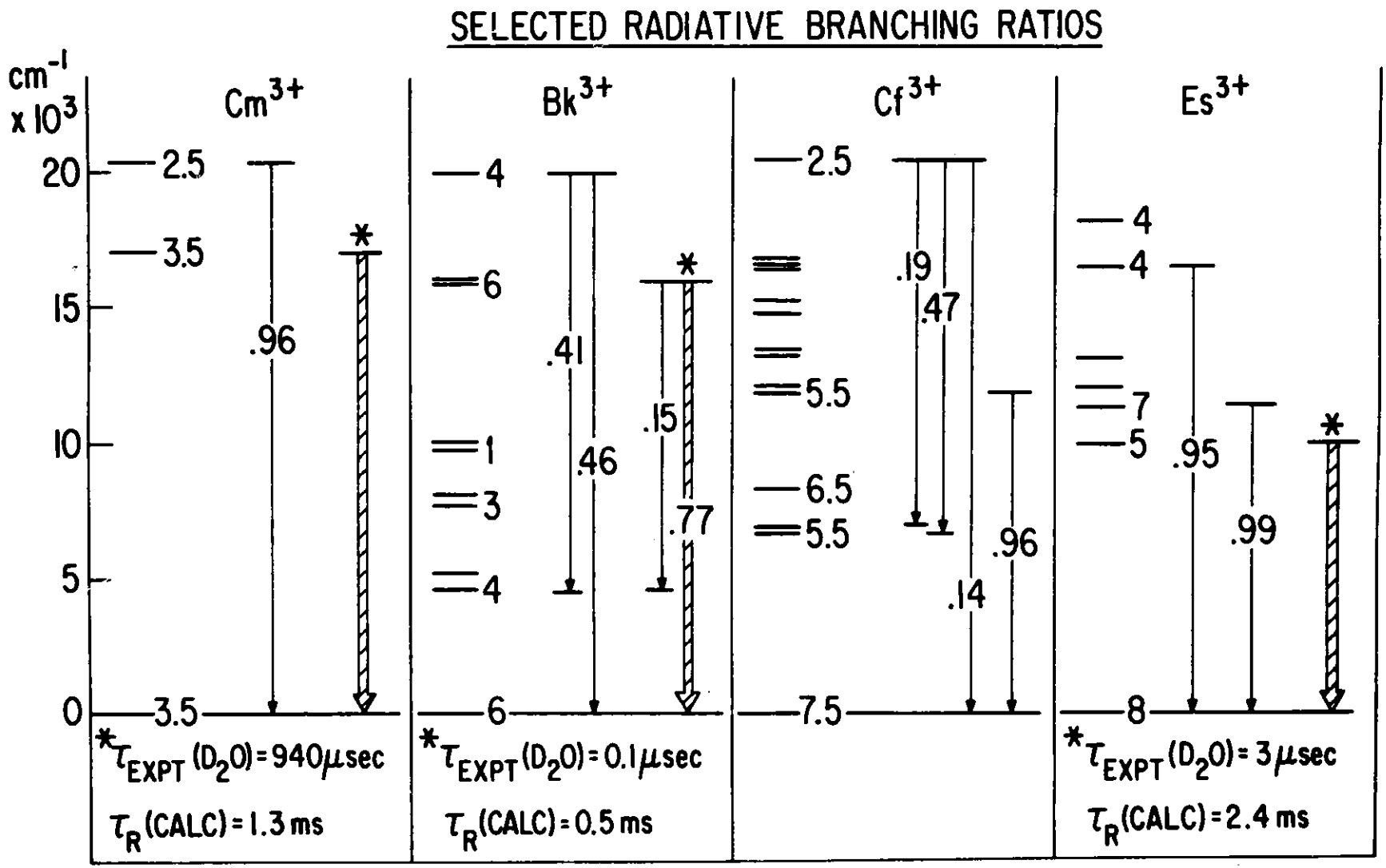

Fig. 14. Energy Level Schemes with Selected Branching Ratios for Radiative Relaxation of Cm^{3+}(aquo) Through Es^{3+}(aquo). J-values for f^N with N Odd Are Given in Decimal Form, thus, J = 5.5 Means J = 11/2.

energy-level structure for the heavier An^{3+}(aquo) ions, only in the case of Cm^{3+}(aquo) does the observed lifetime of 0.94 ms in D_2O compare well with the computed radiative lifetime, τ_R = 1.3 ms. With smaller energy gaps, the non-radiative relaxation rate clearly becomes rate determining. Inability to observe a fluorescing state for Cf^{3+}(aquo) in preliminary experiments suggests that lifetimes may be in the nanosecond time range, Beitz et al. (1981).

In addition to computing radiative lifetimes, it is instructive to establish the most probable pathway for fluorescence from a given state. The latter is clearly indicated by a comparison of branching ratios, where the branching ratio, β_R, from a given relaxing state to a particular final state is

$$\beta_R(\psi J, \psi' J') = \frac{A(\psi J, \psi' J')}{A_T(\psi J)} \qquad (14)$$

As indicated in Figure 14 for Cf^{3+}, β_R = .47 for emission from an excited (J=5/2) state to a lower-lying (J=11/2) state, while β_R = .14 for emission to the ground state. In the case of the J=5/2 state, it would be appropriate to monitor for fluorescence near 13000 cm^{-1} as well near 20000 cm^{-1}.

The identification of the mechanisms of non-radiative relaxation of actinide ions in solution as well as in solids, Hessler et al. (1980), remains an important area for further research. Extensive experimental results for lanthanide systems are available for comparison with those obtained for actinide ions. It should be possible to explore with considerable sensitivity the bonding differences between selected actinides and lanthanides by examining their excited-state relaxation behavior. For example see Beitz and Hessler (1980).

3.8. Interpretation of the Intensities of $f^N \rightarrow f^{N-1}d$ Transitions in Trivalent Actinide Aquo Ion Spectra.

In the preceding sections we have dealt mainly with transitions within the $4f^N$ and $5f^N$-configurations, and referred to the energies of the lowest-lying level in a given $f^{N-1}d$-configuration. In this section we extend our model calculations to gain some insight into the actual structure expected in the $f^{N-1}d$-configurations and compare these calculations to observations of aquo ion spectra. In some cases the energy of the lowest-lying $f^{N-1}d$ state in the aquo ion is not well established, and arguments based on the apparent effects of hydration on free-ion spectra of neighboring ions are examined. The availability of iso-f-electronic ion spectra such as that of Bk^{3+}(aquo) and Tb^{3+}(aquo) provides opportunities for comparison of the effects of the environment on the $f^{N-1}d$-configuration in two series as well

as the behavior of the excited $f^{N-1}d$-relative to the (ground) f^N-configuration for a given ion.

For present purposes we restrict attention to the f^N and $f^{N-1}d$-configurations, since, as indicated in Figure 15 for An^{3+} and Ln^{3+}, Brewer (1971b, 1983) the $f^{N-1}d$ is consistently the lowest-lying excited configuration of opposite parity to the ground f^N-configuration. For the light actinides, the energy of the ground electronic state in the $5f^{N-1}6d$-configuration is considerably lower than that of the corresponding $4f^{N-1}5d$. In addition, the curve shapes (AnIV and LnIV) are quite different in the first half of the the two series but similar at N>7.

3.8.1 Comparison of the Energies of Low-lying Free-Ion States of the $f^{N-1}d$-Configuration with Those Deduced for An^{3+}(aquo) and Ln^{3+}(aquo)

The absorption features observed in the spectra of Ce^{3+}, Bk^{3+} and Tb^{3+} aquo ions at > 30000 cm^{-1}, Figure 16, represent a particularly interesting contrast. In each case the spectroscopic features are effectively those of an excited d^1-configuration. Extensive analysis of the free-ion spectra of both Tb IV and Ce IV has been reported, Martin et al. (1978). Spin-orbit coupling in Ce IV gives rise to two free-ion states in the $4f^1$-configuration, $^2F_{5/2}$ (0 cm^{-1}) and $^2F_{7/2}$ (2253 cm^{-1}). We assume that the crystal-field splitting of the $4f^N$ free-ion states for any Ln^{3+} aquo ion is small with respect to the crystal-field splitting in the $4f^{N-1}5d$-configuration, and thus we neglect effects that might arise from populating excited crystal-field components in the ground state. We also neglect such effects for An^{3+} ($5f^N$) since the crystal-field splitting, while larger than for Ln^{3+}, is still relatively inconsequential for present purposes.

Transitions from the ground $4f^1(^2F_{5/2})$ state to excited $5d^1$ ($^2D_{3/2}$ and $^2D_{5/2}$) states in Ce IV occur at 49737 and 52226 cm^{-1}, respectively. The next higher-lying free-ion state ($^6S_{1/2}$) is at 86602 cm^{-1}. The structure we observe for Ce^{3+}(aquo) in the 32000-52000 cm^{-1} range (the UV-limit for observation of aquo ion spectra), must therefore be interpreted in terms of the states available to a single 5d-electron.

The absorption spectrum of Ce^{3+} doped into $La(C_2H_5SO_4)_3 \cdot 9H_2O$, where the symmetry is approximately D_{3h}, Okada *et al.* (1981), and that of Ce^{3+}(aquo) appear to be very similar in the 37000-52000 cm^{-1} range. While the broad weak band centered near 34000 cm^{-1} in Ce^{3+} (aquo), Figure 16, was not observed in absorption in the crystal, two bands observed in fluorescence at 77 K at 30000 and 32000 cm^{-1} could reasonably be assigned as transitions from a band origin at 32000 cm^{-1} to the two ^2F-states of $4f^1$ which are separated by ~ 2000 cm^{-1}. For Ce^{3+} in single crystal CaF_2, SrF_2 and BaF_2 an excited state near 32000 cm^{-1} has been reported by several authors including Kaplyanskii *et al.* (1963), Crozier (1965) and Loh (1967), as well as for Ce^{3+}:$LiYF_4$, Ehrlich *et al.* (1979). Extensive structure was noted by Loh who observed a relatively intense band in the 30000-40000 cm^{-1} range and at

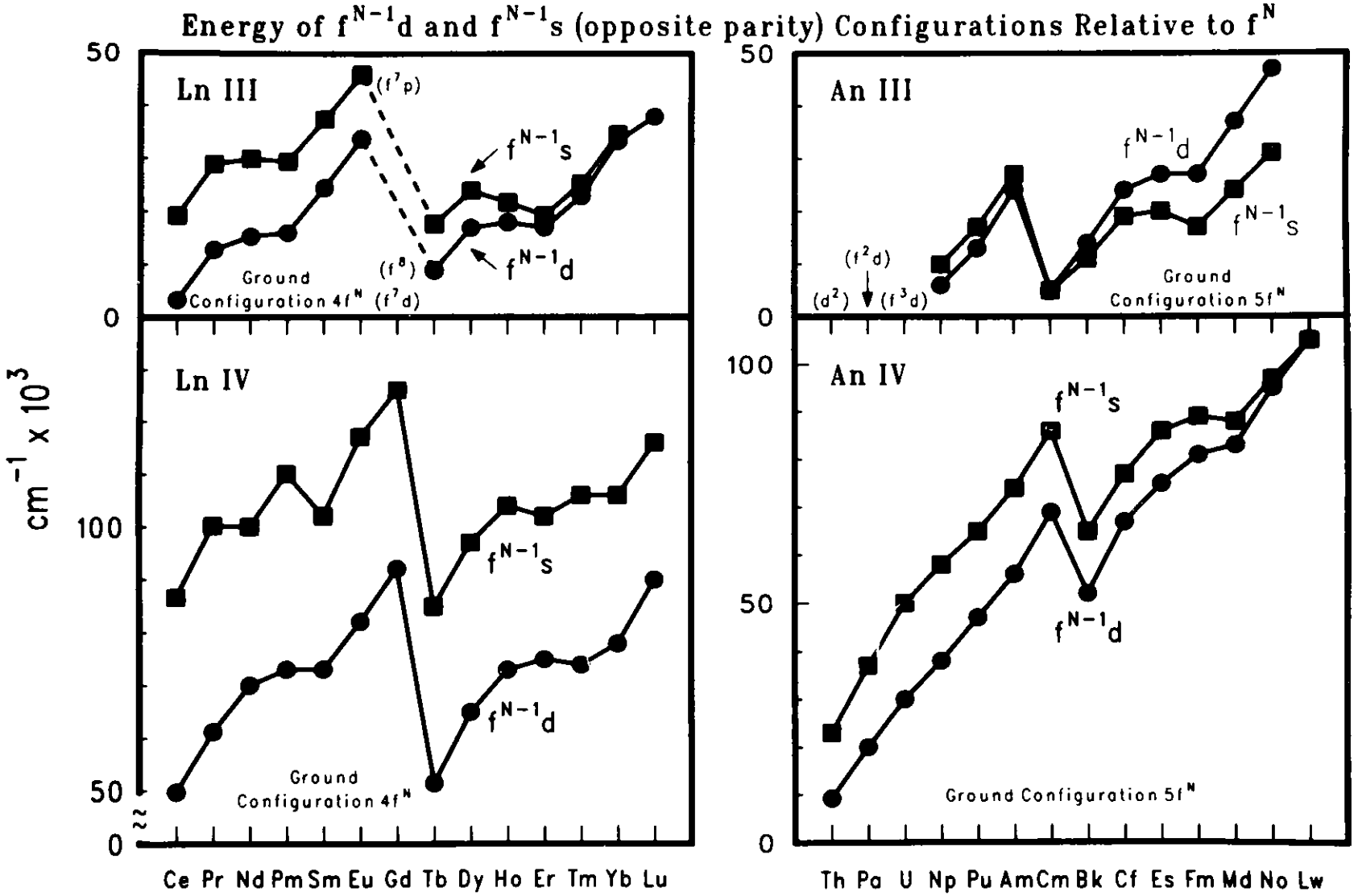

Fig. 15. Energies of Low-lying An IV and Ln IV Configurations Relative to the Ground State of the f^N-Configuration. Only the Energy of the Lowest Energy State is Indicated in Each Case, Brewer (1971b,1983).

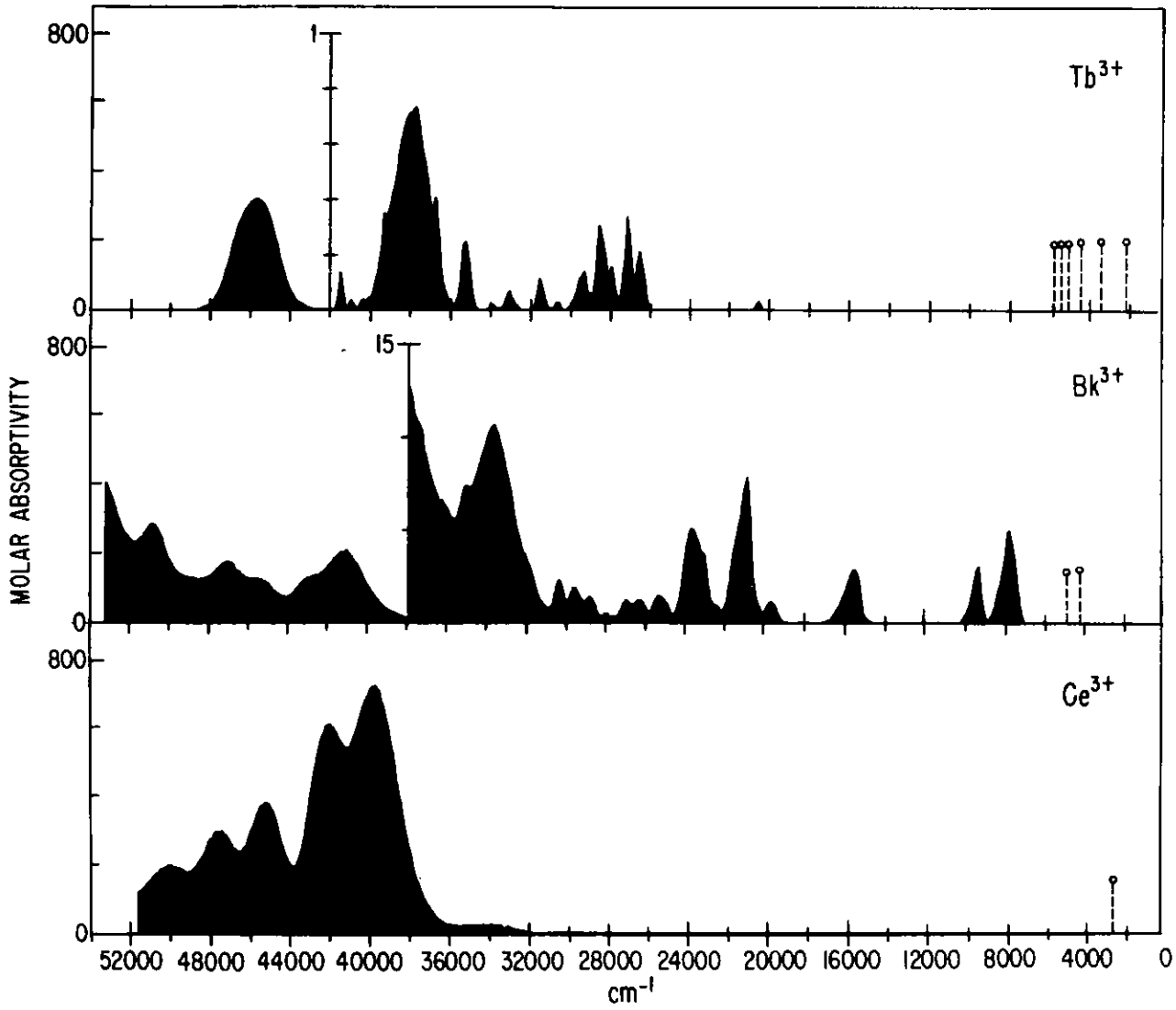

Fig. 16. Absorption Spectra of Tb^{3+}, Bk^{3+}, and Ce^{3+} Aquo Ions in the 0-52000 cm^{-1} Energy Range. Dashed Lines Indicate Computed Levels Lying Outside the Range of Observation.

least three bands or absorption features in the 40000-60000 cm^{-1} range in each matrix. He also found evidence for additional structure at higher dopings of Ce^{3+} attributed to cluster ion absorption that was distinct from the single isolated ion absorption, although as Schlesinger and Szczurek (1973) point out, such added structure may result from the existence of two or more different site symmetries.

An interesting example of the sensitivity of the 5d states in Ce^{3+} to medium effects is illustrated by the structure observed for Ce^{3+} doped into $Y_3Al_5O_{12}$ where the lowest energy f→d transition occurs near 22000 cm^{-1}, Weber (1973). It should be noted that the energies of the $4f^N$-states in Ce^{3+}: and Pr^{3+}: $Y_3Al_5O_{12}$ agree well with those in the ethyl sulfate crystal matrix, Okada et al. (1981), Dieke (1968). It is the energies of the d-states with respect to a relatively fixed f^N-electronic structure that vary markedly.

If we identify the lowest f → d band for Ce^{3+}(aquo) with the weak band centered near 34000 cm^{-1} comparable to the $Ce^{3+}:CaF_2$, $Ce^{3+}:LiYF_4$ and $Ce^{3+}:La(C_2H_5SO_4)_3 \cdot 9H_2O$ cases, then the energy difference between this state and that of the f → d transition in the free-ion is ΔE = 49737 - 34000 or ~16000 cm^{-1}.

If we adopt a spin-orbit parameter, ζ = 2/5 (52226-49737) = ~1000 cm^{-1}, consistent with the free-ion results, then it is necessary to assume a very large crystal-field to account for the ^2D-structure. Jørgensen has suggested that the 34000 cm^{-1} band may be due to the presence of more than one complex in solution, i.e. $Ce^{3+}(H_2O)_8$ as well as $Ce^{3+}(H_2O)_9$, Reisfeld and Jørgensen (1977), and this interpretation was accepted by Okada et al. (1981). However, the fact that there are apparently five absorption features in the Ce^{3+}(aquo) spectrum (37000-51000 cm^{-1}), Jørgensen and Brinen (1963), does not necessarily imply five corresponding zero-phonon origins.

Turning to Tb^{3+} ($4f^8$), the structure in the ultraviolet-visible range offers a considerable contrast to that observed for Ce^{3+} even though the promotion of an f to a d-electron gives the $4f^7$5d-configuration, which is treated as a single d-electron built onto the stable core ($4f^7$) of a half-filled shell. One interpretation would be that the accessibility of the f^{N-1}d-shell to bonding orbitals is quite different from that in Ce^{3+}. The $4f^N$-configuration in Tb^{3+} is assumed to be well shielded from the environment. One expects the same to be true of the excited fd-configuration, and this could be responsible for the apparent reduction in crystal-field splitting relative to the Ce^{3+} case.

An analysis of the free-ion structure in the $4f^7$5d-configuration of Tb IV has already been reported, Table 8, Carnall et al. (1984). We assume electric dipole selection rules J→J, J±1; $\Delta L = 0, \pm 1$. Transitions from the ground $^7F_6$ state of $4f^8$ to low-lying ^9D and ^7D-states must be considered. Transitions to a ^9D-state will be highly spin-forbidden, but if we assume a

TABLE 8

Free-ion Energy Levels for Ln IV[a,b]

Free-ion Energy Levels for Ce IV

Configuration	Term	J	Level (cm^{-1})
$4f^1$	^2F	5/2	0
		7/2	2253
	^2D	3/2	49737
		5/2	52226
	^2S	1/2	86602

Free-ion Energy Levels for Pr IV

Configuration	Term	J	Level (cm^{-1})[a]	Fit Energy (cm^{-1})[c]	Eigenvector
$4f^2$	^3H	4	0	0	$-0.986\ ^3H - 0.166\ ^1G$
		5	2152.09	2106.7	$1.0\ ^3H$
4f5d	^1G	4	61170.9	61171	$0.789\ ^1G + 0.549\ ^3H$
	^3F	2	61457.4	61459	$-0.830\ ^3F - 0.542\ ^1D$
	^3G	3	63355.9	63355	$-0.874\ ^3G - 0.417\ ^3F$
	^3H	4	63580.5	63577	$0.826\ ^3H - 0.481\ ^1G$
	^3F	3	64123.5	64121	$-0.904\ ^3F + 0.424\ ^3G$
	^3H	5	65239.3	65239	$0.999\ ^3H + 0.039\ ^3G$

Free-ion Energy Levels for Tb IV

Configuration	Term	J	Level (cm^{-1})[a]	Fit Energy (cm^{-1})[d]	Eigenvector
$4f^8$	^7F	6	0	0	$0.978\ ^7F - 0.145\ ^5G1$
		5	2051.6	2047.7	$0.985\ ^7F - 0.100\ ^5G1$
$4f^7(^8S)5d$	^9D	2	51404.0	51707	$0.980\ ^9D + 0.149\ ^7P$
		3	51800.8	52057	$-0.973\ ^9D + 0.144\ ^7D$
		4	52399.6	52585	$0.965\ ^9D - 0.184\ ^7D$
		5	53316.6	53389	$0.962\ ^9D - 0.201\ ^7D$
		6	54882.5	54737	$0.985\ ^9D + 0.173\ ^7F$
$4f^7(^8S)5d$	^7D	5	62680.6	62605	$-0.952\ ^7D - 0.215\ ^9D$
		4	63281.4	63188	$0.951\ ^7D + 0.199\ ^9D$
		3	63746.2	63631	$-0.957\ ^7D - 0.155\ ^9D$
		2	64081.4	63950	$0.964\ ^7D + 0.120\ ^5P$

TABLE 8 (cont'd.)

[a]Experimentally established free-ion levels, Martin et al. (1978). For Pr IV see Crosswhite et al. (1965), Sugar (1965a). Sugar's parameters for Pr IV were revised by Crosswhite and Crosswhite (1984a), but the interpretation of the lowest energy fd-states was not changed significantly.

[b]Spin-orbit coupling parameters are:

$$\zeta_{4f} = \frac{2253}{7/2} = 644 \text{ cm}^{-1}, \quad \zeta_{5d} = \frac{2489}{5/2} = 996 \text{ cm}^{-1}.$$

[c]The energies and eigenvectors fit to the levels of the $4f^2$-configuration are results for $Pr^{3+}:LaF_3$, Carnall et al. (1983); The parameters used in the fit to the 4f5d-configuration are from Crosswhite and Crosswhite (1984a): $\zeta_f = 853.2$, $\zeta_d = 1064.0$, $F^2(fd) = 22362$, $F^4(fd) = 18263$, $G^1(fd) = 10526$, $G^3(fd) = 12000$, $G^5(fd) = 8043$, all in cm^{-1}.

[d]The energies and eigenvectors quoted for $4f^8(^7F_{6,5})$ are results fit to $Tb^{3+}:LaF_3$. The parameters used in the fit to the $4f^7(^8S)5d$-configuration are given in Table 9.

small mixing-in of septet character, weak transitions from the ground $^7F_6$ to J=5 and 6 states at 53316 and 54882 cm^{-1} could result in observable bands. In this case we assume J=6 → J' = 2, 3, and 4 will exhibit lower transition probability. The J=2 state at 51404 cm^{-1} is the level recorded by Brewer (1983). A weak band attributed to an f → d transition is observed at 38000 cm^{-1}, Fig. 16. For comparison with the Ce^{3+} case this gives a host dependent energy separation, ΔE = 53300-38000 = 15300 cm^{-1}.

The lowest energy septet states in Tb IV are those of ^7D-character at 62680 cm^{-1} (Table 8), and a corresponding band in Tb^{3+} aquo centered near 46000 cm^{-1} gives ΔE = 62680-45000 = 16680 cm^{-1}. The spin-forbidden band at ~ 38000 cm^{-1} (^9D) exhibits apparent structure which can be quite accurately accounted for by assuming that $4f^8$-states are superimposed on a structureless Gaussian curve, Carnall et al. (1983). While f^8-states also overlap the more intense broad band at 46000 cm^{-1}, they are too weak to observe and the single absorption band exhibits no apparent structure, but spans approximately 4000 cm^{-1}. The intensity of the band in Tb^{3+} at 46000 cm^{-1} is actually much reduced compared to that of the ^2D states in Ce^{3+}, Figure 16, possibly suggesting lesser coupling of vibronic states to the more shielded D-states. Schlesinger et al. (1976) also report a single band in $Tb^{3+}:CaF_2$ centered near 46000 cm^{-1}.

In contrast to the above, the spectrum of Bk^{3+} in the ultraviolet range is more like that of Ce^{3+}, Figure 16. Two factors need to be considered. Our analysis of the Bk^{3+} spectrum, Carnall et al. (1984) suggested that more than one excited state in the $5f^7$6d-configuration may be accessible whereas this was not true for Tb^{3+}. There is also evidence for a much larger crystal-field interaction in Bk^{3+} than in Tb^{3+}, and a greater overlap between the f and d-configurations as reflected in the relatively more intense f → f transitions. We attribute the extensive structure at > 36000 cm^{-1} primarily to crystal-field splitting of $5f^7$6d states that are more exposed to the environment than are the $4f^7$5d-states of Tb^{3+}.

Along with Tb^{3+} and Ce^{3+}, Pr^{3+} is the only other Ln^{3+}(aquo) ion to exhibit an absorption feature attributable to f → d transitions. We observe a weak shoulder near 46500 cm^{-1}. The intensity here has some of the same character as for the $f^8 \rightarrow f^7d$ (^9D) transition in Bk^{3+} or the 34000 cm^{-1} band in Ce^{3+}(aquo) relative to that expected for allowed transitions. Jørgensen and Brinen (1963) reported a further maximum in Pr^{3+}(aquo) at 52910 cm^{-1} with $\varepsilon \sim 400$. The excitation spectrum of Pr^{3+}(aquo) very closely reproduces the absorption features in the 40000-50000 cm^{-1} range, Svetashev and Tsvirko (1981).

The free-ion analysis of Pr IV placed the lowest $4f^2 \rightarrow 4f5d$ state (nominal $^1G_4$) at 61170 cm^{-1}, Martin et al. (1978). The next accessible states are ~ 2000 cm^{-1} higher in energy. A transition from $4f^2$ ($^3H_4$) to 4f5d ($^1G_4$) would be formally spin forbidden, but as indicated in Table 8, there is also considerable triplet character in the latter state. The

energy difference, i.e. free-ion energy less that estimated for the lowest energy Pr^{3+}(aquo) band, 61200-46500 = ~ 15000 cm^{-1}, is of the order of the other ΔE values deduced here.

3.8.2 Theoretical Considerations in Computing the Structure of $\ell^N\ell'$-Configurations

As indicated in Wybourne (1965), the calculation of matrix elements for the electrostatic interaction in configurations of the type $\ell^N\ell'$, in this case f^Nd, proceeds in two steps: first, the calculation of matrix elements within the f^N-core, and then calculation of the matrix elements for the interaction with the added 5d electron. See also Crosswhite and Crosswhite (1984a).

In addition to the usual Slater-Condon F^K integrals encountered in treatment of the $4f^N$-configuration, we add the G^N- or exchange integrals where N = 1,3,5, and F^K(fd) (direct interaction) where K = 2,4, for the fd-configuration. Spin-orbit coupling parameters for both the f and d-configurations must be defined, Crosswhite (1971).

As in calculations involving the f^N-configuration, a systematic set of energy level parameters was developed and the energies calculated for lower-lying states of An IV ($f^{N-1}d$). Since there is very little free-ion data that has actually been interpreted to yield reliable values for the required parameters, extensive use was made of available Hartree-Fock results computed using an approximate relativistic correction (HFR), Section 3.2. As a reasonable approximation, we used the results for U V, Wyart et al. (1980) and Van Deurzen et al. (1984), as the basis for estimates for An IV. The parameter sets are given in Table 9.

3.8.3 Comparison of An^{3+}(aquo) Spectra with Model Calculations of the Structure in Low-Lying $5f^{N-1}6d$ States

In U^{3+}(aquo), Figure 2, we observe a broad very strong absorption at >23000 cm^{-1} which appears to reach a maximum and decrease such that much weaker transitions occur in the ~ 44000-50000 cm^{-1} range. A model energy level calculation for the lower energy region in the U IV (f^2d)-configuration adjusted to bring the computed lowest energy computed state to ~ 24000 cm^{-1} is given in Table 10. Spectra of U^{3+}:$LaCl_3$ in the 23000-50000 cm^{-1} range, Crosswhite et al. (1980), show absorption features at 77K similar to those observed for U^{3+}(aquo). The structure observed in this energy range in U^{3+}:$LaCl_3$ at 4 K is attributed to crystal-field splitting in the f^2d-configuration, but we assume that vibronic as well as electronic features are superimposed. We note from Figure 15 that the $f^{N-1}s$-configuration is nearly coincident in energy with the $f^{N-1}d$. Strong configuration mixing is expected so that the designations $f^{N-1}d$ or $f^{N-1}s$ are only formal and transitions (involving d-character) to both should be observed.

TABLE 9

Free-ion Parameters for $f^N d$-Configurations[a,b]

	U IV	Np IV	Pu IV	Am IV	Cm IV	Bk IV	Cf IV	Es IV	Tb IV
$F^2(ff)$	42900	46100	49100	52000	54800	57500	60200	62700	98500
$F^4(ff)$	39900	42000	44000	46000	47900	49700	51400	53200	68000
$F^6(ff)$	25600	27200	28700	30200	31600	32900	34200	35500	49500
ζ_f	1780	2070	2370	2690	3020	3370	3740	4120	1800
$F^2(fd)$	22552	22593	22605	22596	22565	22513	22447	22365	21000
$F^4(fd)$	23121	22945	22769	22596	22422	22246	22071	21896	11500
$G^1(fd)$	14627	13873	13207	12613	12085	11565	11160	10752	8500
$G^3(fd)$	14565	14119	13718	13353	13020	12709	12420	12149	9000
$G^5(fd)$	9929	9625	9348	9093	8859	8638	8430	8234	6000
ζ_d	2455	2629	2801	2972	3136	3300	3462	3622	1300

[a] All values in cm^{-1}. For U IV, N=2; For Np IV, N=3, etc.

[b] The $F^N(ff)$ parameters are those characteristic of An IV or Ln IV compounds; ζ_{5f} are obtained by reducing the HFR-values for An IV($5f^N6d$) by 280 cm^{-1}; the remaining parameters were obtained from the same HFR-results but corrections were based on experimental results for U V. Similar results for LnIV are discussed by Crosswhite and Crosswhite (1984a). The following parameters were also included in each individual calculation, all in cm^{-1}:

α = 23	T^2 = 250	T^6 = -300
β = 800	T^3 = 50	T^7 = 400
γ = 1200	T^4 = 100	T^8 = 350
P^2 = 500		

TABLE 10.

Free-ion Energy Levels for U IV[a,b,c]

	OBS. LEVEL	J	LS-TERM
f^3	0	9/2	>85% 4 I

$f^3 = f^2f$ -- parent states both ^3H and ^3F.

			EIGENVECTORS					
			LEADING COMPONENT			NEXT COMPONENT		
	CALC. LEVEL(cm^{-1})	J	CORE LEVEL	MAGNITUDE	LS STATE	CORE LEVEL	MAGNITUDE	LS STATE
f^2d	24050	11/2	(^3H)	0.864	^4K	(^3H)	-0.331	^2I
	25854	9/2	(^3H)	0.787	^4I	(^3H)	-0.548	^2H
	27868	7/2	(^3F)	-0.672	^4H	(^3H)	-0.502	^4H
	30192	11/2	(^3H)	-0.521	^2H	(^3H)	-0.404	^4I
	30330	9/2	(^3H)	0.553	^2H	(^3H)	-0.462	^4I
	31535	7/2	(^3F)	0.534	^4G	(^3H)	0.489	^4H
	31718	11/2	(^3H)	0.865	^4I	(^1G)	0.274	^2H
	32704	9/2	(^3F)	-0.718	^4H	(^3H)	-0.552	^4H
	35105	9/2	(^3F)	-0.544	^4G	(^3F)	-0.366	^4H
	36508	11/2	(^3H)	-0.483	^2H	(^3H)	0.396	^4G
	36304	7/2	(^3H)	0.404	^2F	(^3H)	-0.391	^2G
	36644	9/2	(^3H)	0.650	^4H	(^3F)	-0.493	^4H
	37823	9/2	(^3H)	-0.611	^4G	(^3F)	0.432	^4G
	37836	7/2	(^3H)	0.645	^4G	(^3F)	0.534	^4G
	38521	7/2	(^3F)	-0.631	^2F	(^3H)	-0.303	^4G
	38975	7/2	(^3F)	0.545	^4F	(^3H)	-0.422	^4F
	39265	11/2	(^3H)	0.635	^4H	(^3F)	-0.451	^4G
	40781	11/2	(^3F)	0.537	^4G	(^3F)	-0.521	^4H
	41012	9/2	(^3H)	-0.513	^4F	(^3F)	0.467	^4F

[a] adjusted to an energy consistent with the lowest-lying fd-band observed for U^{3+}(aquo).

[b] Parameters for the calculation given in Table 9.

[c] The L-S term for the f^3 ground state is taken from calculations for An^{3+}(aquo).

For U IV ($5f^3$) → $5f^2 6d$ the allowed states will include $5f^2(^3H, ^3F)$ + ^2D → $^{4,2}K$, I, H, G, F, D, P and the relevant transitions can be identified assuming electric dipole selection rules, J → J, J ± 1; ΔL = 0, ± 1. Thus, since the ground state in $5f^3$ has J = 9/2, the stronger transitions are assumed to be limited to J = 9/2 → 7/2, 9/2, 11/2. Numerous allowed transitions from the ground $5f^3$ ($^4I_{9/2}$) to $5f^2 6d$-states built on the $5f^2$-core, ^3H and ^3F are indicated in Table 10. However above 40000 cm^{-1}, the excited states increasingly exhibit appreciable doublet character. The much reduced absorption intensity actually observed is consistent with the increasingly spin-forbidden character of the transitions. No attempts have yet been made to analyze the crystal-field structure in the f^2d-configuration, although in appropriate host crystals a great deal of structure can be observed. As in the d-configuration in Ce^{3+}, we interpret the extensive structure over a large energy range as indicative of a strong interaction with the environment.

In Np^{3+}, Pu^{3+}, and Am^{3+} there is evidence for a progression of the $f^{N-1}d$-configuration to higher energies with respect to the ground state energy of the corresponding f^N-configuration. In Np^{3+}:$LaCl_3$, resolved structure in the fd-bands is observed, Carnall et al. (1980). There is also an apparent shoulder as the lowest-energy feature of the spectrum, Figure 2. In each case Np^{3+}, Pu^{3+}, Am^{3+}, the approximate energy level calculations for the $f^{N-1}d$ configuration do predict one or two lower-lying states separated by 4000-6000 cm^{-1} from a higher energy group that spans a very wide region of energy, Table 11. Except for Am^{3+}, the low-lying states are expected to exhibit normal intensities so the weaker shoulder may simply result from a lower population of levels. Any perceived structure is attributed to crystal-field splitting of states that are relatively exposed to the environment and thus expected to be sensitive to changes in bonding character, as observed in the 4d and 5d-transition elements. It is interesting to note that these 6d-states are the analogs of those expected in the ground configurations of elements beyond 104! In the case of Bk^{3+} ($5f^7 6d$), the next higher Z-element in which a 6d electron could occur in a ground configuration, (the analog of Re^{6+}) would be element 107. With the observed trends, we would not expect, nor do we observe, at <50000 cm^{-1} any structure in the spectrum of Cm^{3+} ($5f^7$) attributable to f → d transitions. Incidently, the value for ζ_d in Bk IV is similar to that for Re^{6+} ($6d^1$).

In Am^{3+} (aquo) there is an apparent marked decrease in the f → d transition intensity. This observation appears to be consistent with the special case posed by transitions originating in $5f^6$ ($^7F_0$). Allowed transitions can only occur to J=1 states of $5f^5 6d$ (^7F, ^7G). The computed free-ion energy level structure, Table 11, gives significant energy differences between the lowest-energy states in the $5f^5 6d$-configuration.

The Bk^{3+} ($5f^8$ → $5f^7 6d$) transitions, Table 12, were discussed earlier and compared to the results for Tb^{3+}. Beginning with the structure observed

TABLE 11.

Computed Levels and Eigenvector Components for Np IV, Pu IV, Am IV[a,b,c]

	OBS. LEVEL	J	LS - TERM					
Np IV(f^4)	0	4	>80%	^5I				
			EIGENVECTORS					
			LEADING COMPONENT			NEXT COMPONENT		
	CALC. LEVEL (cm^{-1})	J	CORE LEVEL	MAGNITUDE	LS STATE	CORE LEVEL	MAGNITUDE	LS STATE
f^3d	37438	5	(^4I)	.814	^5K	(^4I)	.393	^3I
	43639	4	(^4I)	.770	^5I	(^4I)	.476	^3H
	46010	5	(^4I)	-.484	^3I	(^4I)	.445	^5K
	46625	4	(^4I)	.499	^5H	(^4F)	.452	^5H
	47489	4	(^4I)	.375	^3G	(^4I)	-.366	^3H
	47935	3	(^4F)	-.630	^5H	(^4I)	.440	^5G
	48010	5	(^4I)	-.914	^5I	(^4I)	-.242	^3H
	48887	3	(^4I)	-.422	^5H	(^4F)	-.294	^3F
	49264	4	(^4G)	.789	^5I	(^4I)	.253	^3G

	OBS. LEVEL	J	LS - TERM					
Pu IV(f^5)	0	5/2	>65%	^6H				
			EIGENVECTORS					
			LEADING COMPONENT			NEXT COMPONENT		
	CALC. LEVEL (cm^{-1})	J	CORE LEVEL	MAGNITUDE	LS STATE	CORE LEVEL	MAGNITUDE	LS STATE
f^4d	40569	7/2	(^5I)	-.653	^6I	(^5I)	.499	^4H
	41453	5/2	(^5I)	-.534	^4G	(^5I)	-.352	^6G
	45585	7/2	(^5I)	.421	^4G	(^5I)	.365	^6G
	46236	3/2	(^5I)	.610	^6G	(^5F)	.543	^6G
	46342	7/2	(^5F)	-.491	^6H	(^5I)	.460	^6H

TABLE 11 (cont'd.)

Computed Levels and Eigenvector Components for Np IV, Pu IV, Am IV[a,b,c]

			EIGENVECTORS					
			LEADING COMPONENT			NEXT COMPONENT		
	CALC. LEVEL (cm^{-1})	J	CORE LEVEL	MAGNITUDE	LS STATE	CORE LEVEL	MAGNITUDE	LS STATE
	46429	5/2	(^{5}F)	-.561	^{6}H	(^{5}I)	-.383	^{6}H
	47657	5/2	(^{5}I)	.497	^{6}H	(^{5}I)	.299	^{4}G
	48045	7/2	(^{5}I)	.559	^{6}I	(^{5}I)	-.347	^{4}H
	49977	5/2	(^{5}F)	.402	^{6}H	(^{5}I)	.390	^{6}G

	OBS. LEVEL (cm^{-1})	J	LS - TERM	
Am IV(f^6)	0	0	>47%	^{7}F

			EIGENVECTORS					
			LEADING COMPONENT			NEXT COMPONENT		
	CALC. LEVEL (cm^{-1})	J	CORE LEVEL	MAGNITUDE	LS STATE	CORE LEVEL	MAGNITUDE	LS STATE
f^5d	44000	1	(^{6}H)	-.624	^{5}F	(^{6}H)	-.419	^{7}G
	46567	1	(^{6}F)	-.700	^{7}G	(^{4}F)	-.344	^{5}F
	47758	1	(^{6}H)	.502	^{7}G	(^{6}F)	-.420	^{7}G
	51248	1	(^{6}F)	.487	^{7}F	(^{6}H)	-.394	^{7}G

[a]Parameters for the calculation given in Table 9.

[b]The energy of the lowest f → d transition was adjusted to be consistent with that of the lowest-lying fd-band observed for An^{3+}(aquo).

[c]The LS term for the $5f^N$-ground states was taken from calculations for An^{3+}(aquo).

TABLE 12

Computed Levels and Eigenvector Components for Bk IV, Cf IV, Es IV[a,b]

	OBS. LEVEL	J	LS - TERM					
Bk IV(f^8)	0	6	>64%	^7F				
			EIGENVECTORS					
			LEADING COMPONENT			NEXT COMPONENT		
	CALC. LEVEL (cm^{-1})	J	CORE LEVEL	MAGNITUDE	LS STATE	CORE LEVEL	MAGNITUDE	LS STATE
f^7d	34000	5	(^8S)	-.779	^9D	(^8S)	.358	^7D
	38756	6	(^8S)	.882	^9D	(^6P)	.434	^7F
	46847	5	(^8S)	-.679	^7D	(^8S)	-.472	^9D
	53067	5	(^6I)	-.385	^7L	(^4H)	.332	^5K

	OBS. LEVEL	J	LS - TERM					
Cf IV(f^9)	0	15/2	>64%	^6H				
			EIGENVECTORS					
			LEADING COMPONENT			NEXT COMPONENT		
	CALC. LEVEL (cm^{-1})	J	CORE LEVEL	MAGNITUDE	LS STATE	CORE LEVEL	MAGNITUDE	LS STATE
f^8d	35000	13/2	(^7F)	.602	^8G	(^7F)	.444	^8F
	37561	15/2	(^7F)	.709	^8G	(^5G)	-.358	^6H
	44700	13/2	(^7F)	.569	^8H	(^7F)	-.483	^8F
	45828	15/2	(^7F)	.520	^8G	(^7F)	.515	^6H
	45909	17/2	(^7F)	-.850	^8H	(^5G)	.449	^6I
	48032	13/2	(^7F)	.566	^8F	(^7F)	.408	^8H

TABLE 12 (cont'd.)

	OBS. LEVEL	J	LS - TERM	
Es IV(f^{10})	0	8	>74%	^5I

			EIGENVECTORS					
			LEADING COMPONENT			NEXT COMPONENT		
	CALC. LEVEL (cm^{-1})	J	CORE LEVEL	MAGNITUDE	LS STATE	CORE LEVEL	MAGNITUDE	LS STATE
f^9d	57000	8	(^6H)	-.650	^7H	(^6H)	-.395	^7H
	57425	7	(^6H)	.551	^7H	(^6H)	.456	^7G
	61104	9	(^6H)	.574	^7I	(^6H)	-.445	^5K
	67722	8	(^6H)	-.535	^7H	(^6H)	.344	^7I
	67998	7	(^6H)	.587	^7I	(^6H)	-.416	^7G
	68557	9	(^6H)	.609	^7I	(^6H)	.509	^5K

[a]Parameters for the calculation are given in Table 9.

[b]The energy of the lowest f → d transition was adjusted to be consistent with that of the lowest observed fd-band in An^{3+}(aquo).

[c]The L-S term for the $5f^N$-ground states was taken from calculations for An^{3+}(aquo).

in the $5f^{N-1}6d$-configuration in Bk^{3+}, all the heavy 3+ actinides will have low-lying states of both the same spin as the ground state and one spin unit larger, i.e. for Bk^{3+}:$5f^8$ (^7F) → $5f^7 6d$ (^9D, ^7D). The formally spin-forbidden ^7F → ^9D-transition in Bk^{3+} (aquo) is clearly identified even though it is very weak. It is apparently not resolved in Cf^{3+} (aquo).

At least partial structure attributable to the ($5f^8 6d$) states is observed in Cf^{3+}, but assignments based on the observed spectrum alone would be difficult to justify. In his tabulation of energy levels, Brewer (1971b) cites the energies of the lowest spin-forbidden states in the heavy half of both the 4f and 5f series for the lowest f^N → $f^{N-1}d$ transitions. For Bk IV, this would give ΔE = 52000-34000 = 18000 cm^{-1}. If we use this latter value together with Brewer's tabulated f^8d-state energy for Cf IV we obtain $E(^8G_{15/2})$ $-\Delta E$ = 64000-18000 = 46000 cm^{-1}. Referring to Figure 3 we observe a broad feature in the spectrum of Cf^{3+} (aquo) near this energy. The computed level scheme for Cf^{3+} in Table 12 was correspondingly adjusted to place levels expected to show some intensity in the 46000 cm^{-1} region. This locates a (relatively weak) transition to a J = 15/2 state near 37561 cm^{-1}, but suggests that much of the observed intensity increase in the ultraviolet range is probably due to radiation induced solvent decomposition.

The absorption spectrum of Es^{3+} (aquo) is strongly perturbed by the rapid generation of H_2O_2 due to solvent decomposition in the presence of the intensely radioactive ^{253}Es isotope. It is, therefore, unclear from the observed spectrum where f → d transitions might occur. As an estimate, we use the result ΔE = ~18000 cm^{-1} and locate the lowest energy spin-forbidden transition at 75000-18000 = 57000 cm^{-1} using Brewer's estimate. This places f → d bands outside of the energy range accessible with aqueous solutions, Table 12, and indicates that all observed general absorption in the ultraviolet range for Es^{3+} (aquo), Figure 3, can quite reasonably be ascribed to solvent radiation decomposition products.

The experimentally observed transition intensities for the f → d transitions in Bk^{3+} indicate that the lowest energy spin-allowed f → d transitions may be a factor of ten less intense than similar transitions in the light part of the series. This suggests qualitatively the same overall intensity trend as exhibited by transitions in the $5f^N$-configuration, where a very significant decrease in average transition intensity was apparent from U^{3+} through Bk^{3+}, Carnall *et al.* (1985).

4.0. Correlation of Energy-Level Structures in Free-Ion and Condensed-Phase Spectra of f-Elements

A full quantum-mechanical description of the electronic states for actinide ions in condensed-phase environments would include a detailed treatment of the surrounding ions as well. However, because the f-shell orbitals are relatively well shielded, a great deal of progress has been made by taking the point of view of an isolated (free) ion perturbed by

complex surroundings. In adopting a group-theoretical framework, the general aspects of the problem are formulated without regard to specific details.

In order to progress beyond a comparison of parameters for actinide ions in various hosts, we describe here some preliminary attempts to compare them directly with the unperturbed-ion situation. This will provide a basis for understanding the physical processes brought into play when the ions are introduced into the crystalline medium, and appropriately follows the discussion of modeling trivalent ion spectra because many of the comparisons involve the 3+ valence state. In spite of the fact that these tentative results are very fragmentary, they are suggestive enough to warrant description in some detail.

As was pointed out earlier, because of the different techniques used in studying condensed-phase and free-ion spectra, few configurations are available for direct comparison of the two cases. When crystals or solutions are cooled to near 4K so that only the lowest (ground) electronic state is populated, the resultant absorption spectrum is directly interpretable in terms of energy levels. Except for complications of superimposed vibronic bands and the added perturbations of crystal-field effects themselves, the analysis can proceed directly to the study of atomic parameter variations. In free-ion emission studies, on the other hand, many overlapping transition arrays between the multiple configurations indicated in Figure 1 are obtained simultaneously, and one must first disentangle these. This can only be done with the aid of additional tags on the energy levels such as isotope-shift, hyperfine-structure or Lande g-factor information, which requires in fact that multiple experiments be carried out. Of the many configurational analyses that finally result, most are too heavily involved with s, p and d orbitals for easy comparison with the f-shell cases with which we are concerned here. Nevertheless, with some assistance from theory, cases are available from which a beginning can be made to construct a useful interpretative and predictive model.

We consider first the analogous lanthanide situation, Martin et al. (1978). Except for the uncertain assignment of the ^1S state, all $4f^2$ atomic states are known for the free-ion Pr IV, Sugar (1965a), Crosswhite, et al. (1965), Table 13. The ^1S state and most of the multiplet levels have also been identified in the $LaCl_3$-host Pr^{3+} case, Rana and Kaseta (1983), Rana et al. (1984) as well as in LaF_3, Carnall, et al. (1969), Yen et al. (1981), Cordero-Montalvo and Bloembergen (1984). The corresponding parametric results are given in Table 14. This is the only example yet available for either the lanthanides or actinides for which this direct comparison can be made. For this reason we examine this case in considerable detail beginning with a reappraisal of the ^1S assignment in Pr IV.

The $^1S_0$ level value originally reported by Crosswhite et al. (1965) was subsequently questioned on theoretical grounds, Morrison and Rajnak (1971). Because of the importance of having the complete configuration for

TABLE 13.

Free-ion Energy Levels and Parameters for Pr IV ($4f^2$)[a]

Largest[b] Eigen.	Component	Next Largest[b] Eigen.	Component	Observed Energy (cm^{-1})	Fit Energy (cm^{-1})	Calc G Value
0.985	$^3H_4$	0.167	$^1G_4$	0.0	1	0.8056
1.0	$^3H_5$	—		2152.09	2150	1.0334
0.999	$^3H_6$	-0.054	$^1I_6$	4389.09	4389	1.1665
0.988	$^3F_2$	0.151	$^1D_2$	4996.61	4998	0.6736
1.0	$^3F_3$	--		6415.24	6414	1.0835
0.806	$^3F_4$	-0.579	$^1G_4$	6854.75	6853	1.1597
0.798	$^1G_4$	0.591	$^3F_4$	9921.75	9922	1.0848
-0.946	$^1D_2$	0.288	$^3P_2$	17334.39	17334	1.0342
0.996	$^3P_0$	0.092	$^1S_0$	21389.81	21401	0
1.0	$^3P_1$	—		22007.46	21989	1.5012
0.999	$^1I_6$	0.054	$^3H_6$	22211.54	22211	1.0005
-0.958	$^3P_2$	-0.287	$^1D_2$	23160.61	23169	1.4592
0.996	$^1S_0$	-0.092	$^3P_0$	50090.29	50090	0

Parameters (cm^{-1})[c]

E_{ave}	10223	α	23.960 (0.5)	M^0	1.937 (.6)
F^2	72549 (49)	β	-604.48 (28)	M^2	1.08
F^4	53718 (137)	γ	727.82 (25)	M^4	0.74
F^6	36057 (55)	P^2	123 (86)		
ζ_{4f}	766.96 (4)	P^4	92	σ	14
		P^6	62		

a. Experimental data from Crosswhite et al. (1965), Sugar (1965a).

b. The largest and next largest eigenvector components are given with their phases.

c. Parameter errors are shown in parentheses; P^2 was freely varied but P^4 and P^6 were constrained by the relations $P^4 = 0.75\ P^2$ and $P^6 = 0.5\ P^2$; similarly M^0 was varied but M^2 and M^4 were constrained: $M^2 = .56\ M^0$ and $M^4 = .38\ M^0$.

TABLE 14.

Comparison of Free-ion Pr IV Energy Levels and Parameters with those for Pr^{3+} in LaF_3 and $LaCl_3$ Hosts[a] (units of cm^{-1})

	Theoretical				Experimental		
a. Parameters	HF		Many-Body		Free Ion[b]	LaF_3	$LaCl_3$
E_{ave}	13496		11505		10223	10163	9931
F^2	104089		82270		72549	69305	68441
F^4	65507		52434		53718	50675	50192
F^6	47192		23874		36057	32813	32974
α	0		27.94		23.9	[21][c]	22.8
β	0		-616		-604	-842	-679
γ	0		1612		728	1625	1453
b. Levels		O-C[d]		O-C			
$^3H_5$	2275	-123	2311	-159	2152	2303	2137-2283
$^3F_3$	8551	-2136	7587	-1172	6415	6568	6283-6357
$^1G_4$	8553	1368	10586	-665	9921	10001	9592-9926
$^1D_2$	24647	-7313	18716	-1382	17334	17047	16630-16780
$^3P_1$	31581	-9574	27074	-5067	22007	21514	21066-21096
$^1I_6$	29548	-7337	24859	-2648	22211	21743	21298-21521
$^1S_0$	68282	-18192	49907	183	50090	46986	46450

[a]Crosswhite (1977)
[b]Table 13
[c]Parameter not varied.
[d]Observed-calculated.

comparison with the Pr^{3+} crystal levels recently been reported for $LaCl_3$, Rana, et al. as well as for LaF_3, Carnall, et al. (1969), Yen et al. (1981, Cordero-Montalvo and Bloembergen (1984), it is worth while looking at this question in more detail.

The two-body electrostatic operator $G_2(R_7)$ is parametrized by γ in the notation used here (Section 3.3, Eq. 8). Matrix elements are such that this parameter and the ^1S position are closely associated with each other, the parametric values being 1453 and 1625 cm^{-1} for $LaCl_3$ and LaF_3 respectively. Superficially, one could say from this that γ should be somewhat higher for the free ion.

Morrison and Rajnak (1971) used many-body theory to calculate corrections to the atomic electrostatic parameters derived from a single-configuration Hartree-Fock procedure. Results for the uncorrected and corrected radial integrals respectively are given in columns 2 and 4 of Table 14(a). The correction calculations of column 3 also include parameter values for the two-body effective electrostatic operators α β, and γ discussed in Section 3.3. Experimental determinations are given in column 6 for the case in which the ^1S value of 50090 cm^{-1} is assumed to be correct. To judge from the experimental F^2 values, which dominate the Hamiltonian and determine the overall scale of the energy-level spread, the scale reductions for the LaF_3 and $LaCl_3$ cases are roughly in a ratio 4/5. One might then expect the other parameters to follow this same trend. Some do, and others show scatter, but the free-ion value for γ of 723 cm^{-1} would seem to be far out of line compared to the relative consistency of γ and β in the three cases. The many-body calculation, on the other hand, gives a value for γ of 1612 cm^{-1}. It was from this result that Morrison and Rajnak concluded that the 50090 cm^{-1} value must be spurious.

It must be remembered, however, that the Hamiltonian operators defined in this way do not form an orthogonal set, Judd and Crosswhite (1984); values for γ in particular will depend on results for the F^k, which show some large discrepancies. Rather than discussing the parameters in this form, let us examine the energy levels themselves, as given in Table 14(b) for the same five conditions. For convenience in consideration of these electrostatic interactions we have only used the middle levels of the triplet terms, since they are each close to their corresponding multiplet centers. For the "theory" diagonalizations, a Hartree-Fock value of 820 cm^{-1} has been assumed for the spin-orbit interaction and the position of the configuration center has been adjusted such that the ground $^3H_4$ state has the value 0 cm^{-1}. The scale of the level diagram corresponding to the original HF calculation is far too large. The many-body calculations correct this in large measure, predicting a ^1S position of 49907 cm^{-1}, but with an uncertainty, as judged by the scatter of other levels, of some 2000 cm^{-1}. The high position of the postulated 50090 cm^{-1} level would seem to be in acceptable agreement with this and, particularly, with the assump-

tion of a 4/5 ratio in the $LaF_3/LaCl_3$ shielding effects. On the other hand, the residual errors of the many-body calculation (column 5 of Table 14(b)) show a pronounced energy dependence, reminescent of the proposal by Wilson and Fred (1969), which would favor an even lower theoretical value. A more accurate theoretical calculation is needed to clarify this question.

Two other points can be made in favor of the 50090 cm^{-1} value for the free-ion ^1S state. (1) In the Hamiltonian which was used for the diagonalization, operators for both the spin-other-orbit and spin-spin relativistic corrections were included. These in theory should be parametrized by the same Marvin integrals M^k, Marvin (1947). In the present case, they were varied independently, but the experimentally-determined values were within the estimated error of each other, bracketing the Hartree-Fock-calculated value. On the other hand, if the 50090 cm^{-1} value was removed and γ fixed at the theoretical value of 1612 cm^{-1}, the spin-spin parameters dropped to about 60% of their theoretical value. (2) The $^1S_0$ level of the actinide U V $5f^2$ has been reported by Van Deurzen et al. (1984) on similar evidence (three weak lines). The value for γ reported for this case was 744 cm^{-1}.

For the more detailed comparisons of free-ion/crystal parameters which we will now make, we will carry out two parallel calculations, with and without this determination of the ^1S position.

In columns 2 and 3 of Table 15 are given the parameters found by a least-squares fit for the two cases: (1) no $^1S_0$ assumed but γ fixed at 1612 cm^{-1}, and (2) a $^1S_0$ value of 50090 cm^{-1} assumed but γ varied freely. Along with a variable configuration average, eleven parameters (column 1) in all were used to fit the thirteen levels in the second case, and one less of each in the first, with a mean error in each case of less than two cm^{-1}. The two sets of Marvin M^k parameters were varied independently, with $M^2/M^0 = 0.56$ and $M^4/M^0 = 0.38$ in each case. The p^k were varied as a single parameter in the customary ratios $P^4/P^2 = 0.75$ and $P^6/P^2 = 0.50$. Experimental parameters for the $LaCl_3$-host case are given in column 4. (No spin-spin operator was used here because of the somewhat larger mean error, 8 cm^{-1}.) The shifts of these parameters derived from the crystal environment from each of the free-ion sets are given in the respective columns 5 and 6, in cm^{-1}, and in columns 7 and 8 as a percentage change from the free-ion values. Two points should be noted: (1) the shifts derived for α and β do not depend greatly on the value used for γ, and (2) the results for the F^k do, the shifts found for the second case being much more consistent with those found in the actinide spectra discussed below. From the foregoing we conclude that the theoretical grounds for previously rejecting the 50090 cm^{-1} value for the $^1S_0$ level are not as strong as first believed.

In passing, it is worth noting that this discussion might well have been less convoluted had the recently-proposed orthogonal operators, Judd and Crosswhite (1984), been used in the analysis instead of the conventional ones.

TABLE 15.

Parameter Shifts for Pr^{3+} Ions in $LaCl_3$[a]

	Free Ion (in cm^{-1})		$LaCl_3$	Medium Shift (cm^{-1})		Medium Shift (%)	
	no $^1S_0$	with $^1S_0$	(in cm^{-1})	no $^1S_0$	with $^1S_0$	no $^1S_0$	with $^1S_0$
F^2	71585	72549	68441	-3144	-4108	-4.39	-5.65
F^4	51268	53717	50192	-1076	-3525	-2.10	-6.67
F^6	33199	36057	32974	-225	-3083	-0.68	-8.55
α	23.90	23.96	22.83	-1.07	-1.13	-4.5	-4.5
β	-592	-604	-679	-87	+75	+15	+14
γ	[1612][b]	728	1453	---	+725	---	+101
ζ	764.2	766.9	749	-15	-18	-2.0	-2.0
$M^0(SOO)$	1.91	1.84	1.7	0	0	0	0
$M^0(SS)$	1.23	2.11	---	0	0	0	0
P^2	225	123	238	0	0	0	0

[a]Crosswhite (1977).

[b]Not varied.

Returning to the comparison of free ion and crystal matrix results for this unique $4f^2$ case, an examination of the parametric results in Table 15 reveals significant differences for the major parameters F^k and zeta, and lesser ones for α and β. Here we refer to the columns showing shifts with assignment of $^1S_0$ in Pr IV. Any possible differences in the M^k and P^k values are masked by the statistical uncertainties. The parameter shifts attributed to the Pr^{3+} environment are given in column 6 and the relative change of the crystal values, compared to those of the free ion, in column 8. The most striking change seems to be for beta, which shows an increase in magnitude of some 10-15%. However, until this result is confirmed by comparison of more complex cases (such as nf^3), it must be regarded as possibly spurious.

The $5f^2$ free-ion configurations are completely known for both Th III, deBruin et al. (1941), and U V, Wyart et al. (1980), Van Deurzen, et al. (1984), but the Th^{2+} condensed-phase analogue is not known, and analyzed data for U^{4+} are limited in scope. The $4f^3$ Pr III configuration is nearly completely known, Table 16, Sugar (1963), Crosswhite et al. (1968), but there is no corresponding divalent crystal case for comparison. On the other hand, both the Nd^{3+}:$LaCl_3$, Crosswhite, et al. (1976), and U^{3+}:$LaCl_3$, Crosswhite, et al. (1980) spectra are very well documented, but analysis for the experimental spectra of Nd IV and U IV, Crosswhite and Crosswhite (1984d) are both incomplete. In fact, except for thorium, there are no doubly- or triply-ionized actinide free-ion analyses known.

Although we lack the appropriate free-ion data for direct comparison, it nevertheless appears plausible that an indirect approach could be tried to approximate the higher valent free-ion cases by making use of Hartree-Fock estimates of adjustments to available lower-ionization analyses. Three cases from first and second spectra of the actinides are known which yield atomic parameters which are well enough defined that serious study seems indicated: uranium, plutonium and californium, all derived from emission experiments using microwave-excited discharge tubes containing microgram quantities of specific isotopes. Instances in which the free ion contains an additional $7s^2$ shell relative to the condensed-phase example form the simplest case. A direct comparison of the spectra can in fact be made. The shifts due to the crystalline environment and those due to the addition of the $7s^2$ shell are found to be nearly the same. Thus for initial identifications, the crystal absorption lines can be directly related to the free-ion energy levels themselves, at least in those cases for which the crystal field can be treated in the weak-field approximation. For more complex cases a more elaborate comparison of the appropriate atomic parameters is necessary.

TABLE 16.
Free-ion Energy Levels and Parameters for Pr III ($4f^3$)[a]

Largest[b] Eigen.	Component	obs. (cm^{-1})	calc. (cm^{-1})	Δ	Largest[b] Eigen.	Component	obs. (cm^{-1})	calc. (cm^{-1})	Δ
0.986	$^4I_{9/2}$	0.0	-2.6	2.6	0.989	$^2D1_{5/2}$	19046.09	19025	21
0.995	$^4I_{11/2}$	1398.34	1392	7	0.721	$^2P_{3/2}$	20856.86	20876	-19
0.998	$^4I_{13/2}$	2893.14	2888	5	0.905	$^4D_{3/2}$	23091.70	23098	-6
0.995	$^4I_{15/2}$	4453.76	4456	-3	0.887	$^4D_{5/2}$	23245.99	23234	12
0.973	$^4F_{3/2}$	9370.66	9369	1	0.975	$^4D_{1/2}$	23465.43	23510	-45
-0.771	$^2H2_{9/2}$	10032.92	10038	-5	-0.918	$^2I_{11/2}$	24357.98	24381	-23
0.989	$^4F_{5/2}$	10138.18	10138	0.5	0.992	$^4D_{7/2}$	24886.51	24852	35
-0.965	$^4F_{7/2}$	10859.06	10859	0	0.984	$^2L_{15/2}$	25244.61	25255	-11
0.975	$^4S_{3/2}$	10950.24	10948	2	-0.996	$^2I_{13/2}$	25391.75	25391	0
-0.884	$^4F_{9/2}$	11761.69	11763	-1	1.0	$^2L_{17/2}$	26477.88	26415	33
0.903	$^2H2_{9/2}$	12494.63	12513	-18	0.894	$^2D2_{3/2}$	26921.49	26910	11
0.638	$^2G1_{7/2}$	13887.60	13876	12	0.934	$^2H1_{9/2}$	27178.80	27147	32
-0.993	$^4G_{5/2}$	14187.35	14194	-6	-0.766	$^2D2_{5/2}$	27597.13	27626	-29
0.869	$^4G_{7/2}$	15443.48	15445	-2	-0.833	$^2H1_{11/2}$	28101.77	28146	-44
-0.732	$^4G_{9/2}$	15705.13	15708	-2	-0.648	$^2F2_{5/2}$	-	30610	-
0.994	$^2K_{13/2}$	16089.14	16106	-17	0.780	$^2F2_{7/2}$	31787.93	31768	20
-0.666	$^4G_{9/2}$	16763.98	16767	-3	0.763	$^2G2_{9/2}$	39225.60	39208	18
0.699	$^2D1_{3/2}$	17095.63	17100	-4	0.765	$^2G2_{7/2}$	39940.72	39947	-6
0.972	$^4G_{11/2}$	17409.58	17407	2	0.786	$^2F1_{7/2}$	53092.80	53130	-37
-0.979	$^2K_{15/2}$	17642.06	17631	11	0.746	$^2F1_{5/2}$	54184.37	54153	31
0.975	$^2P_{1/2}$	18693.65	18666	27					

Parameters (cm^{-1})[c]

E_{ave}	19717	T^2	451 (13)	M^0	1.458 (0.4)
F^2	59946 (40)	T^3	33.8 (7)	M^2	0.816
F^4	39977 (159)	T^4	81.2 (10)	M^4	0.554
F^6	26454 (101)	T^6	-222 (15)	P^2	172 (58)
ζ_{5f}	665.05 (3)	T^7	309 (23)	P^4	129
α	30.686 (.36)	T^8	258 (27)	P^6	86
β	-814.04 (22)				
γ	2208 (27)	σ = 24			

a. Experimental data from Sugar (1963).

b. The largest eigenvector component is given with its phase.

c. Parameter errors are shown in parentheses; M^0 was freely varied, but M^2 and M^4 were constrained by the relations $M^2 = 0.56\ M^0$, $M^4 = 0.38\ M^0$; P^2 was freely varied, but P^4 and P^6 were constrained by the relations $P^4 = 0.75\ P^2$, $P^6 = 0.5\ P^2$. The mean error is given by σ.

4.1. Uranium

By far the most favorable case for these studies is uranium, both from the point of view of the additional extensive body of experimental spectra for the triply and quadruply-ionized cases, Crosswhite and Crosswhite (1984d), which will in time yield the energy levels themselves for direct comparison, and also from the point of view of computational complexity, which is more modest that for the more central elements in the period. A sketch of the low U I and U II configurations is given in Figure 17, in which the solid bars represent the lowest levels, where known, of the indicated configuration and the dotted ones the estimated positions of the remainder, Brewer (1971b). Since we are interested in comparisons with the levels of U^{3+}:$LaCl_3$, Crosswhite *et al.* (1980), we will concentrate particularly on configurations containing $5f^3$. The most straightforward cases are $5f^37s^2$ and $5f^36d7s$ of U II, for which it is possible to diagonalize both configurations simultaneously without truncation, and to include the interaction with $5f^36d^2$ as well, Crosswhite and Crosswhite (1984b). Because this group of three configurations is fairly well removed from the next-higher ones, neglecting the effects of the latter should be a good approximation.

Parametrization of $5f^37s^2$ would appear to be the most appropriate choice, since one then has only to make allowance for the effects of the closed $7s^2$ shell to obtain an estimate of the desired $5f^3$ free-ion parameters and levels. In practice, this is complicated by the configuration-interaction perturbations. The $5f^36d7s$ problem is more involved, requiring many additional parameters to accommodate interactions between the 5f and 6d orbitals. However, partly because of the 20-fold redundancy of the $5f^3$ core states, the final results turn out to be more extensive than those of the $5f^37s^2$ configuration itself.

One of the difficulties in dealing with atomic-spectra analyses of this type is that because of the complexity of configurations containing inequivalent electrons, false minima can rather easily be generated by the least-squares process, depending on the particular correlations of experimental and theoretical levels assumed. One must then rely on additional experimental characterizations of the levels, such as isotope shifts and Zeeman splitting factors, to verify a particular solution. The results given in Table 17 correspond to one such solution for which almost all such comparisons are in good agreement with experimental data, up to the point that additional interference from levels of the incompletely-characterized $5f^36d^2$ configuration become important. These results were arrived at by beginning with initial constraints suggested by the parametric model developed at Argonne, Crosswhite and Crosswhite (1984a, 1984c).

A third possible configuration for study is U I $5f^36d7s^2$, which is intermediate in complexity between the two discussed above, but requires simultaneous solution with the companion configurations $5f^36d^27s$ and

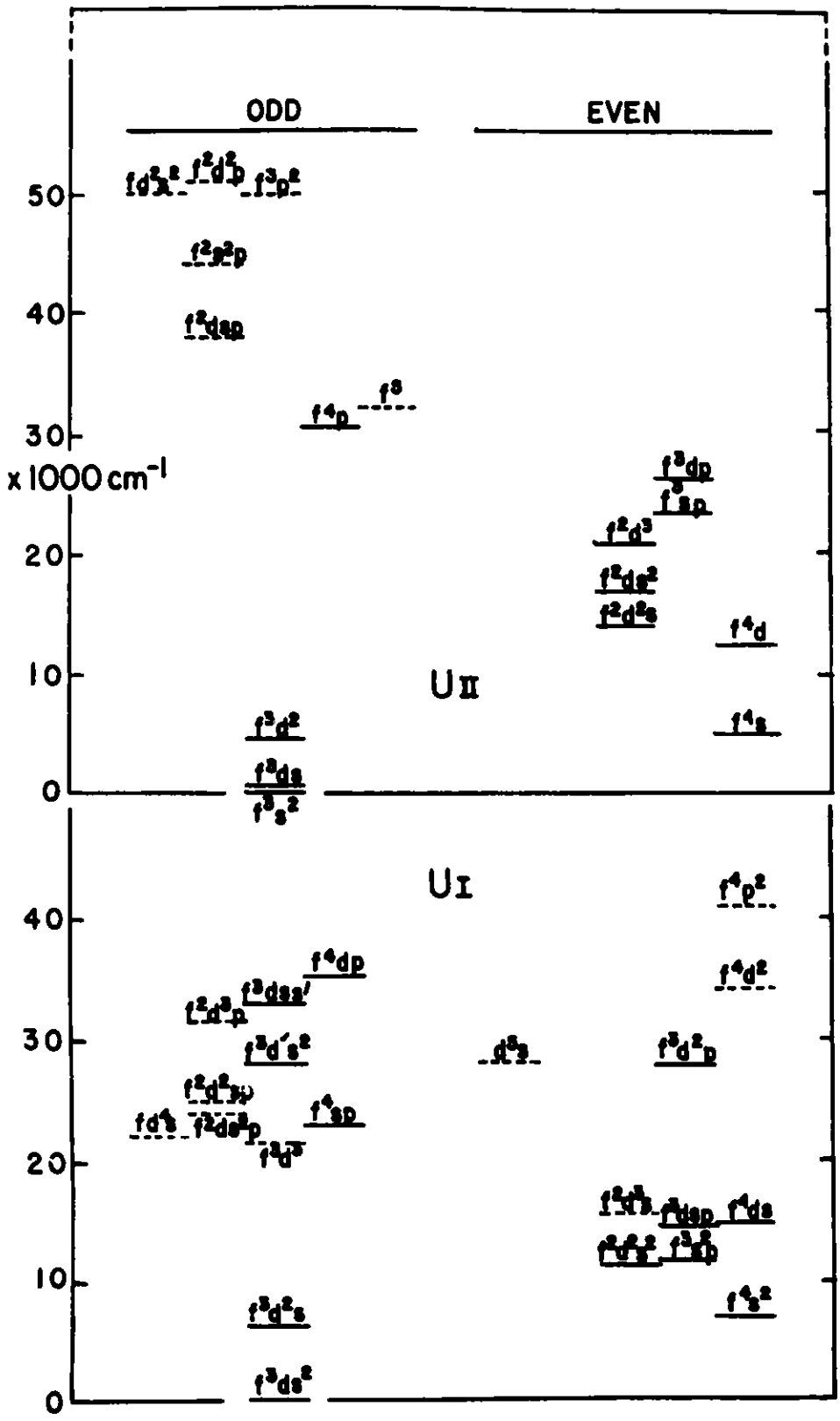

Fig. 17. The Lower Energy Configurations of U I and U II. Only the Ground State is Indicated for Each Configuration.

TABLE 17.

Parameter Values and Shifts for Uranium Spectra[a]

	Exp. (cm^{-1})	HFR[b] Adjustment	U IV $5f^3$ (estimated)	$U^{3+}:LaCl_3$[c]	Medium Shift	Relative Shift
U II f^3ds						
F^2	41691	2442	44133	39715	-4418	-10%
F^4	36718	1753	38463	33537	-4926	-13%
F^6	27066	1334	28400	23670	-4730	-17%
U II f^3s^2						
F^2	42826	1332	44158	39715	-4743	-11%
F^4	33505	955	34460	33537	-923	-3%
ζ	1719	37	1756	1623	-133	-8%
U I f^3ds^2						
F^2	42862	2750	45612	39715	-5897	-13%
F^4	34404	1974	36378	33537	-2841	-8%
F^6	24572	1501	26073	23670	-2403	-9%
U V f^2						
F^2	51906	-5282	46624	39715	-6909	-16%
F^4	42706	-3829	38877	33537	-5340	-14%
F^6	27701	-2942	24759	23670	-1089	-4%
α	35.4		(35.4)	27.6	(-7.8)	(-22%)
β	-658		(-658)	-722	(-54)	(+8%)
ζ	1969	-212	1757	1623	-134	-8%
P^2	496	-	(496)	1276	(780)	(+157%)

[a]References given in Section 4.0.

[b]From Tables 1-4

[c]From Table 5

$5f^3 6d^3$. The resultant problem is much too large for complete diagonalization, but a very satisfactory approximation method has been worked out, Crosswhite and Crosswhite (1984c). This configuration has the advantage of having about twice the number of known experimental levels as the U II case discussed above. The parametric results and the extracted estimates for the $5f^3$ free ion are also given in Table 17.

Another independent estimate of the free-ion U IV $5f^3$ parameters can be derived from the analysis of U V $5f^2$ levels, Wyart, et al. (1980), Van Deurzen, et al. (1984), Crosswhite and Crosswhite (1984a), by applying the HFR adjustments. Table 17 also includes comparison of these with the U^{3+}:$LaCl_3$ crystal results. In deriving U IV $5f^3$ from U V $5f^2$ results, the parenthetical uncertainties (the simple sum of those for free-ion and crystal analyses) are much smaller, and the comparison more extensive, than for derivations from U I and U II spectra. The real uncertainty in this case might be the systematic errors inherent in the HFR adjustments. In spite of these reservations, the magnitudes of the medium shifts are in general agreement with those for the lanthanide case Pr IV/Pr^{3+} in Tables 14 and 15, including the increase in magnitude of beta for the crystal, relative to that for the free ion.

4.2. Plutonium

The energy level structure of Pu^{3+}:$LaCl_3$ (and $PuCl_3$) has been analyzed in considerable detail. The closest approximation to the unknown $5f^5$ Pu IV configuration now available is Pu II $5f^3 7s^2$, of which seven levels are known from the work of Blaise et al. (1984a, 1985). These levels are embedded in the more complex $5f^5 6d7s$ configuration, but satisfactory simultaneous diagonalizations of these two have been carried out, Blaise, et al. (1983), using a truncation method similar to that for U I above.

Fortunately, as is characteristic of actinide spectra, the large spin-orbit interaction generates enough mixing such that the nominal ground ^6H multiplet contains considerable character of higher SL states. As a result, several electrostatic parameters can be determined as well as the spin-orbit parameter itself, Crosswhite and Crosswhite (1984c). These parameters are compared with those derived from an analysis of Pu^{3+}:$LaCl_3$ data in Table 18.

4.3. Californium

Eleven levels are known for the ground configuration $5f^{10}7s^2$ of atomic californium, Cf I, Blaise et al. (1984b). A parametric analysis by Crosswhite and Crosswhite (1984a), is listed in Table 18. Using HFR differences, we get the estimates for doubly-ionized Cf III $5f^{10}$ given in column 4. Parametric results for divalent Cf^{2+} in $CfCl_2$ are listed in column 5, and the medium shift in column 6. The medium shifts for F^2, F^4, F^6, and zeta are all similar to those encountered in the Pu case.

TABLE 18

Parameter Values and Shifts for Plutonium and Californium Spectra

	Exp. (cm^{-1})	HFR[a] Adjustment	Pu IV $5f^5$ (estimated)	Pu^{3+}:$LaCl_3$[b] exp.	Medium Shift	Relative Shift
Pu II f^5s^2						
F^2	49066	949	50015	48670	-1345	-3%
F^4	39640	682	40322	39188	-1134	-3%
F^6	26946	520	27466	27493	+27	0
ζ	2275	30	2305	2241	-35	-2%

	Exp. (cm^{-1})	HFR[a] Adjustment	Cf III $5f^{10}$ (estimated)	Cf^{2+}[c] $CfCl_2$	Medium Shift	Relative Shift
Cf I $f^{10}s^2$						
F^2	56774	574	57348	56711	-637	-1%
F^4	41713	405	42118	41172	-946	-2%
F^6	35559	306	35856	35274	-582	-2%
ζ	3382	17	3399	3446	+47	+1%

[a]From Tables 1-4.

[b]Table 5

[c]Estimated from an analysis of the spectrum of $CfCl_2$, Table 21.

4.4. Suggested Future Research

From the tentative nature of the above results, it appears that much more work is needed before the desirable goal of quantitative findings regarding the nature of electronic orbitals in the solid phase can be reached. The most direct approach, and the one more likely to give definitive results, would be to press ahead with the analysis of U IV. U VI and U V are now known, and, from the work of Berg, et al. (1980), a number of lines in the visible and near-ultraviolet have been characterized as being resonance lines of U IV. Extensive uranium spark spectra have been measured, Crosswhite and Crosswhite (1984d), but there is not yet enough additional characterization of these lines that term analysis can be attempted. Since it is unlikely that isotope-shift or Zeeman data of comparable quality will be available in the forseeable future, a new approach is needed. A very fruitful one would be to apply modulated-absorption laser techniques to the lines in this region to see which lines have common behavior as the lower level of one of them is depopulated. This would then tie all the lines of this subgrouping to a common lower level, leaving only a simple coincidence search to tie the groupings together into an energy-level scheme. Current laser technology is such that experiments of this type would be possible with equipment in place in a number of laboratories.

The secondary source of such free-ion data, namely, the related configurations of lower ionization discussed above, could also be made more significant by improved theoretical interpretations. New and planned experimental work at Los Alamos and Berkeley (both in cooperation with Kitt Peak) on U and Pu, respectively, promises extension of the neutral and singly-ionized level characterizations.

Preliminary studies of crystals with other than a valence of three have indicated a possible need for further extension of crystal-field theory to better accommodate those cases with much larger local fields. While some attempts have been made to extend the theory beyond the first-order approximation, it is likely that a much greater effort will be needed in this direction before the available spectra of higher valent actinides can be fully analyzed.

5.0. Spectra and Electronic Structure Interpretation in the Divalent and Quadrivalent Oxidation States of the Actinides

While spectra of compounds and solutions containing actinides in other than the tripositive valence state are well known, similar systematic analyses of the electronic structure have not yet been developed. Extensive analysis is limited to a few isolated cases. In this context it is important to use an effective method for the extrapolation from characterized cases to neighboring ones as means of extending the analysis as well as

simply for predicting the energies of transitions in valence states not previously observed.

In the discussion of trivalent ion spectra it was shown that the extensive effective operator model was capable of satisfactorily reproducing the experimentally observed spectra. A model for extrapolation of the energy level parameters was not necessary since for practically every member of the series the data were sufficient for a completely independent determination of those parameters, Table 5. When plotted directly against atomic number, the Slater and spin-orbit coupling parameters exhibit a regular but not the linear dependence originally assumed, Carnall and Wybourne (1964). In fact, as suggested by the results given in Table 6, the trend in the experimentally determined parameters very closely matches that in the corresponding Hartree-Fock values, since the difference ΔP is found to be nearly constant over the series. From Table 5 it is apparent that the independently determined values of the two-body and three-body effective operators are to a first approximation essentially constant over the series, and the magnitudes of these parameters for the actinides are very nearly those deduced for the lanthanides, Crosswhite (1977).

In view of the consistency of the ΔP values for trivalent actinides, Table 6, we have adopted an approach based on use of ΔP for extrapolation of parameters where the data base is extremely limited, i.e. in the 2+, 4+, and higher valent spectra. The Hartree-Fock values for the Slater and spin-orbit integrals relevent to each valence state are given in Tables 1-4. While these integrals were computed using a code with a relativistic correction, Section 3.2, consistent use of other published results such as those tabulated in Varga et al. (1970) and spin-orbit integrals given by Lewis et al. (1970), should also prove useful. In principle, for any given valence state, we need a single case in which the energy level parameters have been determined from experimental data. We then establish the approximate values of ΔP for the system and are in a position to extrapolate over the entire series.

As we consider other than the trivalent actinides, the role of the two-body and three-body correction terms is not known in detail. We assume in every case a set of values for the correction terms consistent with those established for the trivalent case, and these are included in the calculation. This appears to be a reasonable approximation. For the divalent case, the electrostatic and spin-orbit integrals which we use are comparable in magnitude to those established for the trivalent case. However, with increasing valence, there is an increase in the relative importance of both spin-orbit coupling and the crystal field interaction relative to the electrostatic term. Since the electrostatic interaction in effect decreases in importance, so does the importance of the attendent correction terms which act primarily to correct the electrostatic interaction.

5.1. Divalent Actinide Ion Spectra

Efforts to prepare divalent actinide compounds and analyze their spectra have been less successful than was the case for the lanthanides, for which the divalent ion for each member of the series could be stabilized in CaF_2, McClure and Kiss (1963), Figure 18. In both $Am^{2+}:CaF_2$, Edelstein et al. (1966), Edelstein et al. (1967), Baybarz et al. (1972), and $Es^{2+}:CaF_2$, Edelstein et al. (1970), intense absorption bands were observed. They could be attributed to either f→d or charge-transfer transitions. The presence of divalent actinide ions in these cases was established by measurements of the electron paramagnetic resonance spectra, not on the basis of the observed optical spectra. In contrast to the more intense absorption bands reported for $Es^{2+}:CaF_2$, weak absorption bands consistent with the intensities expected for f→f transitions have been identified in the 10000-20000 cm^{-1} region in both $EsCl_2$ and $Es^{2+}:LaCl_3$, Fellows et al. (1978). The relatively narrow band structure exhibited by the Es^{2+} halides was also found to be characteristic of the Cf^{2+} halides, Peterson et al. (1977), Wild et al. (1978), Figure 19.

While it has not been possible to stabilize Cm^{2+} in CaF_2 under the same conditions that yielded evidence for Am^{2+} and Es^{2+}, evidence for the formation of both Am^{2+} and Cm^{2+} in pulse radiolysis studies of aqueous solutions has been obtained. Broad intense bands were observed near 33000 cm^{-1}; however, the nature of the absorption process is not clear, and a charge-transfer mechanism cannot be excluded, Gordon et al. (1978).

Since the available spectroscopic results for divalent actinides are fragmentary, it is of particular interest to apply a consistent interpretative method which can account for observed spectral features and predict the energies of characteristic bands not yet observed but accessible to observation. As a first approximation the parameters for a tentative model for divalent actinides can be deduced from data for divalent lanthanide spectra.

The free-ion spectra of Pr IV, Pr III, and Ce III are known. The published energies and the corresponding parameters are given in Tables 13, 16, and 19, respectively. Initial estimates of F^k and ζ_{4f} values appropriate to Ln^{2+} in condensed phases can be made by assuming that the change observed in these parameters for iso f-electron couples such as Ce III/Pr IV (both $4f^2$) will also be characteristic of the couple Ce^{2+}/Pr^{3+} in condensed phases. Parameters for Nd IV can be inferred from Pr IV by use of the Hartree-Fock difference method already cited. As shown in Table 20, for both $4f^2$ and $4f^3$ couples there is a reduction of 20-30% in comparing values of F^k and ζ_{4f} for divalent compared to isoelectronic trivalent-ion cases. If we also compare the results of Downer et al. (1983) for $Eu^{2+}:CaF_2$ with those for $Gd^{3+}:LaF_3$, Carnall et al. (1971), we see that the parameters for $Eu^{2+}(4f^7)$ are ~82-86% of those for $Gd^{3+}(4f^7)$. This latter result is similar to that for the decrease in the parameters for $Eu^{3+}:LaCl_3$ necessary to approximate the first few levels in $Sm^{2+}:LaCl_3$, Dieke (1968). The little information available on

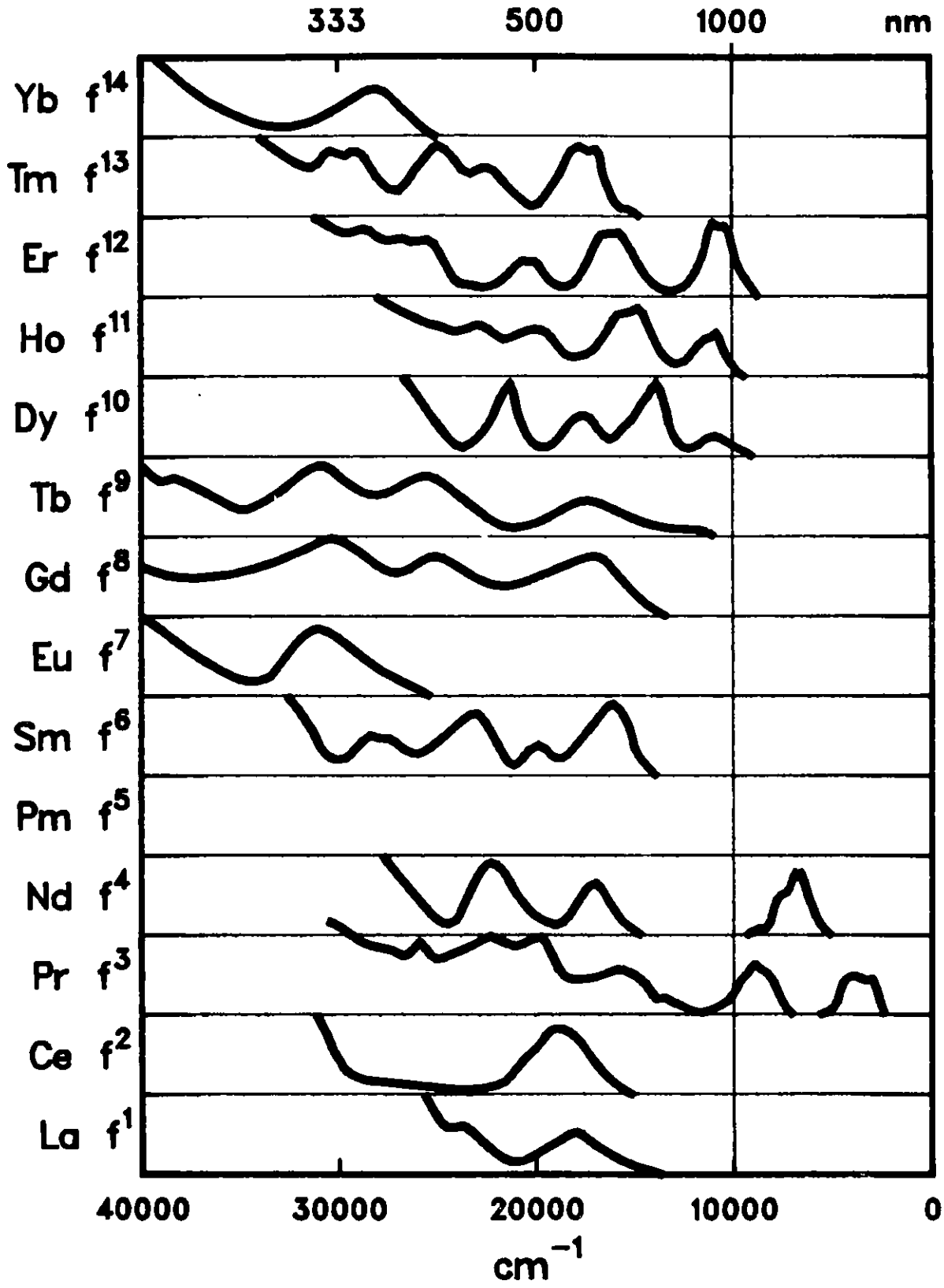

Fig. 18. Absorption Spectra of the Divalent Lanthanides, $Ln^{2+}:CaF_2$, Adapted from McClure and Kiss (1963).

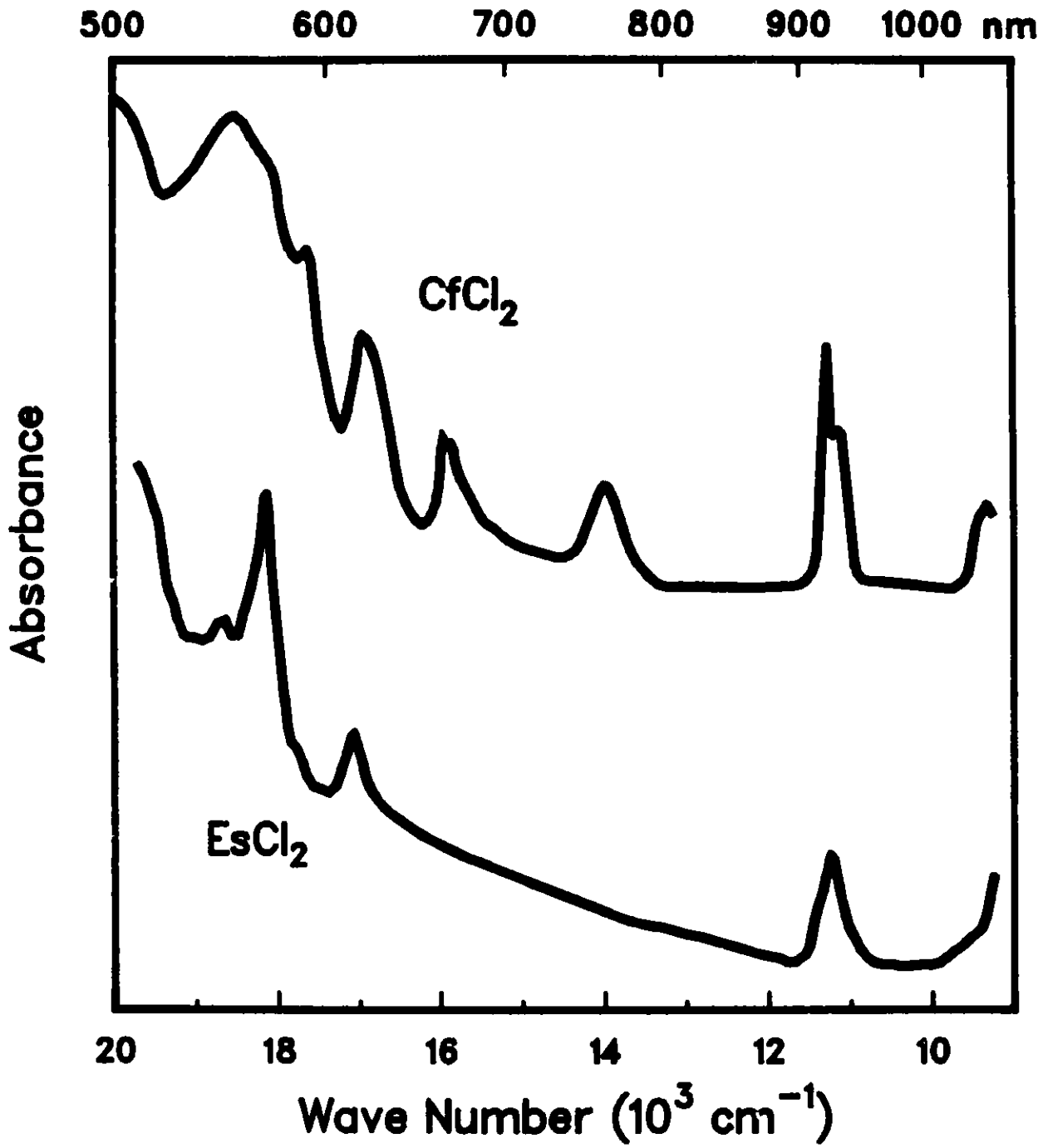

Fig. 19. The Absorption Spectra of $CfCl_2$ and $EsCl_2$ Adapted from Peterson et al. (1978) and Fellows et al. (1978).

TABLE 19.

Free-ion Energy Levels and Parameters for Ce III ($4f^2$)[a]

Largest[b] Eigen.	Component	Next Largest[b] Eigen.	Component	Observed Energy (cm^{-1})	Fit Energy (cm^{-1})	Calc G Value
0.985	$^3H_4$	0.167	$^1G_4$	0.0	0.4	
1.0	$^3H_5$	--		1528.32	1528	
0.999	$^3H_6$	-0.047	$^1I_6$	3127.10	3125	1.6667
0.989	$^3F_2$	0.146	$^1D_2$	3762.75	3766	0.6731
1.0	$^3F_3$	--		4764.76	4764	1.0835
0.778	$^3F_4$	-0.615	$^1G_4$	5006.06	4999	1.1484
0.771	$^1G_4$	0.627	$^3F_4$	7120.00	7125	1.0961
-0.954	$^1D_2$	0.262	$^3P_2$	12835.09	12836	1.0275
0.994	$^3P_0$	0.110	$^1S_0$	16072.04	16074	0
1.0	$^3P_1$	--		16523.66	16520	1.5011
-0.965	$^3P_2$	-0.261	$^1D_2$	17317.49	17318	1.4663
0.999	$^1I_6$	0.047	$^3H_6$	17420.60	17421	1.0003
0.994	$^1S_0$	-0.110	$^3P_0$	32838.62	32838	0

Parameters (cm^{-1})[c]

E_{ave}	7631	α	42.179 (.2)	M^0	[1.393]
F^2	54864 (20)	β	-1060.3 (11)	M^2	[0.767]
F^4	35301 (50)	γ	2705.3 (10)	M^4	[0.518]
F^6	21070 (20)	P^2	150 (25)		
ζ_{4f}	543.71 (1)	P^4	112	σ	5.4
		P^6	75		

a. Experimental data from Martin et al. (1978), Sugar (1965b), Johannson and Litzen (1972).

b. The largest and next largest eigenvector components are given with their phases.

c. Parameter errors are shown in parentheses; parameters in brackets were not varied; P^2 was freely varied but P^4 and P^6 were constrained by the relations $P^4 = 0.75\ P^2$ and $P^6 = 0.5\ P^2$.

TABLE 20.

Values for F^k and ζ_{4f} for Iso-f-Electronic Trivalent Compared to Divalent Lanthanides

	Pr IV ($4f^2$)[a]	Ce III ($4f^2$)[b]	% Reduction 3+ → 2+
F^2	72549	54864	24.4
F^4	53718	35301	34.3
F^6	36057	21070	41.6
ζ_{4f}	766.9	543.7	29.1
	Nd IV ($4f^3$)[c]	**Pr III ($4f^3$)[d]**	
F^2	75819	59946	20.9
F^4	54352	39977	26.4
F^6	35712	26454	25.9
ζ_{4f}	896.4	665.0	25.8
	$Gd^{3+}:LaF_3$ ($4f^7$)[e]	**$Eu^{2+}:CaF_2$ ($4f^7$)[f]**	
F^2	85587	70834	17.2
F^4	61361	50902	17.0
F^6	45055	38891	13.7
ζ_{4f}	1503.5	1228	18.3

a. Data from Table 13.

b. Data from Table 19.

c. Data extrapolated from values for Pr IV.

d. Data from Table 16.

e. Carnall *et al.* (1971).

f. Downer *et al.* (1983).

divalent lanthanide ion crystal-field splitting within the f^N-configuration in Sm^{2+} and Eu^{2+} suggests a relatively small crystal-field interaction, consistent with that for the trivalent case in similar hosts.

Based on a small crystal-field splitting for the divalent lanthanides, we assumed as a first approximation that corresponding actinide crystal-field splitting would be small. The fragmentary spectroscopic data for An^{2+}, Figure 19, do not appear to be inconsistent with this estimate. The initial model was consequently limited to free-ion considerations, and the F^k and ζ_{5f} parameters for An^{2+} were estimated to be 85-90% of those for the iso-f-electronic An^{3+}:$LaCl_3$ ion. The effects of configuration interaction for An^{2+} were assumed to be the same as those for An^{3+}, as indicated earlier. The results of the initial calculations were slightly modified by adjusting the computed levels to more accurately reproduce experimental data where available. The final results are given in Tables 21 and 22. Reductions in the iso-f-electronic An^{3+} F^k and ζ_{5f} parameters for comparison with the results shown in Table 21 were in the 10-15% range except for F^6, which approached the value for An^{3+}. The "model ΔP values" for the difference between the Hartree-Fock and deduced parameters shown in Table 21 can be compared with values for the +3 series in Table 6. It must be emphasized that each set in Table 6 corresponds to an independent determination, and that we observe a small decrease in the ΔP values over the series. Any attempt to average would cause distortion in some of the fits. Considering the small amount of data available, results given in Table 21 may be expected to undergo some adjustment as further experiments are carried out. The model energy level schemes for An^{2+} are plotted in Figure 20 where the lowest levels in the $5f^{N-1}s$ and $5f^{N-1}d$ configurations, Figure 15, are also indicated. For Cf^{2+} and Es^{2+}, the correlation between calculated and experimentally observed absorption features shown in Table 22 appears to be quite satisfactory. Additional absorption features not previously reported are predicted in the near infrared range in both Cf^{2+} and Es^{2+}. The value of the "predictions" for f→f transitions in other cases depends strongly on the extent of the optical windows to be expected, i.e. the energy at which the absorption due to f→d transitions will first be observed.

As noted earlier, the energies quoted by Brewer (1971b) are for the gaseous free-ion. We need an estimate of the extent to which the free-ion energy will be lowered by ligand-field interaction, as discussed in Section 3.8.1. As with the trivalent spectra we refer first to observations of divalent spectra of the lanthanides. In their survey of the spectra of divalent lanthanides in CaF_2, McClure and Kiss (1963) identified the energies of the lowest-lying d-states in most cases. Their estimates have been confirmed by later investigations in which both the absorption and fluorescence spectra of divalent lanthanides in CaF_2, SrF_2, and often in BaF_2 were measured at low temperatures. For example, Loh (1968) gives the lowest energy f→d transition for Ln^{2+}:CaF_2 at approximately 15000 cm^{-1} in Sm^{2+}, 24000 cm^{-1} in Eu^{2+}, 10000 cm^{-1} in Dy^{2+}, 14000 cm^{-1} in Tm^{2+}, and

TABLE 21.

Energy Level Parameters (all in cm^{-1}) for An^{2+} Based on a Consistent Predictive Model[a]

	Np	Pu	Am	Cm	Bk	Cf	Es	Model Δ-Value
F^2(HFR)[a]	68843	72563	76031	79292	82379	85340	88198	
F^2(Est)[b]	40210	43930	47400	50660	53750	56711	59569	
ΔP	28633	28633	28631	28632	28629	28629	28629	28630
F^4(HFR)	44355	46868	49208	51405	53481	55471	57385	
F^4(Est)	30055	32570	34910	37105	39180	41172	43085	
ΔP	14300	14298	14298	14300	14301	14299	14300	14300
F^6(HFR)	32343	34220	35968	37609	39159	40644	42073	
F^6(Est)	26970	28850	30600	32240	33790	35274	36700	
ΔP	5373	5370	5368	5369	5369	5370	5373	5370
ζ(HFR)	1959	2255	2565	2888	3227	3583	3956	
ζ(Est)	1820	2118	2428	2750	3090	3446	3819	
ΔP	139	137	137	138	137	137	137	137

a. Computed using Hartree-Fock methods and including an approximate relativistic correction (HFR), Cowan and Griffin (1976), Crosswhite (1977), with, in addition to the parameters shown,

$\alpha = 30$ $T^2 = 200$ $T^6 = -300$ $P^2 = 500$

$\beta = -800$ $T^3 = 50$ $T^7 = 400$ $P^4 = 375$

$\gamma = 1200$ $T^4 = 100$ $T^8 = 350$ $P^6 = 250$

b. Estimated parameter value used to compute the energy level structure.

TABLE 22.

Computed Energy Level Structures for the f→f Transitions in An^{2+}.[a]

Np^{2+} ($5f^5$)		Pu^{2+} ($5f^6$)		Am^{2+} ($5f^7$)		Cm^{2+} ($5f^8$)	
SLJ	Calc. (cm^{-1})	SLJ	Calc. (cm^{-1})	SLJ	Calc. (cm^{-1})	SLJ	Calc. (cm^{-1})
$^6H_{5/2}$	0	$^7F_0$	0	$^8S_{7/2}$	0	$^7F_6$	0
$^6H_{7/2}$	2467	$^7F_1$	1993	$^6D_{7/2}$	15504	$^7F_4$	3840
$^6H_{9/2}$	4770	$^7F_2$	3988	$^6P_{5/2}$	17925	$^7F_5$	4066
$^6F_{3/2}$	5177	$^7F_3$	5787	$^6I_{7/2}$	19548	$^7F_3$	6357
$^6F_{1/2}$	5241	$^7F_4$	7401	$^6P_{3/2}$	19744		
$^6F_{5/2}$	5321	$^7F_5$	8832	$^6I_{9/2}$	20466		
$^6H_{11/2}$	6845	$^7F_6$	9996	$^6I_{11/2}$	22354		
		$^7F_0$	10450	$^6I_{17/2}$	22390		
		$^5D_1$	14325	$^6D_{9/2}$	22653		
				$^6I_{13/2}$	23123		
				$^6I_{15/2}$	23427		

TABLE 22 (continued).

Bk^{2+} ($5f^9$)		Cf^{2+} ($5f^{10}$)			Es^{2+} ($5f^{11}$)		
SLJ	Calc. (cm^{-1})	SLJ	Calc. (cm^{-1})	obs.[b] (cm^{-1})	SLJ	Calc. (cm^{-1})	obs.[c] (cm^{-1})
$^6H_{15/2}$	0	$^5I_8$	0	-	$^4I_{15/2}$	0	-
$^6F_{11/2}$	5621	$^5F_5$	8368	-	$^4F_{9/2}$	7102	-
$^4F_{9/2}$	5693	$^5I_7$	9271	9200	$^2H_{11/2}$	8682	9000?
$^6H_{13/2}$	6703	$^3D_2$	10284	-	$^2P_{3/2}$	10657	11100
$^6H_{11/2}$	9685	$^5I_6$	11183	11000	$^4I_{13/2}$	11225	
$^6F_{3/2}$	10360	$^5F_4$	13951	14000	$^4F_{5/2}$	16718	17300
$^6H_{9/2}$	10984	$^5I_4$	15428	15400	$^4I_{9/2}$	17199	
$^6F_{7/2}$	11212	$^5I_5$	16038	16000	$^4I_{11/2}$	18425	18500
$^6H_{7/2}$	12507	$^5G_6$	16896	17000	$^4F_{7/2}$	18824	18900
$^6F_{5/2}$	12897	$^3K_8$	17636	17600	$^4S_{3/2}$	20083	
		$^5S_2$	17662	-			
		$^5G_4$	17975	-			
		$^5F_3$	18669	-			

a. The energy range shown in each case is that corresponding to the energy gap between the ground state and the onset of intense absorption.

b. Peterson *et al.* (1977).

c. Fellows *et al.* (1978).

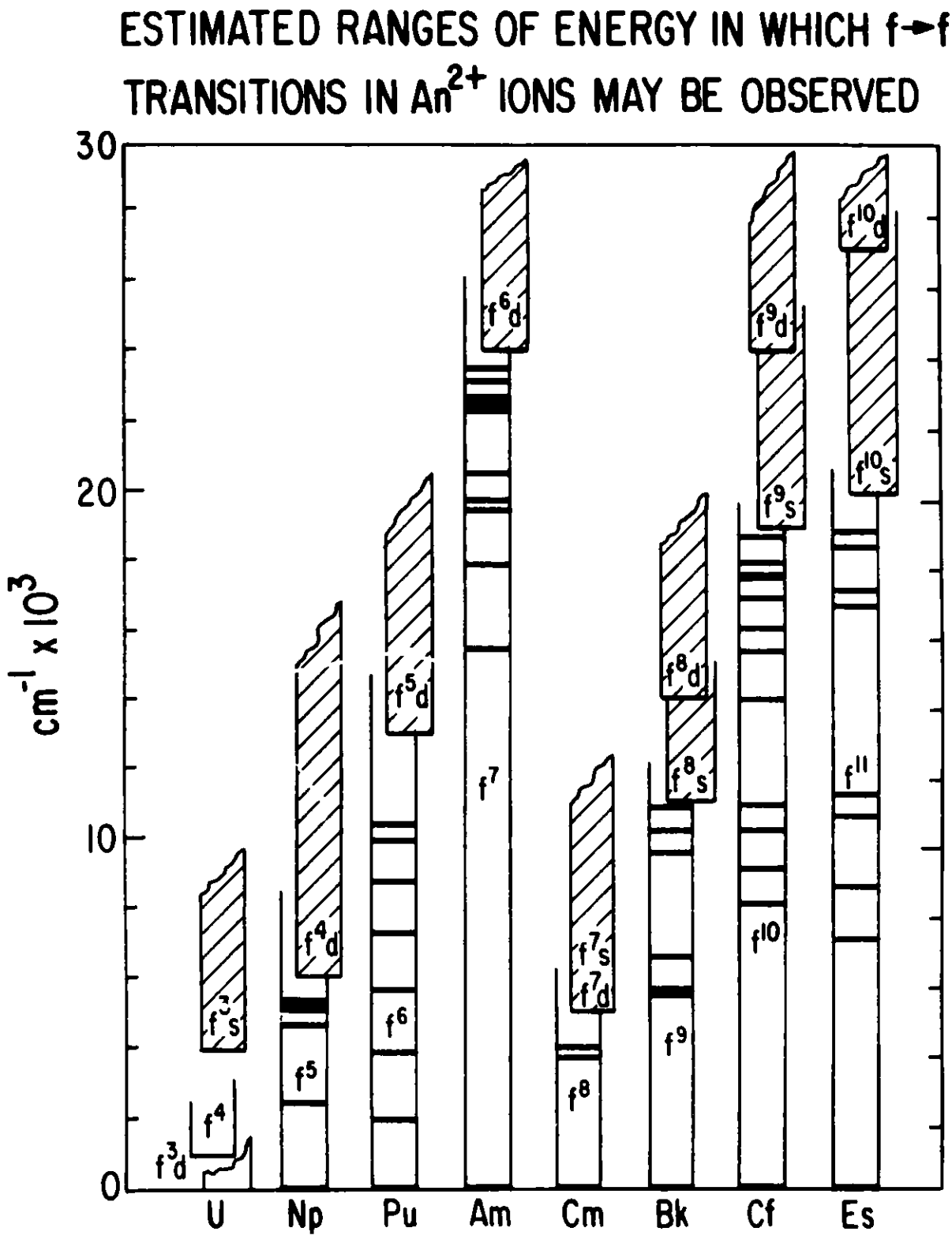

Fig. 20. Predicted Energy Level Structure for f→f Transitions in An^{2+} and Predicted Energies of First Excited States in $f^{N-1}s$ and $f^{N-1}d$ Excited Configurations.

27000 cm^{-1} in Yb^{2+}. See also Chase (1970) $Eu^{2+}:CaF_2$; Loh (1969) Eu^{2+} and $Yb^{2+}:CaF_2$, Loh (1973) $Yb^{2+}:CaF_2$, and Eremin (1970) $Yb^{2+}:CaF_2$. All of these results show that for $Ln^{2+}:CaF_2$, the energy difference, (lowest energy free-ion state) less (energy of leading edge of first f→d band in absorption in the host CaF_2 crystal), is $\Delta E \sim 8000$ cm^{-1}. There are several members of the Ln^{2+} series in which the ground state is not in the $4f^N$-configuration, and this is also indicated to be the case for An^{2+} in Figure 15, but these exceptions are not of primary concern here. We proceed to examine the relevance of a medium shift of ~ 8000 cm^{-1} for An^{2+}, Figure 20.

In Figure 15 we note that while $5f^{N-1}d$ states lie lowest over $5f^N$ for the light half of the series, this changes at Cm^{2+}. In the heavier members the ground state of the $5f^{N-1}6s$ configuration is predicted to be lower in energy than that of $5f^{N-1}d$. In $Ce^{3+}:CaF_2$, Loh (1967), it was reported that the $f^N \rightarrow f^{N-1}s$ transitions were a factor of 100 weaker than those corresponding to $f^N \rightarrow f^{N-1}d$. We assume here that configuration mixing occurs between $5f^{N-1}d$ and $5f^{N-1}s$, but the transitions to formed $5f^{N-1}s$ states may still give rise to relatively weaker band structure. The effect of inserting these two nominal $f^{N-1}s$ and $f^{N-1}d$-configurations into a matrix may also not result in identical medium shifts in the respective lowest energy states. It is interesting to note that if we assume the f → d transitions in Es^{2+} and Cf^{2+} occur ~ 8000 cm^{-1} lower in energy than that predicted for the lowest free-ion f → d transition, then we would expect strongly increasing absorption near 19000 cm^{-1} and 16000 cm^{-1}, respectively. In both cases broad absorption features do appear to increase in intensity near these energies, Figure 19. Of course transitions to $f^{N-1}s$-configurations that are not subjected to large medium-induced energy shifts would also be consistent with the observations, Figure 20. If we examine the case of Am^{2+}, the correlation with experiment is even clearer since intense broad bands earlier attributed to possible f→d transitions are reported in the expected range, Edelstein et al. (1967).

We are left with interesting predictions for the An^{2+} not already cited. In Bk^{2+} and Pu^{2+} as in Am^{2+} we might be able to observe the first excited state in the f^N-configuration before f→d absorption becomes predominent, but in each case the only f→f transition expected to be observable will lie well into the infrared range, Figure 20. In Np^{2+} and Cm^{2+}, the ground configuration will probably be $f^{N-1}d$ instead of f^N because of the stabilization energy. The $5f^36d$-configuration lies lowest in U III; Th^{2+}, Pa^{2+} and U^{2+} have similar non-f^N ground configurations. Consequently, they are not considered here. The most interesting experiment to pursue would center on Am^{2+}. Because of the predicted large energy gap between the ground ($^8S_{7/2}$) and first excited ($^6P_{7/2}$) states, fluorescence near 14000 cm^{-1} may be observable.

The lanthanide analog, Eu^{2+}, is known to fluoresce in certain hosts. Dieke (1968) shows the diagram comparing Eu^{2+} in CaF_2 and SrF_6--in both

cases cubic sites. However the f → d transitions are shifted slightly higher in energy in $SrCl_2$ and the lowest ^6P-state is observed via fluorecence.

Weber (1980) discusses the broad band Stokes shifted 5d → 4f emission of Eu^{2+} in many hosts. Fluorescence in the 400-500 nm range has a lifetime of 1-2 μsec. Attempts to observe laser action from $Eu^{2+}:CaF_2$ or Eu^{2+} (glass) were unsuccessful, due either to excited state absorption or color centers. Corresponding experiments with Am^{2+} should be carried out.

5.2. Quadrivalent Actinide Ion Spectra

The absorption spectra of tetravalent actinides, with features similar to those observed for f→f transitions in the trivalent series, have been reported in a number of different solvents and in the vapor phase as well as in solid compounds. The observations are consistent with trends suggested in Figure 1 that the $5f^N$ configuration will lie lowest and that the energy gap between the ground state ($5f^N$) and the lowest energy state in the next higher-lying configuration ($5f^{N-1}6d$), will be greater than in corresponding cases for trivalent ions.

The lowest f→d transition in the atomic spectrum of U V was placed at 59183 cm^{-1}, Wyart et al. (1980). Assignment of intense absorption in U^{4+}(aquo) beginning near 43000 cm^{-1} as indicative of the first f→d transition in that condensed phase, Cohen and Carnall (1960), yields a shift from the corresponding free-ion transition energy of ~ 16000 cm^{-1}. The lowest energy f→d transition in $Pa^{4+}:ThBr_4$ was found to occur at 20763 cm^{-1}, Naik and Krupa (1985). The identification of the free-ion energy levels in the U V $5f^2$-configuration is now complete, Table 23, Wyart et al. (1980), Van Deurzen et al. (1984), and provides a valuable basis for comparison with the various analyses of An^{4+} spectra in condensed phases. At present the number of reliable detailed analyses of An^{4+} spectra is very small and primarily involves the Pa^{4+} and U^{4+} ions i.e. $5f^1$ and $5f^2$ cases. An important experimental deficiency is the lack of a suitable host lattice into which a broad range of An^{4+} ions can be doped. Excellent results with $ThCl_4/ThBr_4$ appear to end at neptunium doping where both the 4+ and 3+ oxidation states have been observed, Genet (1984).

Extensive and reliable analyses of the spectra of U^{4+} in both high-symmetry (O_h) and in lower symmetry (D_{2d} and D_2) sites have been published. Somewhat in contrast to observations made with trivalent ions, the magnitude of the crystal field splitting in the two cases differs significantly. A good example of the high-symmetry (O_h) case is that of U^{4+} in Cs_2UCl_6, Johnston et al. (1966a,b), shown in Table 24, where the state labels in terms the major SLJ-component are included. The lower symmetry (D_{2d}) case is illustrated in the analysis of $U^{4+}:ThBr_4$, Delamoye et al. (1983) which is summarized in Table 25. Energy level parameters for both the above cases are given in Table 26.

TABLE 23.

Free-ion Energy Levels and Parameters for U V ($5f^2$)[a]

Largest[b] Eigen.	Component	Next Largest[b] Eigen.	Component	Observed Energy (cm^{-1})	Fit Energy (cm^{-1})	Calc G Value
0.945	$^3H_4$	0.314	$^1G_4$	0.0	-9.7	0.8231
-0.929	$^3F_2$	-0.316	$^1D_2$	4160.65	4158	0.7155
1.0	$^3H_5$	—		6136.88	6146	1.0334
1.0	$^3F_3$	--		8983.53	8983	1.0835
0.706	$^3F_4$	-0.649	$^1G_4$	9433.76	9442	1.1086
0.973	$^3H_6$	-0.232	$^1I_6$	11513.58	11513	1.1580
-0.740	$^1D_2$	0.579	$^3P_2$	16465.30	16475	1.1294
0.702	$^3F_4$	0.693	$^1G_4$	16655.73	16651	1.1183
0.966	$^3P_0$	0.258	$^1S_0$	17128.16	17115	0
1.0	$^3P_1$	--		19818.58	19838	1.5011
0.973	$^1I_6$	0.232	$^3H_6$	22276.05	22276	1.0089
0.811	$^3P_2$	0.567	$^1D_2$	24652.91	24637	1.3220
0.966	$^1S_0$	-0.258	$^3P_0$	43613.58	43614	0

Parameters (cm^{-1})[c]

E_{ave}	12649	α	35.425 (0.7)	M^0	[0.775]
F^2	51906 (64)	β	-658.44 (38)	M^2	[0.434]
F^4	42707 (171)	γ	764.98 (35)	M^4	[0.294]
F^6	27702 (113)	P^2	496 (57)		
ζ_{5f}	1969.2 (3)	P^4	372	σ	17
		P^6	248		

a. Experimental data from Wyart et al. (1980), Van Deurzen et al. (1984).

b. The largest and next largest eigenvector components are given with their phases.

c. Parameter errors are shown in parentheses; parameters in brackets were not varied; P^2 was freely varied but P^4 and P^6 were constrained by the relations $P^4 = 0.75\ P^2$ and $P^6 = 0.5\ P^2$.

TABLE 24.

Observed and Calculated Energy Levels for U(IV) in Cs_2UCl_6 (O_h-site symmetry) (in cm^{-1})[a,b]

Γ	E (obs'd)	E calc'd	Δ	Largest SLJ	Γ	E (obs'd)	E calc'd	Δ	Largest SLJ
1	0	57	-57	$^3H_4$	5		12875	-	$^3H_6$
4	924	971	-47	$^3H_4$	1		13270	-	$^3H_6$
3		1402	-	$^3H_4$	4		13276	-	$^3H_6$
5		2295	-	$^3H_4$	1	14780	14775	13	$^3P_0$
3	5060	4864	195	$^3F_2$	3	15213	15491	-278	$^3F_4$
5	4899	5013	-114	$^3F_2$	4	15754	15622	132	$^3F_4$
4	6343	6396	-52	$^3H_5$	5		16205	-	$^1D_2$
5	7011	7056	-46	$^3H_5$	1	16797	16948	-151	$^3P_0$
4	7267	7123	144	$^3H_5$	3		16982	-	$^1D_2$
3	8197	7941	256	$^3H_5$	5		17600	-	$^1G_4$
1	8469	8392	77	$^3F_4$	4	18824	18742	81	$^3P_1$
5		9314	-	$^3F_3$	1		19913	-	$^1I_6$
4	9232	9373	-142	$^3H_5$	4		20096	-	$^1I_6$
2		9946	-	$^3F_3$	5		20165	-	$^1I_6$
3		10022	-	$^3H_6$	2		21013	-	$^1I_6$
4	10065	10078	-13	$^3F_3$	5	21814	21879	-65	$^1I_6$
5		10971	-	$^3H_6$	3	22183	22029	153	$^1I_6$
3		11335	-	$^3H_6$	5	23329	23276	53	$^3P_2$
5		11338	-	$^3H_6$	3	24700	24741	-41	$^1D_2$
2	12128	12221	-93	$^3H_6$	1		41974	-	$^1S_0$

a. Experimental data of Johnston et al. (1966a,b); further interpretation of similar spectra by Satten et al. (1983).

b. Energy level parameters are given in Table 26.

c. For the O_h-symmetry assumed here the values of B_4^4 and B_4^6 are fixed by the relationship $B_4^4 = 5/\sqrt{70}\, B_0^4$ and $B_4^6 = -\sqrt{7/2}\, B_0^6$.

TABLE 25.
Observed and Calculated Levels for $U^{4+}:ThBr_4$
(D_{2d} - site symmetry) (in cm^{-1})[a,b]

Γ	E_{obs}	E_{calc}	ΔE	Γ	E_{obs}	E_{calc}	ΔE
4	0	-34	34	5	15412	15397	15
5	78	105	-27	2		15630	
1		197		1		15827	
3		587		4		15964	
2		729		5	16003	16038	-35
1		895		3		16743	
5	943	967	-24	2	16997	17008	-11
3		3686		5	17335	17330	5
5		3867		1	19311	19268	43
4		3936		5	19341	19344	-3
1		4041		3		19462	
3		5617		4		19975	
5	5730	5724	6	5	19970	19997	-27
2		5798		2		20071	
4		5961		5	20382	20374	8
5		6058		1	20460	20448	12
5	6450	6414	36	3		20846	
1		6541		4		20941	
2		6552		3		21588	
5	8246	8252	-6	5	21842	21826	16
3		8304		1	22220	22249	-29
2		8314		4		22360	
4		8406		1		37542	
5	8513	8528	-15				
1		8834					
5		8853					
4		8970					
2		9111					
1	9250	9199	51				
3		9443					
5	9530	9497	33				
4		10570					
1	10593	10607	-14				
5	10658	10663	-5				
3		10725					
5		10928					
4		11004					
3		11072					
2		11081					
1		11416					
5		11860					
3		14296					
4		14327					
1	14368	14355	13				
5	14654	14651	3				
1	14899	14914	-15				
1	15204	15224	-20				

a. Results of Delamoye et al. (1983). The energy level parameters derived for this data are shown in Table 26, and are not the same as the above reference since we have additionally allowed γ and P^2 to vary.

b. The mean error σ = 27 for a fit to 26 levels.

TABLE 26.

Summary of Energy Level Parameters (in cm^{-1}) for Pa^{4+} and U^{4+} in Various Hosts[a]

Parameter	$Pa^{4+}:Cs_2ZrCl_6$[b] (O_h)	Cs_2UCl_6[c] (O_h)	$Pa^{4+}:ThCl_4$[d] (D_{2d})	$U^{4+}:ThCl_4$[e] (D_{2d})	$U^{4+}:ThBr_4$[f] (D_{2d})	$U^{4+}:ZrSiO_4$[g] (D_{2d})	$U(BD_4)_4$[h] (O_h)
E_{ave}		12825		11901	11692		
F^2		42562 (925)		42918 (80)	41821 (312)	44257	41121 (236)
F^4		38135 (2302)		39873 (419)	39646 (872)	40293	38849 (1071)
F^6		30230 (1761)		25588 (267)	24674 (926)	31286	21711 (827)
ζ	1514.2 (22)	1781.1 (23)	[1525]	1810.2 (6)	1776.2 (4)	1740	1807 (16)
B_0^2			-1408 (144)	-1129 (94)	-1115 (52)	-2000	
B_0^4	6932 (251)	7271 (300)	1753 (275)	1793 (154)	1167 (91)	2000	-2486 (170)
B_4^4			-2434 (275)	-2617 (94)	-2154 (55)	5125	
B_0^6	239 (261)	1421 (293)	-2428 (1123)	-3016 (323)	-3784 (232)	-5792	-5287 (113)
B_4^6			-206 (508)	342 (246)	733 (161)	-427	
α				[30.12]	29.67 (0.8)	22.8	40 (0.3)
β				[-660]	-686.9 (47)		[-648]
γ_2				[1200]	1704 (297)		[1200]
P^2				[500]	403 (88)		[500]
rms	88	156	41	36	27	112	71
No. of Levels	5	21	7	20	26	30	19

TABLE 26 (contd.)

a. The indicated parameters were derived as part of the present work except where noted. Values in brackets were not varied; values in parentheses are the rms errors in the associated parameter values; for O_h-symmetry the parameters B_0^4 and B_0^6 were freely varied but B_4^4 and B_4^6 were constrained by the relations $B_4^4/B_0^4 = 5/\sqrt{70}$ and by $B_4^6/B_0^6 = -\sqrt{7}/2$; P^2 was freely varied but P^4 and P^6 were constrained by the relations $P^4/P^2 = 0.75$, $P^6/P^2 = 0.5$.

b. Data from Axe (1960); the Γ_8 level was assigned the value 1900 cm^{-1} in the indicated fit.

c. Data from Johnston *et al.* (1966a).

d. Data from Krupa *et al.* (1983).

e. Estimated from Krupa and Khan Malek (1983), Genet (1984), Delamoye *et al.* (1983), and Krupa *et al* (1983).

f. Data from Delamoye *et al.* (1983).

g. Data from Mackey *et al* (1975); the parameters are those determined by Mackey *et al.*

h. Data from Rajnak *et al.* (1984a); parameter values are those determined by Rajank *et al.*, with, in addition to those shown, $P^4 = P^6 = [500\ cm^{-1}]$.

The recent extensive analysis of the data for U^{4+}:$ThBr_4$ and the similar crystal-field parameters deduced for Pa^{4+}:$ThCl_4$, Krupa et al. (1983), Table 26, have provided a new basis for examining other An^{4+} spectra. For example, a reinterpretation of the spectrum of UCl_4, Gamp et al. (1983), has led to energy level parameters quite similar to those for U^{4+}:$ThBr_4$. An extrapolation of the new results for UCl_4 consistent with those for Pa^{4+}:$ThCl_4$, with some adjustment of the parameters to fit partial data for U^{4+}:$ThCl_4$, Krupa and Khan Malek (1983), Krupa et al. (1983), and Genet (1984), leads to the estimate of parameters for U^{4+}:$ThCl_4$ also given in Table 26. The parameters for several other cases are included for reference in the table. The results for Pa^{4+}:Cs_2ZrCl_6, Axe (1960), are related to those for Cs_2UCl_6, while the parameters for U^{4+}:$ZrSiO_4$ refer to a D_{2d}-site symmetry, but with a much larger field than for the $ThBr_4$ host, Richman et al. (1967), Mackey et al. (1975). A large field is also revealed in $U(BD_4)_4$, Rajnak et al. (1984a), Bernstein and Keiderling (1973).

When comparing the magnitudes of different crystal-field strengths it is convenient to use a generalization of Auzel's scalar crystal-field strength parameter, N_v, Auzel and Malta (1983), where

$$N_v/_{(4\pi)^{1/2}} = N'_v = \left[\sum_{k,q} (B_q^k)^2/2k+1 \right]^{1/2}$$

For example N'_v for U^{4+}:$ThBr_4$ = 1617 cm^{-1} while for U^{3+}:$LaCl_3$, N'_v = 605 cm^{-1}. Since both can be considered relatively weak field cases, the comparison is not unreasonable in indicating a much larger splitting in quadrivalent compared to trivalent ions. Both Cs_2UCl_6 with N'_v = 3363 cm^{-1} and $U(BD_4)_4$/ $Hf(BD_4)_4$ with N'_v = 4283 cm^{-1} are strong field cases, as is U^{4+}:$ZrSiO_4$, N'_v = 3113 cm^{-1}. As a group, they exhibit much more complex structure with states of different J-values in close proximity in a given energy range compared to the more isolated purer SLJ states characteristic of U^{4+}:$ThBr_4$, as indicated in Figure 21.

The energy level structure computed for U^{4+}:$ThBr_4$ appears to give a relatively good correlation with the observed spectrum of U^{4+}(aquo), as represented in Figure 21 by centers of gravity of observed absorption bands; the results for U^{4+}:$ThCl_4$ provide an even better approximation of the U^{4+}(aquo) ion level scheme. Actually Auzel et al. (1982) were able to show that the band intensities in the spectrum of U^{4+}(aquo) could be usefully interpreted based on the energy level structure in U^{4+}:$ThBr_4$. This type of analysis would not have been expected to be successful in cases where more extensive J-mixing is indicated, as in Cs_2UCl_6. Jørgensen pointed out some of the "enigmatic aspects" of the U^{4+}(aquo) ion spectrum in a paper published the same year as the Auzel analysis, Jørgensen (1982a).

Comparison of U(IV) spectra in aqueous solution and in molten LiCl-KCl eutectic with that for single crystals of Cs_2UCl_6 had earlier led Gruen and

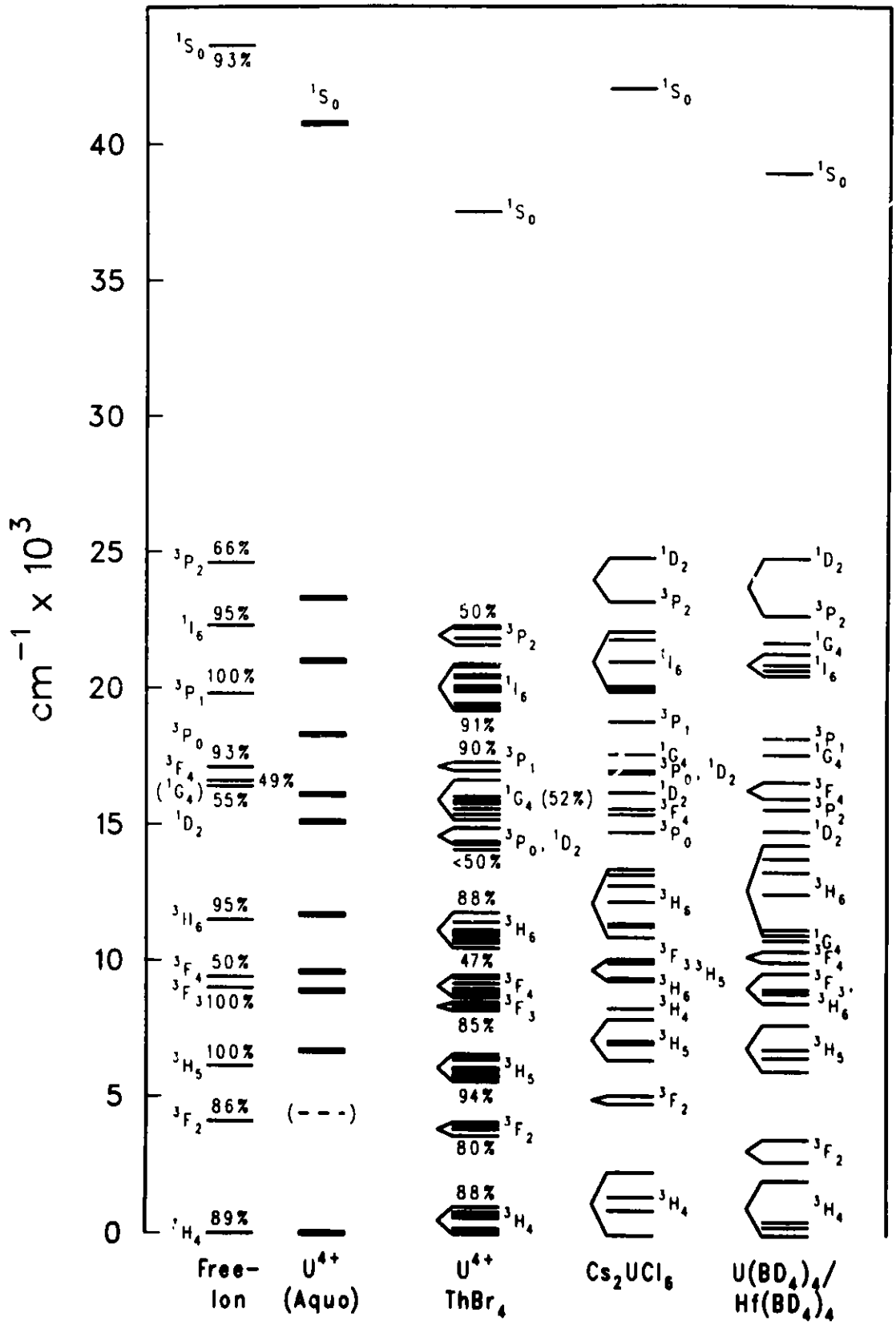

Fig. 21. Energy Level Schemes for U(IV) Species.

McBeth (1959) to suggest a change from 8-fold to 6-fold coordination as the basis for the contrasting spectroscopic results.

If we examine the spectra of U^{3+}(aquo) and Np^{4+}(aquo), both $5f^3$ ions, Figure 22, we find further evidence for interpretation in the weak field limit based on the apparent similarities in the band structure. If it is assumed that the crystal-field splitting in both U^{3+}(aquo) and Np^{4+}(aquo) is relatively small, the apparent shift of corresponding band structure to higher energies in Np^{4+}(aquo) compared to U^{3+}(aquo) is consistent with the expected greater electrostatic and spin-orbit interaction in the Np^{4+} case. That the similarities between band structure observed for iso-f electronic An^{4+}(aquo) and An^{3+}(aquo) ions continues along the series is evident in comparing the spectra of Pu^{4+}(aquo) and Np^{3+}(aquo), Figure 23. Jørgensen (1959) called attention to this type of correlation at a time when much less was known about the extent of the ligand fields involved. While difficult to rationalize in the strong field case, a weaker field in An^{4+}(aquo) similar to that in An^{3+}(aquo) does provide a reasonable basis for understanding the observed similarities in absorption features. Regions of absorption in the spectrum of $PuCl_4$(g) at 928°C are similar to those found in Pu^{4+}(aquo), Gruen and DeKock (1967).

If we adopt the approximate energy level parameters for U^{4+}:$ThCl_4$ in Table 26 as a basis for estimating parameters for the solution spectra of all of the An^{4+} ions, the resulting model parameters are those shown in Table 27. The free-ion energy level structure at <25000 cm^{-1} for the An^{4+} ions as computed using the parameters of Table 27 is then shown in Figure 24. This structure in turn correlates well with the collected solution absorption spectra of An^{4+} ions in Figure 25. An earlier estimate of the interaction integrals characteristic of An^{4+} gave values of F^2 much smaller and values of zeta somewhat larger than those indicated in Table 27, Conway (1964a). It can be seen from the results given in Table 28 that the increase in the electrostatic and spin-orbit parameters estimated for Np^{4+} with respect to the iso-f electronic trivalent ion U^{3+}, is of the same order that was deduced for the reduction of trivalent ion parameters to approximate the data for divalent ions, Table 21, except for F^6.

While in the case of the trivalent actinides the spectrum of the aquo ion of each member of the series from U^{3+} through Es^{3+} could be obtained to give a useful basis for comparison of band energies and intensities, such aquo ion comparisons are limited for An^{4+}. Starting with Am^{4+}, the spectra in Figure 25 are of the ion stabilized in a concentrated CsF-HF solution or for the pure tetrafluoride in the case of BkF_4. Useful Am(IV) and Cm(IV) spectra have also been recorded in H_3PO_4 solutions with absorption features in the visible range similar to those in the fluoride salt solution, Yanir et al. (1969), Myasoedov et al. (1973). Nevertheless the correlation between observed band features and those predicted by the model calculation for the lower energy range is satisfactory. This is not unexpected since in many systems F^- and H_2O coordination give rise to similar spectroscopic

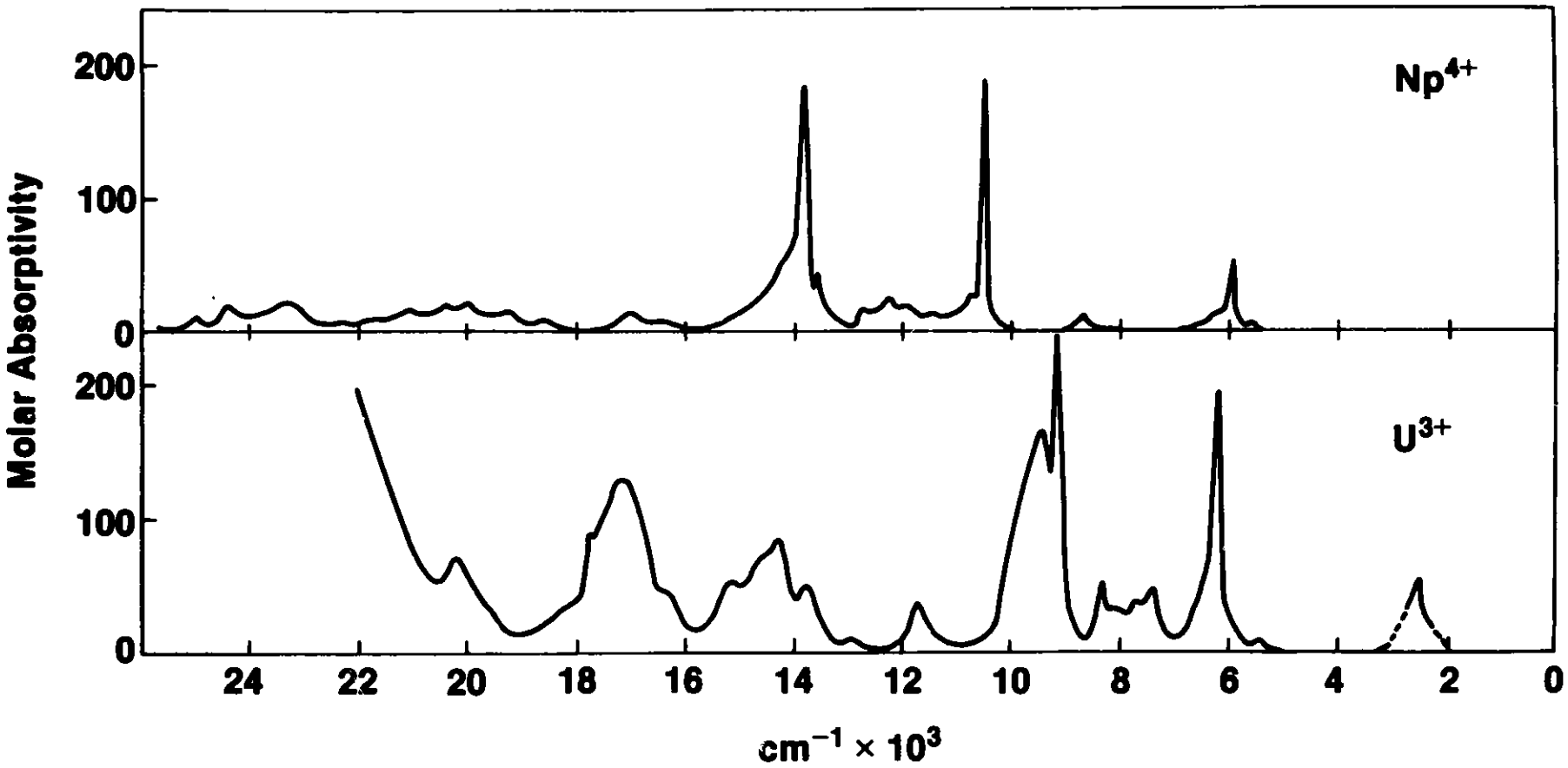

Fig. 22. Solution Absorption Spectra of Np^{4+}(aquo) and U^{3+}(aquo).

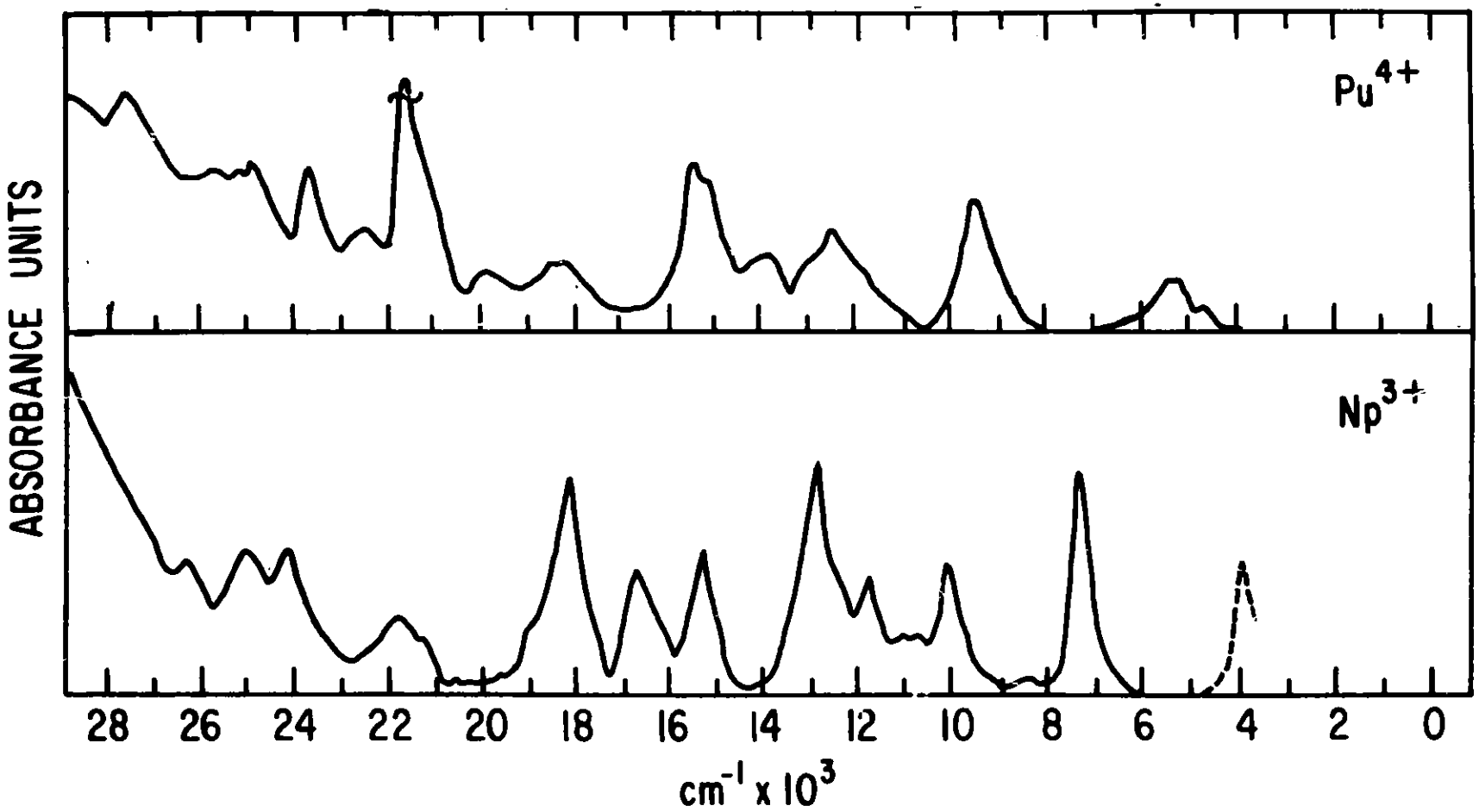

Fig. 23. Solution Absorption Spectra of Pu^{4+}(aquo) and Np^{3+}(aquo).

TABLE 27.

Energy Level Parameters (all in cm^{-1}) for An^{4+} Based on Consistent Predictive Model[a]

	U^{4+}	Np^{4+}	Pu^{4+}	Am^{4+}	Cm^{4+}	Bk^{4+}	Cf^{4+}	Model Δ-Value
F^2(HFR)[b]	76724	79892	82908	85817	88625	91338	93984	
F^2(Est)[c]	42918	46090	49110	52020	54825	57540	60185	
ΔP	33806	33802	33798	33797	33800	33798	33799	33800
F^4(HFR)	50199	52330	54356	56307	58188	60003	61772	
F^4(Est)	39873	42000	44030	45980	47860	49670	51440	
ΔP	10326	10330	10326	10327	10328	10333	10332	10330
F^6(HFR)	36860	38452	39965	41423	42827	44181	45500	
F^6(Est)	25588	27180	28695	30150	31555	32910	34230	
ΔP	11272	11272	11270	11273	11272	11271	11270	11270
ζ(HFR)	2110	2397	2697	3014	3347	3697	4064	
ζ(Est)	1810	2095	2395	2715	3045	3395	3765	
ΔP	300	302	302	299	302	302	299	300

a. In addition to the free-ion parameters shown, the following parameter values (in cm^{-1}) were used in all calculations: $\alpha = 30.12$, $\beta = -660$, $\gamma = 1200$, $B_0^2 = -1129$, $B_0^4 = 1793$, $B_4^4 = -2617$, $B_0^6 = -3016$, $B_6^6 = 342$. $P^2 = 500$, $P^4 = 375$, $P^6 = 250$. For $5f^N$ where $N > 3$, three-body parameters were included and the values assigned were: $T^2 = 200$, $T^3 = 50$, $T^4 = 100$, $T^6 = -300$, $T^7 = 400$, $T^8 = 350$.

b. Computed using Hartree-Fock methods and including an approximate relativistic correction, Cowan and Griffin (1976), Crosswhite (1977).

c. Parameter value used to compute the energy level structure. The set for U^{4+} was estimated for U^{4+}:$ThCl_4$, Krupa and Khan Malek (1983), Genet (1984), based on extrapolation of results for U^{4+}:$ThBr_4$, Delamoye *et al.* (1983) and Pa^{4+}:$ThCl_4$, Krupa *et al.* (1983).

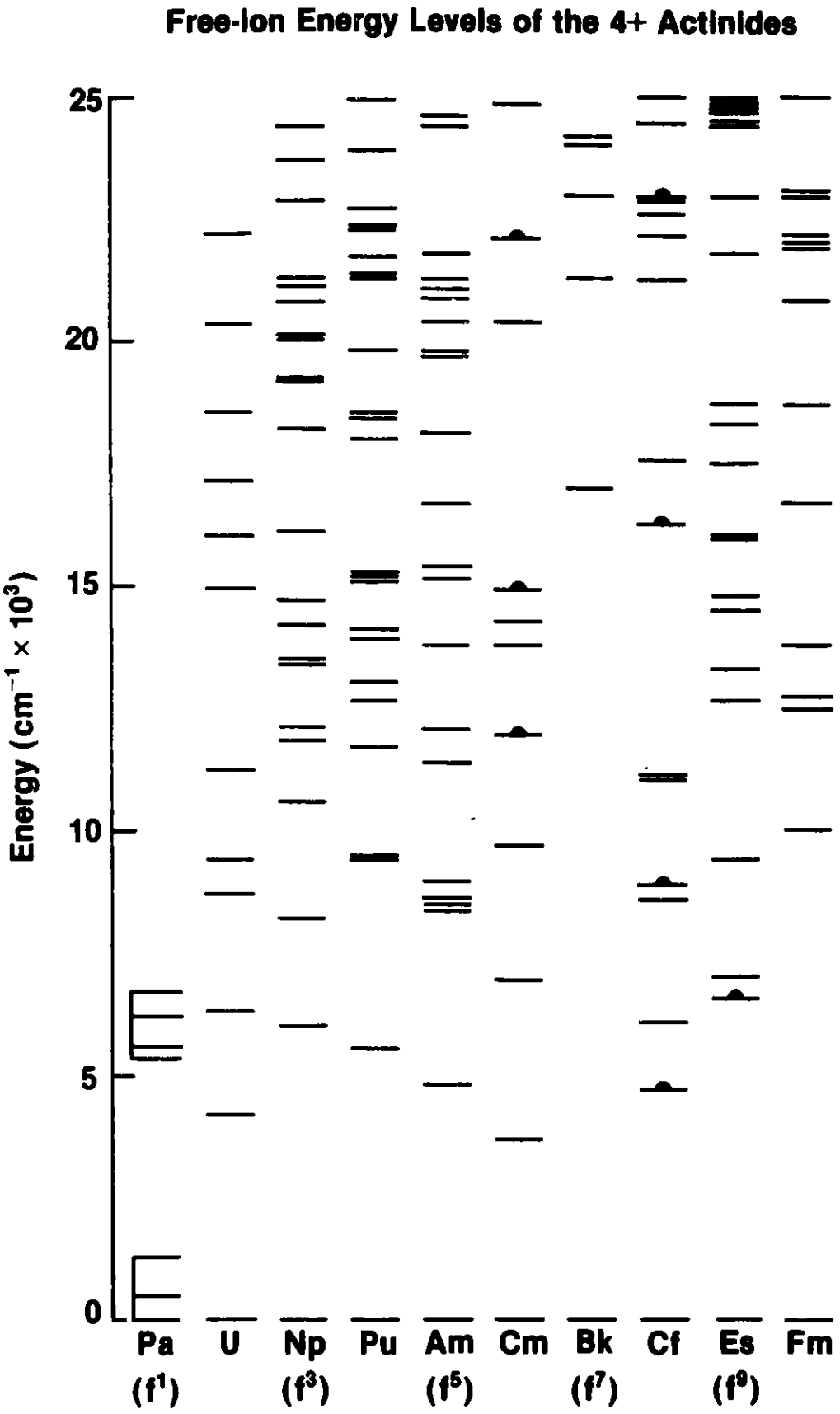

Fig. 24. Computed Free-ion Energy Levels for An^{4+}.

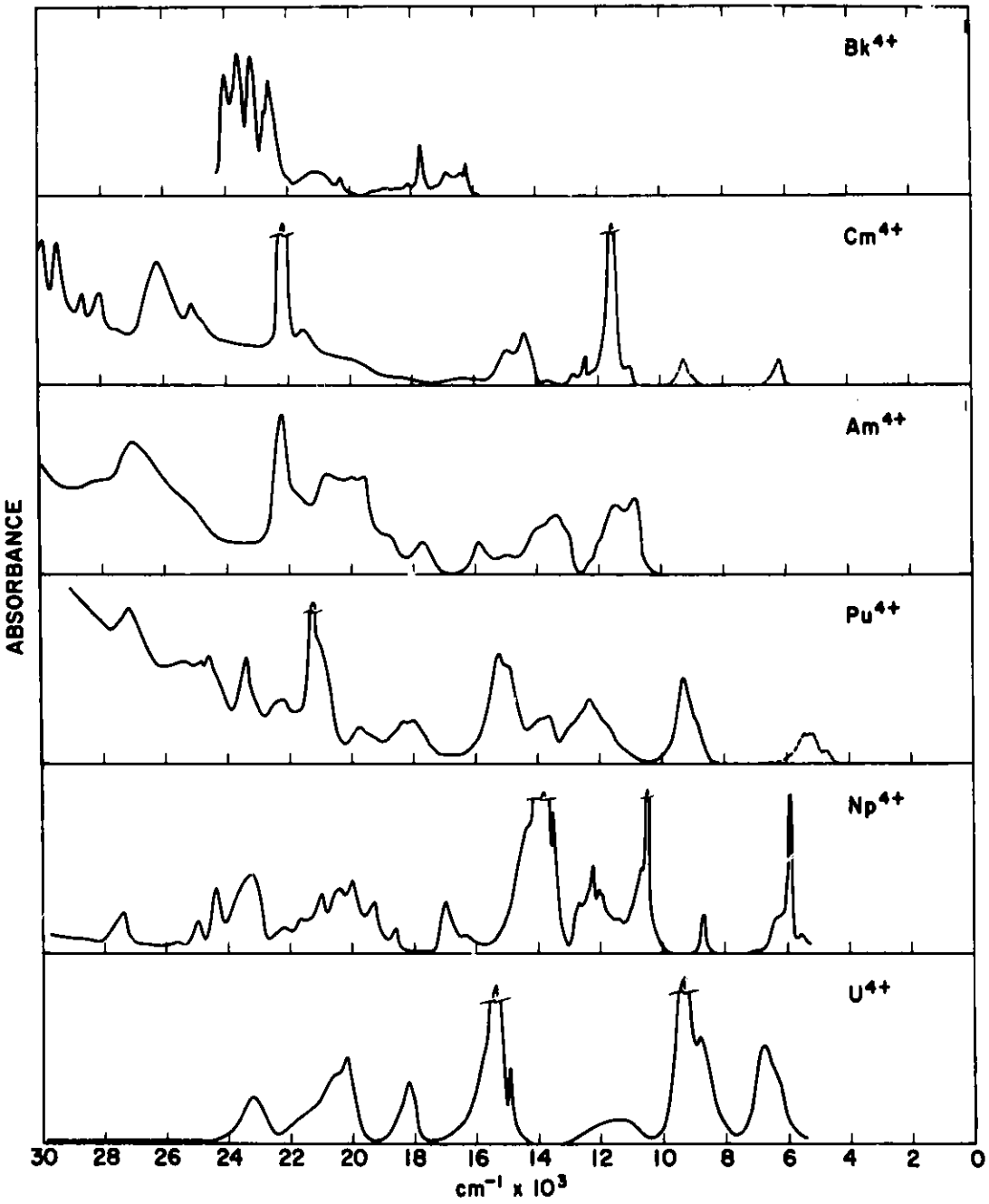

Fig. 25. Absorption Spectra of the Quadrivalent Actinides: U^{4+}:1 M $DClO_4$, [Cohen and Carnall (1960)], Np^{4+}: 1 M $DClO_4$, Waggener (1958), Pu^{4+}: 1 M $DClO_4$, Cohen (1961); ---LiCl-KCl Eutectic at 480°, Swanson (1964); Am^{4+}:15 M NH_4F, Asprey and Penneman (1961); Cm^{4+}:CmF_4, Asprey and Keenan (1958); 15 M CsF, Keenan (1961), BkF_4, Ensor et al. (1981).

TABLE 28.

Comparison of the Magnitudes of the Electrostatic and Spin-Orbit Parameters for An^{4+}, An^{3+}, and An^{2+} (in cm^{-1})

	Np^{4+} ($5f^3$)	U^{3+}:$LaCl_3$ ($5f^3$)	% Increase/Decrease in An^{3+} Parameter
F^2	46086	39715	16
F^4	42004	33537	25
F^6	27180	23670	15
ζ_{5f}	2097	1623	29
	Pu^{3+}:$LaCl_3$ ($5f^3$)	Np^{2+} ($5f^3$)	
F^2	48670	42300	15
F^4	39188	30300	13
F^6	27493	22300	12
ζ_{5f}	2241	1772	13

observations. The spectra of NpF_4 and Np^{4+} in a concentrated CsF-HF solution are shown for comparison in Figure 26. While there are some differences in band shapes and intensities, it is apparent that within the range that can be compared there are strong similarities in the regions of absorption.

In solid compounds such as Cs_2UCl_6 where the 4+ ions occupy sites of inversion symmetry the observed structure is almost exclusively vibronic in character in contrast to the electronic transitions characteristic of most 3+ compounds. The energy level analysis of Cs_2UCl_6 has been described by Satten et al. (1965) and Johnston et al. (1966a). More recently a corresponding intensity analysis was reported by Satten et al. (1983). The electronic origins were deduced from progressions in the vibronic structure, since the electronic transitions were symmetry-forbidden. In some regions, the spectra were too complex to be analyzed, or the transitions associated with predicted states may have been too weak to be observed.

One might have expected the analysis of the spectrum of Cs_2UCl_6 and its precurser, Pa^{4+}:Cs_2ZrCl_6, to serve as a model for Cs_2AnCl_6 where An = Np or Pu. While there is apparently no change in the crystal structure revealed in X-ray studies of samples of the three compounds, An = U, Np, and Pu, it is apparent that the spectrum of Cs_2NpCl_6 does not exhibit the vibronic structure patterns so characteristic of Cs_2UCl_6. It has been suggested that inversion symmetry has been lifted for many of the optical levels in the Np compound, and that the crystal-field splitting is a factor of two smaller than for the Pa^{4+} and U^{4+} analogs, Menzel and Gruber (1971). Further, it was reported that the spectrum of Np^{4+} in $[(C_2H_5)_4N]_2NpCl_6$ is very similar to that of Cs_2NpCl_6, Menzel et al. (1972). It would appear to be profitable to examine individual spectra in greater detail to determine whether a more systematic analysis of Cs_2AnCl_6 spectra can be offered. In each case the crystal field interaction must be treated as an integral part of the calculation of the energy level structure for An^{4+}.

With increasing valence state, the relative importance of the crystal-field interaction increases. The magnitude of the crystal-field in An(IV) compounds appears to intrinsically exhibit a larger variation with increasing Z than that found in the An^{3+}:$LaCl_3$ case. The latter is shown, for example, in comparing the results for Cs_2UCl_6 and Cs_2NpCl_6, Menzel and Gruber (1971). The change in the magnitude of the crystal-field interaction appears to be similar whether it arises as a result of increasing charge state of the central ion while maintaining the same ligand environment, or whether the charge state and identity of the central ion remains constant and the covalency of the ligands is varied. In a comparison of the energy level parameters for $[(C_2H_5)_4N]_2AnX_6$ with An = Pa, U and X = F, Cl, Br, and I, Wagner et al. (1977), a decrease in the Slater parameter F^2 was noted for An =U, but could not be established for zeta for either An = Pa or U. The only marked change was between X = F and Cl, suggesting that structural

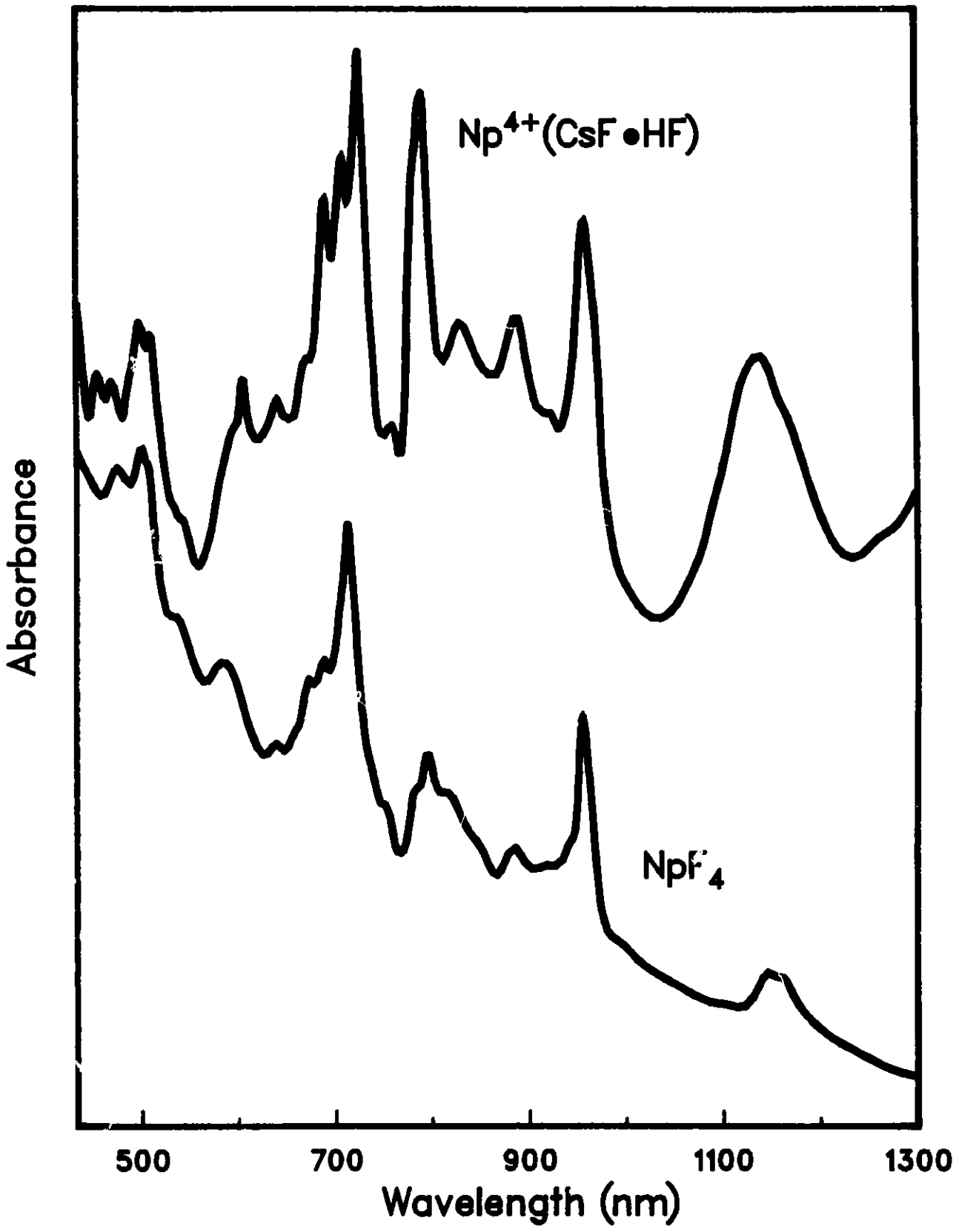

Fig. 26. Absorption Spectrum of NpF_4 and of Np^{4+} in CsF-HF Solution.

differences may have been an important consideration in this instance. The changes in the energy level parameters for a given ion and set of ligands with structural (symmetry) changes, Figure 21, are considerably larger than that referred to above with respect to changing ligands while maintaining the symmetry.

The crystal field strength of the borodeuterides of U^{4+} and Np^{4+} is considerably greater than that of the tetrachloride or tetrabromide and comparable to Cs_2AnCl_6. This is a further example of a spectrum that is largely vibronic in character, but in the T_d symmetry exhibited in this case the origins are allowed. The original $U(BD_4)_4$ optical data of Bernstein and Keiderling (1973) was recently reanalyzed by Rajnak et al. (1984a). It also proved to be possible to interpret $Np(BD_4)_4$ spectra with parameters which were consistent with those for the U-analog, Rajnak et al. (1984b). However the resulting interpretation required the assignment of several weak origins with stronger associated vibronics. An intensity analysis would be necessary to confirm these assignments. If they are correct, the one-particle crystal-field model is clearly adequate for the interpretation. If they are incorrect, the borodeuterides would appear to present a case in which the one-particle crystal-field parameterization is clearly inadequate to a consistent interpretation of the structure.

It is remarkable that in studies of the 4+ actinides, the only reported fluorescence from a U^{4+} compound has been that from U^{4+} in the $ThBr_4$ host, Delamoye et al. (1979). The fluorescence of Np^{4+} in both $ThCl_4$ and $ThBr_4$ has also been reported, Gruber and Menzel (1969).

6.0. Spectra of Actinide Ions in the (V), (VI) and (VII) Valence States

The actinide ions with well-defined, stable, and readily accessible valence states greater than IV are confined to the light half of the 5f-series. A large number of stable compounds are known, and spectra have been recorded in solutions, in the gas phase, as well as in solids. However, there have been relatively few attempts to develop detailed energy-level analyses except for the least-complex cases.

Two types of ionic structure are normally encountered in the higher valent species: the actinyl ions AnO_2^{+} and AnO_2^{++}, and binary and complex halides such as UCl_5, $CsUF_6$, and PuF_6. Mixed oxohalide complexes are also known. In the actinyl ions (An = U, Np, Pu, Am) the axial field imposed by the two nearest-neighbor (-yl) oxygen atoms plays a dominant role in determining the observed energy level structure, Eisenstein and Pryce (1966), Denning et al. (1980, 1985). The analysis of higher-valent actinide halide spectra must incorporate a strong ligand-field interaction, but frequently the analysis is made simpler because the symmetry is octahedral or can be assumed to be approximately octahedral, Eichberger and Lux (1980), Eisenstein and Pryce (1960), Goodman and Fred (1959), Kugel et al. (1976). Typical iso-f-electronic penta- and higher-valent actinide species are noted in Table 29.

TABLE 29.

Iso-f-Electronic Penta- and Higher-Valent Actinide Species

Number of 5f electrons	0	1	2	3	4
	UO_2^{2+}	UO_2^{+}	PuO_2^{2+}	AmO_2^{2+}	AmO_2^{+}
	Np(VII)	NpO_2^{2+}	NpO_2^{+}	PuO_2^{+}	
	UF_6	Pu(VII)	PuF_6	PuX_6^{-}	
	UCl_6	NpF_6	NpX_6^{-}		
		UX_6^{-}			
		UF_5			

X = is a halide ion.

While the results of the Hartree-Fock calculations given in Tables 1-4 extend through the hexavalent state, and can be carried out for any arbitrary state of ionization, the relative importance of the ligand field must also be established in order to develop a useful correlation to experimentally observed spectra. Some insight into the increasing magnitude of the crystal-field and of the spin-orbit interaction with increasing charge state can be gained from the comparison of energy level structures for f^1-configurations shown in Figure 27. Ab initio models of the crystal-field interaction that accurately reproduce, and offer a predictive interpretation of the results of parametrized fits to experimental data, are very difficult to construct and are not generally available. The available spectra of penta- and higher-valent actinides are strong crystal-field cases and the development of correction terms for even the parametrized first-order crystal-field model may well be essential to extensive detailed analysis.

For purposes of the comparisons shown in Figure 27, the energy level structures are all high symmetry O_h or near O_h-cases. Well characterized comparable results for the An^{3+} member of the series, Th^{3+}, are of course not available. We assume that such results would evidence a splitting of a factor of two larger than that shown for Ce^{3+}, but this would still be significantly less than that for the Pa^{4+} case shown. Of course, two effects are involved in the obvious increase in splitting with charge state: the increase in magnitude of the spin-orbit coupling, and the increase in the crystal-field itself. They are difficult to separate, although it appears that increased magnitude of the crystal-field is the principal effect.

Aqueous solution spectra characteristic of the NpO_2^+, and PuO_2^{++} ions, both having the $5f^2$-electronic structure, are shown in Figure 28. Some qualitative similarities in band patterns for these iso-f-electronic ions appear to exist, but detailed analysis of the observed structure in terms of a predictive model has not been published. Electron transfer bands for NpO_2^+, PuO_2^+ and AmO_2^+ apparently lie at such high energies that they have not been reported, but this type of transition in NpO_2^{2+} (20800 cm^{-1}), PuO_2^{2+} (19000 cm^{-1}), and AmO_2^{2+} (~18000 cm^{-1}) has been identified, Jørgensen (1970), Denning et al. (1982a). The spectra of all of the actinyl ions and tabulations of the molar absorptivities of the more intense bands in aqueous solution are given in existing reviews, Carnall (1971, 1982).

Attempts to interpret the spectra of the binary penta- and hexa-halides of the actinides have been published, but the results should be considered preliminary, and only U(V) and Np(VI) compounds, both $5f^1$, have been analyzed in any detail. The magnitude of the spin-orbit interaction is known for U VI. The free-ion spectrum has been interpreted in terms of a coupling constant, $\zeta_{5f} = 2173.9\ cm^{-1}$, based on a $^2F_{5/2} \rightarrow {}^2F_{7/2}$ energy difference of 7608.6 cm^{-1}, Kaufman and Radziemski (1976).

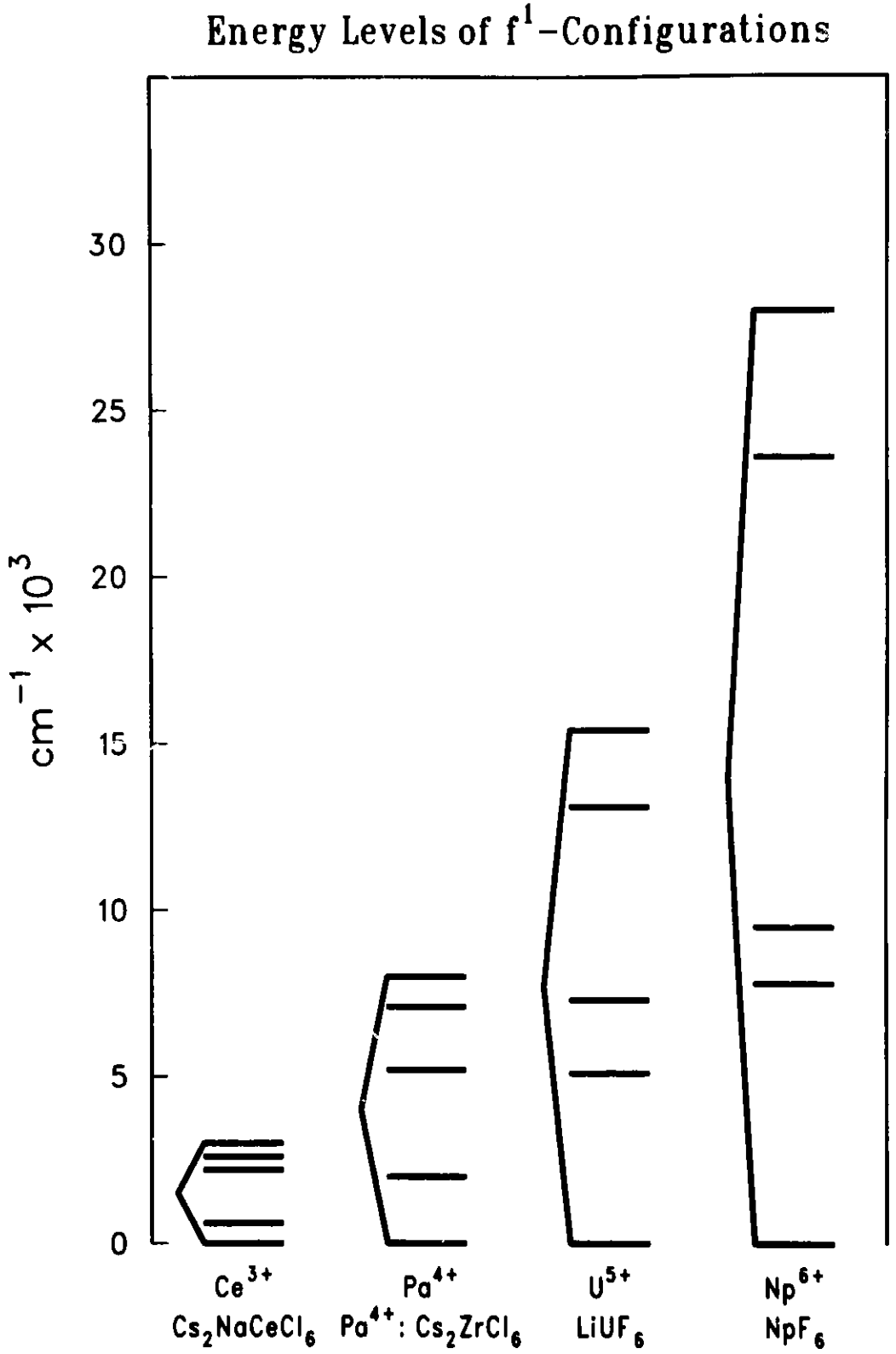

Fig. 27. Energy Levels of f^1-Configurations. Ce^{3+}:$Cs_2NaCeCl_6$, Richardson et al. (1985), Pa^{4+}:Cs_2ZrCl_6, Axe (1960); U^{5+}:$LiUF_6$, Hecht et al. (1985b), Np^{6+}:NpF_6, Goodman and Fred (1959).

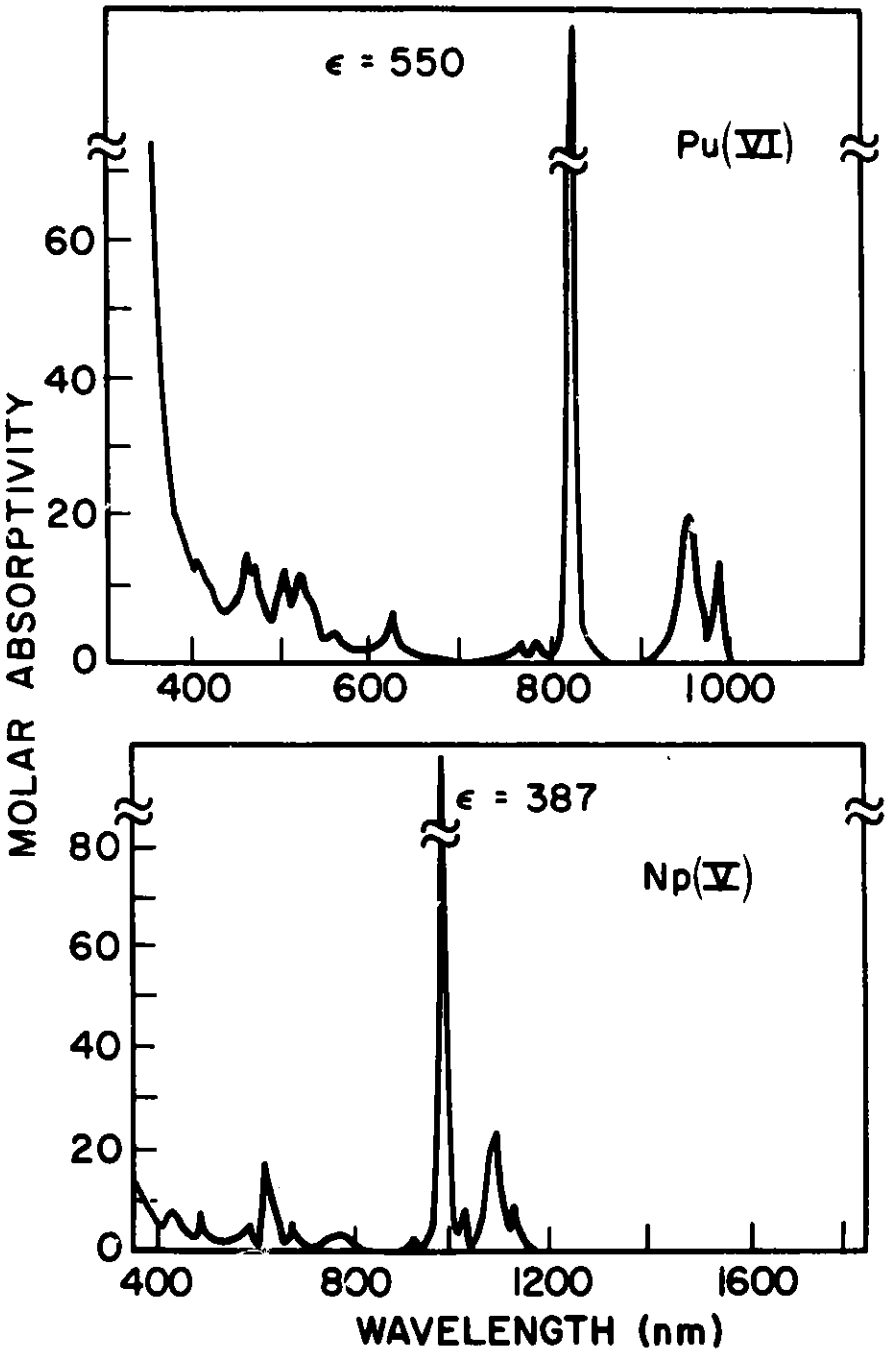

Fig. 28. Solution Absorption Spectra of Np(V) (aquo) and Pu(VI) (aquo). Pu(VI): 1 M $HClO_4$, Cohen (1961); Np(V): 1M $DClO_4$, Waggener (1958).

6.1. Binary and Complex Halides of An(V)

Although there are a number of published attempts to analyze An(V) spectra dating back to the early 1960's, it has been pointed out that in some instances experimental results and thus the interpretation must be questioned because of the presence of impurities. Of the existing analyses, with the exception of that for $CsNpF_6$, all involve U(V).

One of the striking features of the spectra of many of the U(V) compounds considered here is the great similarity in the pattern of the absorption bands. This similarity is apparent whether the spectra are observed in the solid state, in solution or in the gas phase. Thus the spectrum of $CsUF_6$ shown in Figure 29 can be recognized as characteristic of UCl_5 dissolved in $SOCl_2$, Karraker (1964), of UCl_5 single crystals, Leung and Poon (1977), and of the vapor phase $(UCl_2)_2$ or $UCl_5 \cdot AlCl_3$, Gruen and McBeth (1969). It is also recognized in $(C_6H_5)_4$ As UX_6 where X = F^-, Cl^-, or Br^-, Ryan (1971), as well as in $MUBr_6$ salts where M = Na, Cs, and $N(C_2H_5)_4$, Eichberger and Lux (1980). In each case the spectrum is attributed to the UX_6^- entity in nearly octahedral symmetry. However the spectrum of KUO_3 in which U(V) is stabilized in a cubic perovskite site also bears a striking resemblance to the spectra of the penta halides, Kemmler-Sack (1968). Spectra of $RbUBr_6$, Eichberger and Lux (1980) and of $UCl_5 \cdot Al_2Cl_6$ at 596 K, Gruen and McBeth (1969), are shown for comparison in Figure 30.

There have been two recent analyses of U(V)-containing compounds in which the absorption band structure is quite different from that in $CsUF_6$. In α-UF_5 the bond angles can be described in terms of an octahedron subjected to a tetragonal elongation (D_{4h}). The bonding in β-UF_5 is much more irregular with a structure intermediate between a dodecahedron and a square antiprism (D_{4d}), Penneman et al. (1973). Spectra of the two modifications are shown in Figures 31 and 32. Assuming a crystal-field dominated by weak covalent rather than electrostatic interactions, both spectra were analyzed using the angular overlap model relationships given by Urland (1976). The results are shown in Tables 30 and 31, Hecht et al. (1985a). Spectroscopic features attributed to UF_5 molecules generated by laser photolysis of UF_6 have been identified in the 14000-29000 cm^{-1} range, and also near 8000 cm^{-1}, Kim and Laguna (1981), but there appears to be no obvious correlation with the spectra of α-UF_5 and β-UF_5. The second case referred to above is that of $RbUF_6$ in which a crystal-field analysis in dodecahedral symmetry (D_{2d}) was carried out, Amberger et al. (1983). As was the case for UF_5, the molecular orbital approach was taken. These results are also included in Table 30 and 31.

Interpretation of spectra of the $CsUF_6$ type proves to be central to further systematic analysis of energy level structures in An(V) compounds since both $CsNpF_6$ and $CsPuF_6$ have been characterized as isostructural to $CsUF_6$, Penneman et al. (1973). In principle, UF_5 is the first member of another series that could be examined systematically, but while milligram

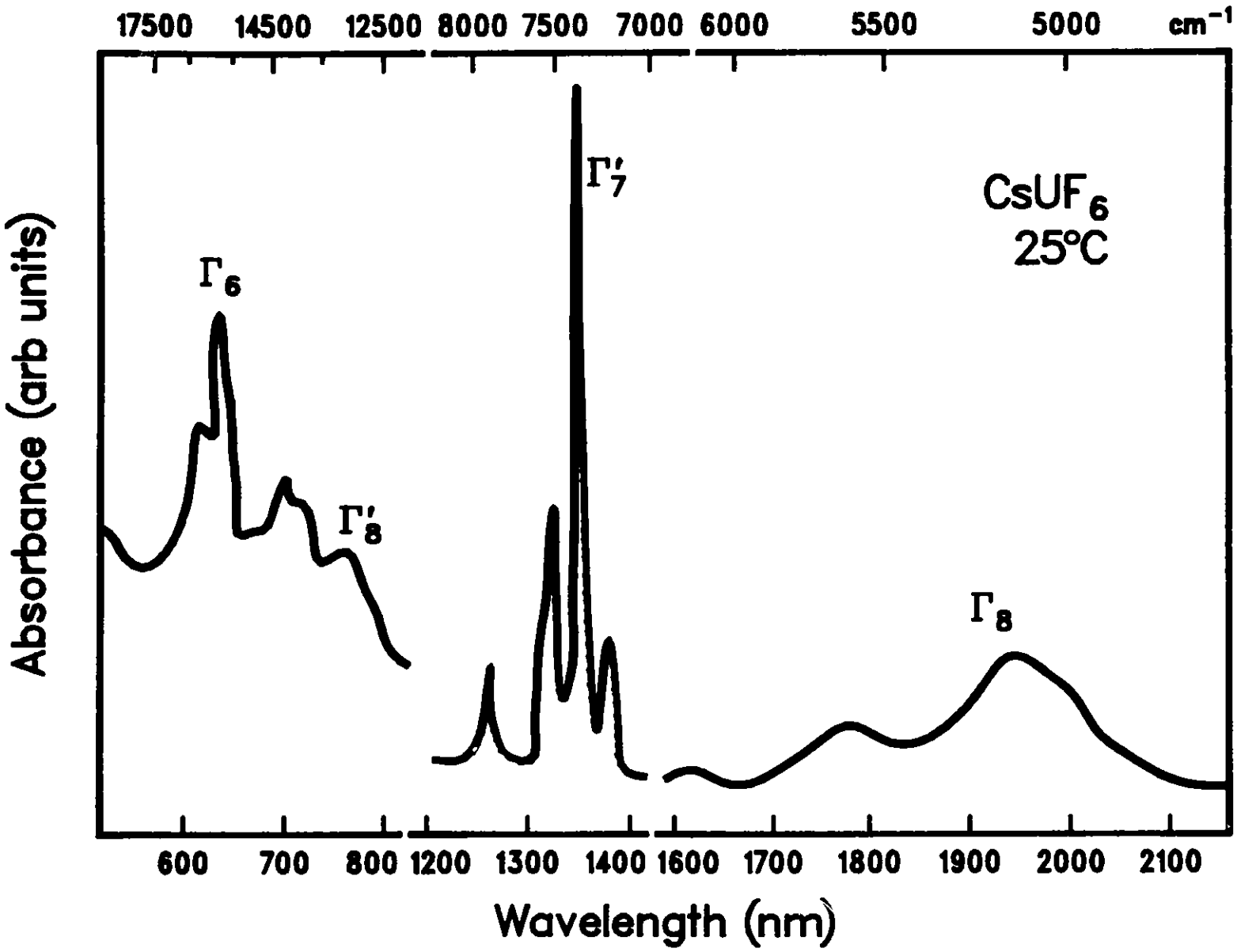

Fig. 29. Absorption Spectrum of $CsUF_6$.

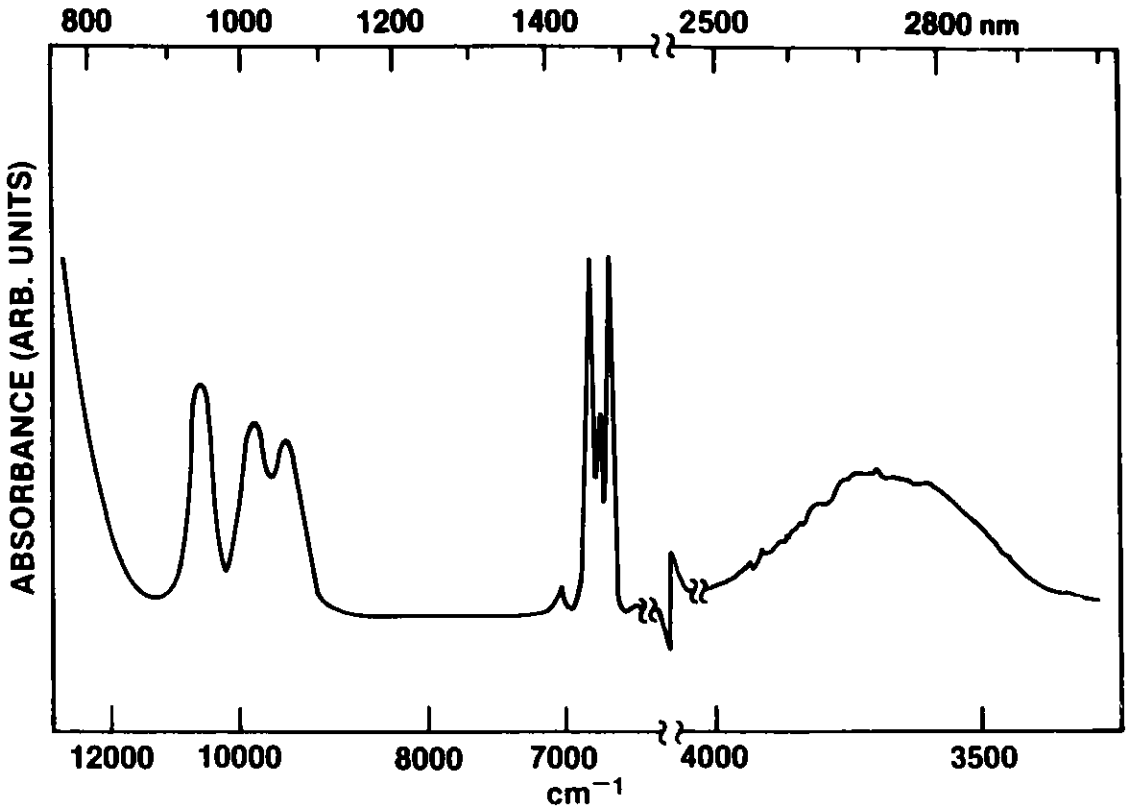

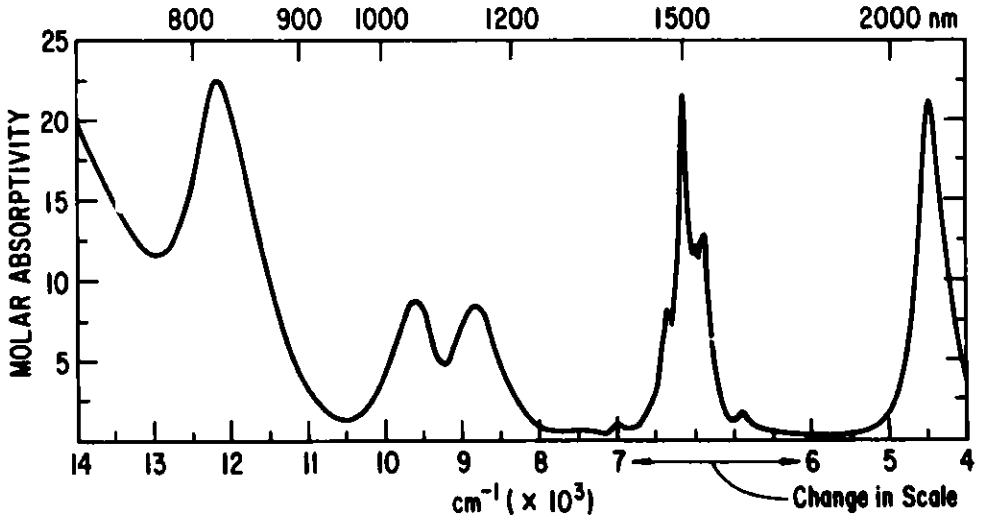

Fig. 30. Absorption Spectra of $RbUBr_6$ (Top), Eichberger and Lux (1980), and $UCl_5 \cdot Al_2Cl_6$ at 596 K, Gruen and McBeth (1969).

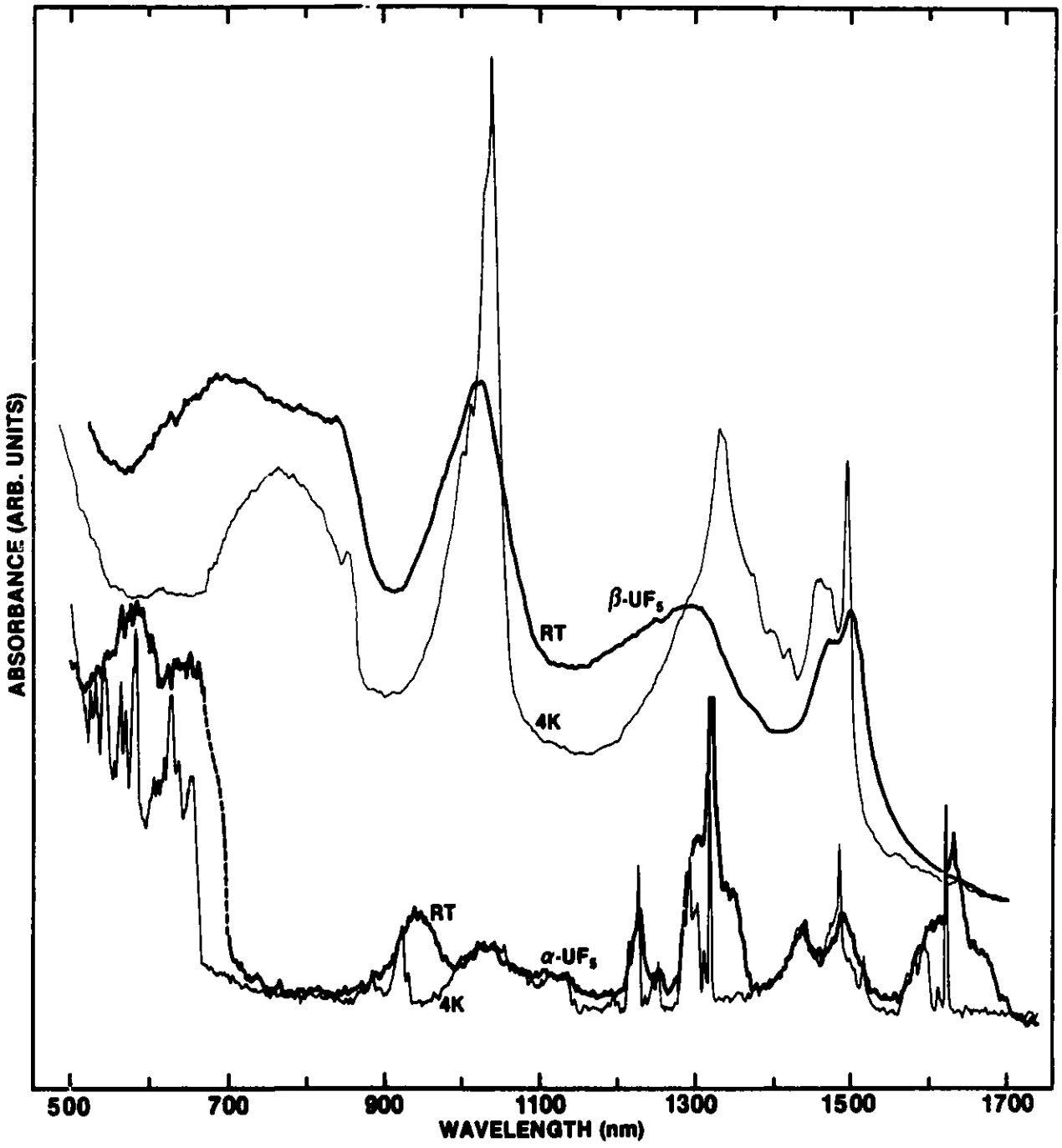

Fig. 31. Absorption Spectra of α-UF_5 and β-UF_5.

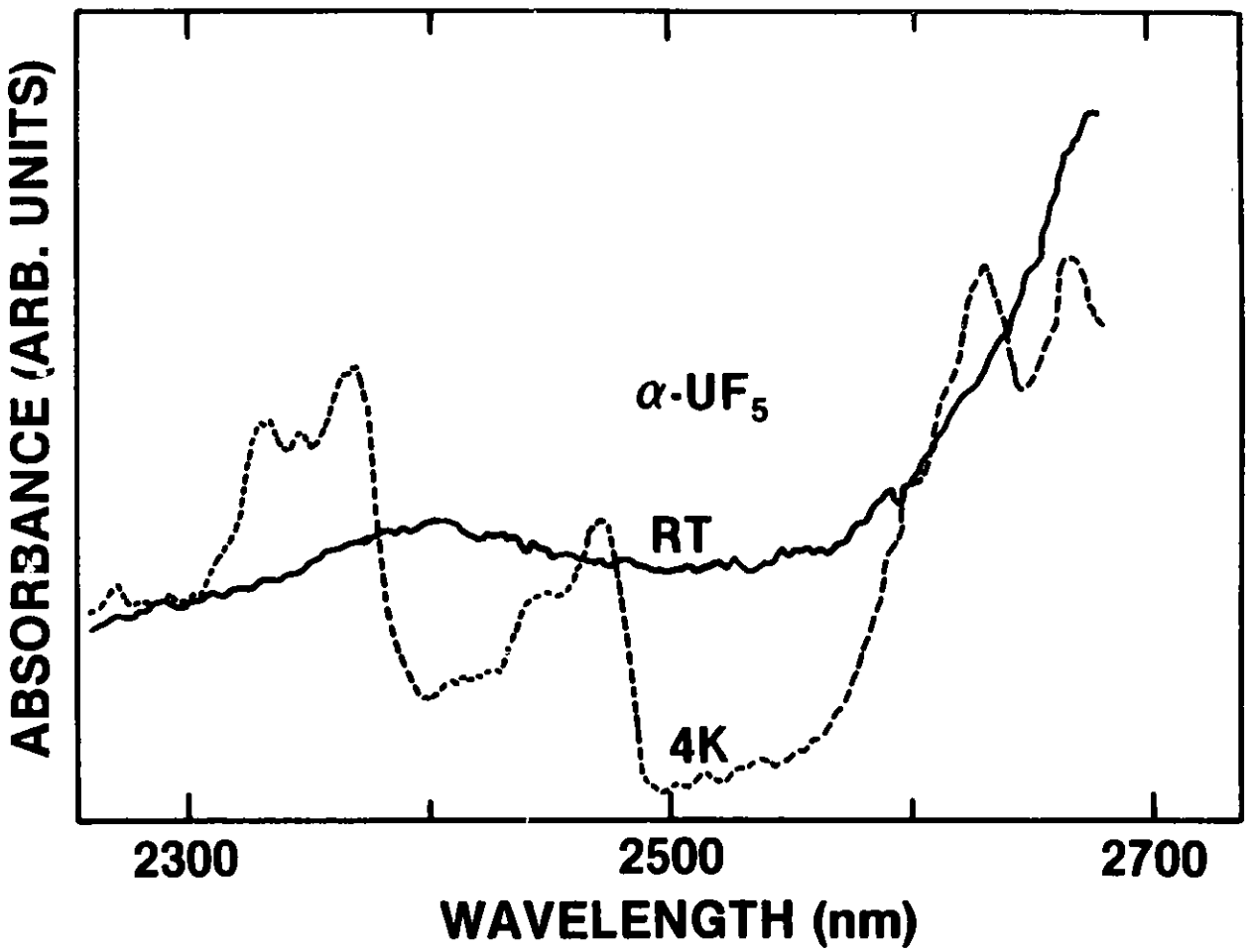

Fig. 32. Absorption Spectra of α-UF_5.

TABLE 30.

Observed and Calculated energy Levels for α-UF_5, β-UF_5, and $RbUF_6$ (all values in cm^{-1})

α-UF_5[a] D_{4h}		β-UF_5[a] D_{4d}		$RbUF_6$[b] D_{2d}	
Assigned Level	Calculated Level[c]	Assigned Level	Calculated Level	Assigned Level	Calculated Level
0	0 (Γ_7^-)	0	0 (Γ_{10}^-)	0	0 (Γ_6)
3650	3773 (Γ_6^-)	-	1136 (Γ_9^-)	1555	1549 (Γ_7)
6161	6030 (Γ_7^-)	-	3061 (Γ_{11}^-)	4599	4598 (Γ_6)
7579	7673 (Γ_7^-)	6671	6671 (Γ_{10}^-)	7087	7122 (Γ_6)
10730	10684 (Γ_6^-)	7474	7474 (Γ_8^-)	7952	7951 (Γ_7)
15152	14919 (Γ_7^-)	9434	9434 (Γ_{11}^-)	11001	11005 (Γ_6)
17182	17399 (Γ_6^-)	11601	11601 (Γ_9^-)	12500	12494 (Γ_7)

[a]Hecht *et al.* (1985a).

[b]Amberger *et al.* (1983).

[c]The parameters used to generate the levels are given in Table 31.

TABLE 31.

Crystal-Field and Spin-orbit Parameter Values

for α-UF_5, β-UF_5, and $RbUF_6$ (in cm^{-1})

	α-UF_5[a]	β-UF_5[a]	$RbUF_6$[b]
B_0^2	-5920	-1185	-5000
B_0^4	16442	-15354	5720
B_4^4	17786		±10518
B_0^6	-2986	3314	-4320
B_4^6	-6298		1212
ζ	1884	1926	1965

[a]Hecht et al. (1985a).

[b]Amberger et al. (1983).

amounts of NpF_5 were recently prepared and fully characterized for the first time, Malm et al. (1985), the successful synthesis and isolation of PuF_5 has not yet been reported. Because there have been a number of criticisms and reinterpretations of the original published spectrum of $CsUF_6$, extensive new experimental studies were carried out, Hecht et al. (1985b). This comprehensive reinvestigation included preparation and spectroscopic characterization of the isostructural compounds $LiUF_6$ and α-$NaUF_6$.

In their pioneering investigation of $CsUF_6$, Reisfeld and Crosby (1965) measured spectra at 298 and at 75 K. They assumed that the U-atoms were not at true O_h sites, but that the distortion was small enough to make it reasonable to model the spectra as if it were an O_h-case. The samples were examined as fluorolube mulls, and some decomposition to U(IV) was specifically cited; however, it was reported that corrections were made to the spectra such that features attributed to U(IV) were subtracted out.

The authors were convinced that structure to the low energy of strong absorption bands in the region near 2000 nm could not be attributed to "hot" bands; they ascribed it to vibrational modes that would not be populated at room temperature. They developed an interpretation which viewed the observed spectral bands as the result of the coupling of normal vibrational modes of the UF_6^- structure to zero phonon centers which themselves were weak or unobserved. Thus, electric dipole transitions in this nearly centrosymmetric environment were viewed as enabled by the simultaneous change of electronic state and a quantum of an odd vibronic mode of the UF_6^- group. A search for electronic centers enabled by strong vibrational modes led to the interpretation shown in Table 32.

Subsequent experimental studies of complex U(V) halides by others, particularly Ryan (1971), noted discrepancies between the spectrum of $CsUF_6$ as published by Reisfeld and Crosby, and that of other compounds containing the UF_6^--entity. Of relevance to the new experimental studies cited here, Ryan referred to work in progress by Morrey and Morgan on the spectra of hexahalide complexes of U(V) at liquid N_2 as well as at liquid He temperatures. This projected investigation was actually not completed, and thus was never published. In discussing the $\Gamma_7 \rightarrow \Gamma_8, + \Gamma_6$ spectral range, Table 32, Ryan was apparently among the first to point out one of the most serious experimental problems with the Reisfeld-Crosby study. By correcting for UF_4, they apparently also removed absorption features characteristic of $CsUF_6$.

Leung (1977) also addressed the $CsUF_6$ spectrum and the necessity for considering a D_{3d} instead of the O_h site symmetry. He used the Reisfeld and Crosby data with his own reinterpretation, finding as did Soulie (1978) that the energy level fit was inconsistent with a $\Gamma_7 \rightarrow \Gamma_6$ assignment near 14000 cm^{-1}. He assumed the corresponding band to be near 16000 cm^{-1} (unobserved).

TABLE 32.

Observed and Computed Energy Level Structure for $CsUF_6$ (in cm^{-1})

Vibrational Modes			Zero Phonon States[a]		
	(Ref. a)	(Ref. b)		OBS (cm^{-1})	CALC (cm^{-1})
ν_1 (A_{1g})	506	608	Γ_7	0	0
ν_2	-	452	Γ_8	4587	3989
ν_3 (T_{1u})	503	505	Γ_7'	6928	6928
ν_4 (T_{1u})	150	130*	Γ_8'	12705	12107
ν_5 (T_{2g})	145	190	Γ_6	14245	14840
		213			
ν_6 (T_{2u})	100	62*			

Parameters for E CALC (cm^{-1})[a]
ζ = 1955
A_4^o = 2351 (B_o^4 = -18808)
A_6^o = 208.8 (B_o^6 = 3341)

[a]Reisfeld and Crosby (1965).

[b]Hecht et al. (1985b). Asterik denotes value obtained from excited-state spectra.

The analysis of the $CsUF_6$ spectrum by Hecht et al. (1985b) is different in a number of respects from any of the interpretations that preceded it; nevertheless one recognizes that many of the concepts used in the analysis are not new. They have been cited by others in their attempts to understand certain aspects of the subject spectral type. The advantage of the reinvestigation lies in careful attention to the preparation of pure samples and in the experimental measurements which included for the first time complete spectra at ~ 4 K. The parallel interpretation of spectra of $LiUF_6$ and α-$NaUF_6$ served to amplify the $CsUF_6$ results.

A fundamental difference between the reinvestigation and previous observations is that structure at 4587 cm^{-1} was not observed. The $\Gamma_7 \rightarrow \Gamma_8$ transitions, assuming D_{3d} symmetry, but for convenience continuing to use the labels of O_h-symmetry, were placed at 5107 and 5203 cm^{-1}, and characterized as transitions due to a magnetic dipole mechanism, Figure 33. In agreement with Drifford and Soulie (1977) and Soulie (1977), the $\Gamma_{7'}$ state was placed at 7326 cm^{-1} where a moderately strong (magnetic dipole) transition is observed, Figure 34. In the region of the $\Gamma_{8'}$ and Γ_6 transitions, Figure 35, the spectrum of $CsUF_6$ does not correspond with the results of Reisfeld and Crosby undoubtedly for the reason cited by Ryan (1971).

Interpretation of the structure associated with the $\Gamma_7 \rightarrow \Gamma_{8'}$, Γ_6 transitions follows directly from that for $\Gamma_7 \rightarrow \Gamma_{7'}$, and $\Gamma_7 \rightarrow \Gamma_8$. In both cases the major features were found displaced from the zero phonon transitions by ~ 130 cm^{-1} and 505 cm^{-1}, consistent with the ν_4 and ν_3 modes proposed by others. A Raman spectrum of $CsUF_6$, together with an infrared spectrum establishing ν_3, gave a set of vibrational mode energies that contrasts with that assumed by Reisfeld and Crosby, Table 32. The assignments to zero phonon transitions, and the computed results based on D_{3d}-symmetry for the three compounds $LiUF_6$, α-$NaUF_6$, and $CsUF_6$ are given together with the parameter values in Table 33, Hecht et al. (1985b).

The energy level structures and parameters for several U(V) compounds are compared in Table 34. The ligand-field parameters in such analyses, Eichberger and Lux (1980), are sometimes reported in terms of Δ and Θ, linear combinations of the normal fourth and sixth degree crystal-field potential terms B_0^4 and B_0^6, together with the so-called orbital reduction factors k and k', Eisenstein and Pryce (1966). The orbital reduction factors provide a basis for discussing the covalency of the bonding. As indicated in Table 34, the data for several U(V) compounds have been analyzed in terms of a spin-orbit parameter of ~2200 cm^{-1} consistent with the free-ion results for U VI. However there has been considerable variation in the ligand-field parameters deduced by different investigators from absorption spectra in which the energies of observed features are surprisingly consistent.

Both the spectra of $CsNpF_6$, Hecht et al. (1979) and $CsPuF_6$, Morss et al. (1983) have been reported. The spectrum of $CsNpF_6$ as originally

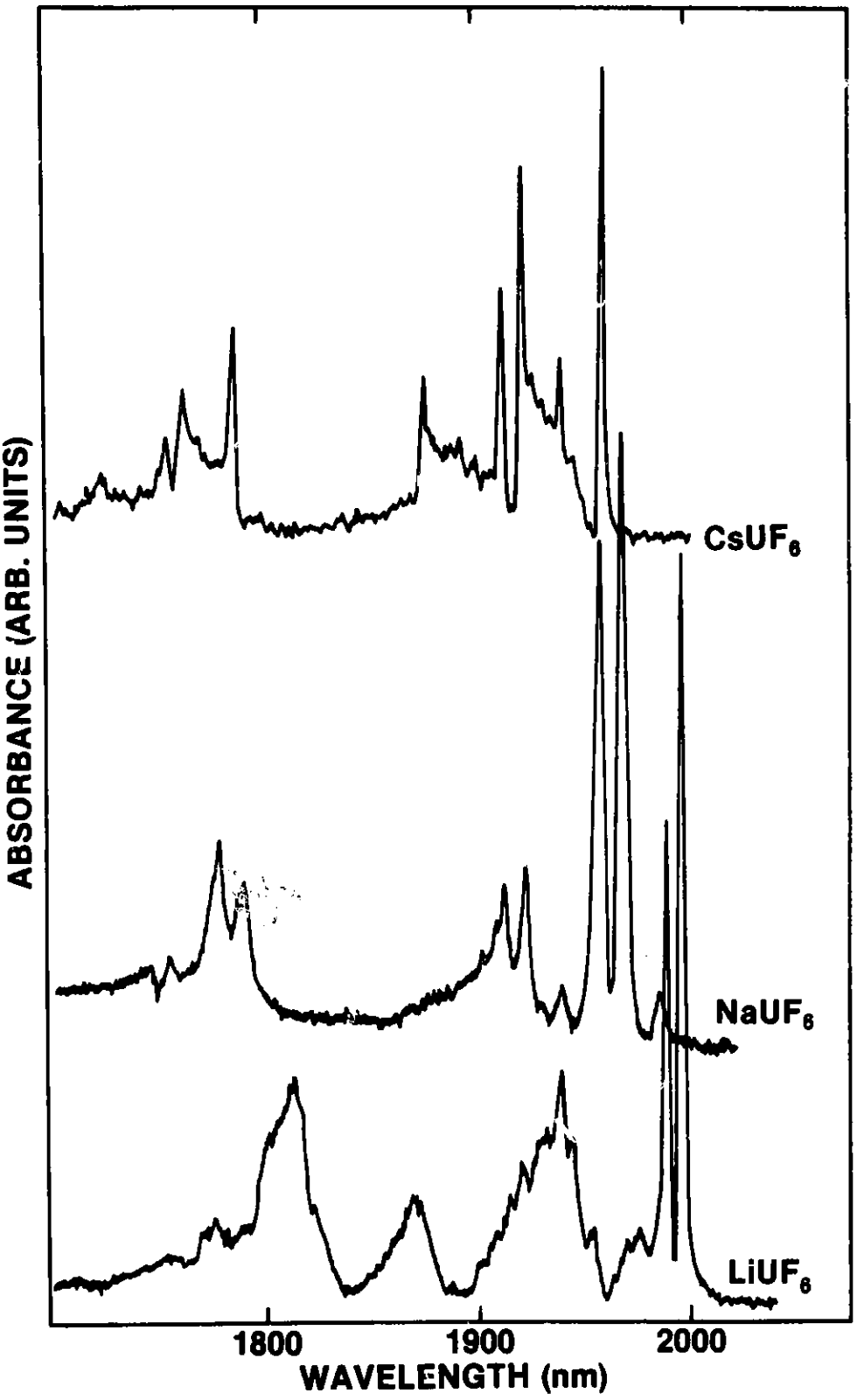

Fig. 33. Absorption Spectra of $LiUF_6$, α-$NaUF_6$ and $CsUF_6$ at 4 K in the 1700-2100 nm Range.

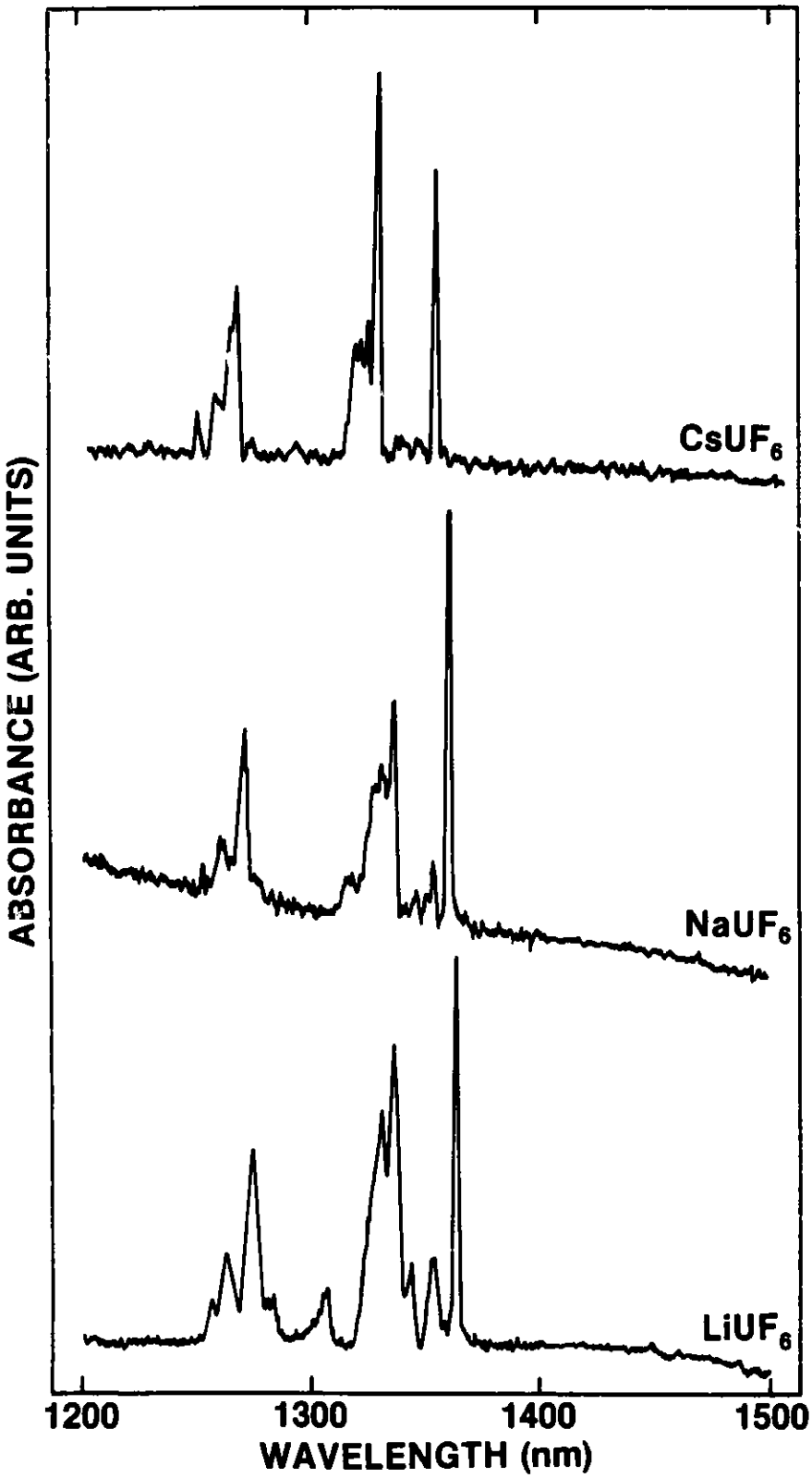

Fig. 34. Absorption Spectra of $LiUF_6$, α-$NaUF_6$ and $CsUF_6$ at 4 K in the 1200-1500 nm Range.

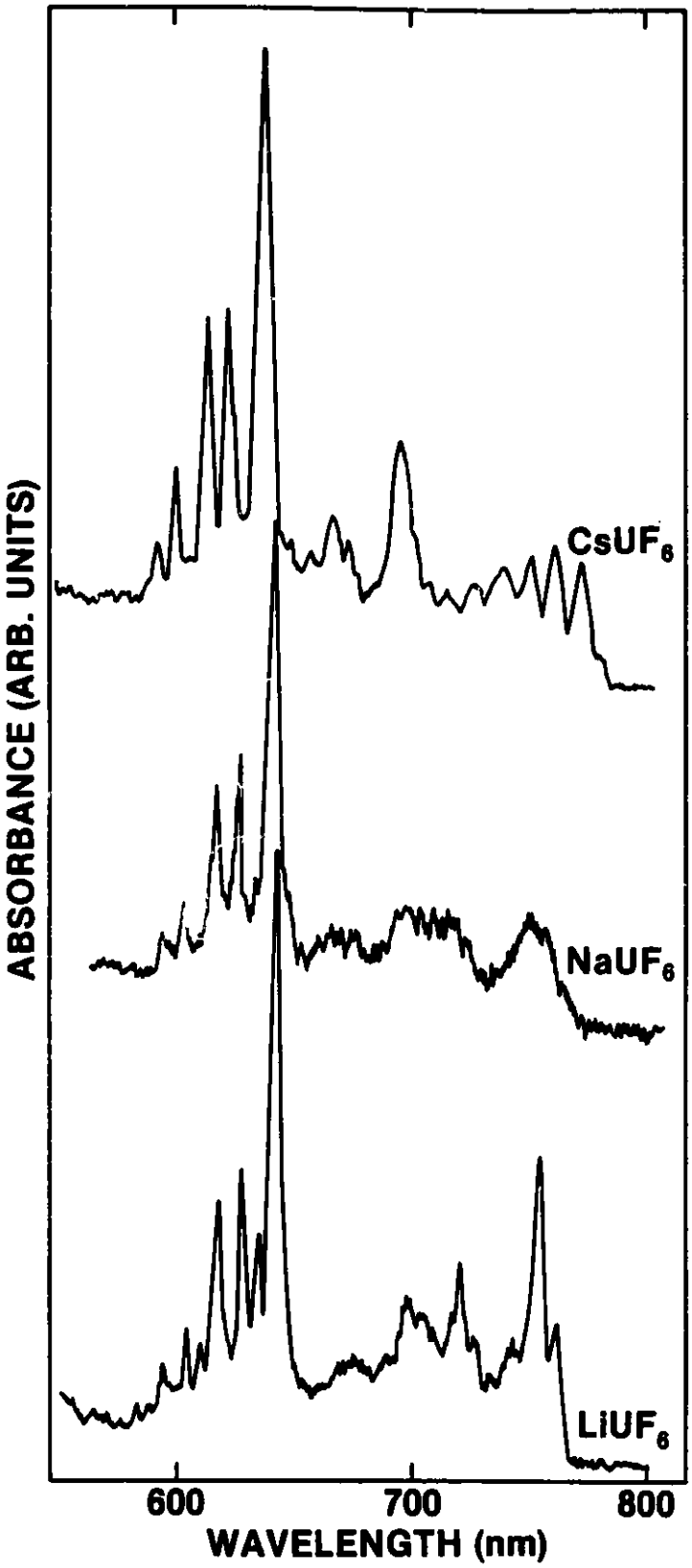

Fig. 35. Absorption Spectra of $LiUF_6$, α-$NaUF_6$ and $CsUF_6$ at 4 K in the 600-800 nm Range.

TABLE 33.

Energy Level Parameters for MUF_6 in D_{3d}-Symmetry (in cm^{-1})[a]

	$LiUF_6$		α-$NaUF_6$		$CsUF_6$		
	obs'd.	cal'd.[b]	obs'd.	cal'd.[b]	obs'd.	cal'd.[c]	calc.[c]
Γ_{6u}	0	0	0	0	0	0	0
	5010	5051	5081	5129	5104	5097	5209
	7339	7344	7364	7365	7396	7394	7440
	13132	12972	13245	13062	12903	12924	12836
	15439	15690	15517	15796	15697	15667	15667
$\Gamma_{4u}+\Gamma_{5u}$	5029	5052	5108	5131	5203	5201	5187
	(13134)	13047	13250	13155	13098	13107	13186
ZETA		1915±62		1908±70		1905±7	1907±33
B_0^2		7.8±687		11.8±766		426±85	-145±150
B_0^4		-14150±326		-14364±366		-14212±40	-14609±180
B_0^6		3989±485		3939±530		3600±57	2934±205
θ		54° 29'		54° 26'		54° 20'	53° 23'
σ[d]		163		182		20	87

[a]Hecht *et al.* (1985b).

[b]O_h = 54° 44'; the value of θ used in this case was arbitrary, but the fit for the value indicated is better than for 54° 44', or 54°.

[c]The crystal structure gives θ = 53° 23'—the arbitrary choice of θ = 54° 20' provides the best fit.

[d]Mean error.

TABLE 34

Energy Level Structures and Parameters (in cm^{-1}) for U(V) Compounds.

	$(NEt_4)UCl_6$[a,b]		$(NEt_4)UBr_6$[b,c]		$RbUCl_6$[c,d]	KUO_3[e]	UCl_5[f]	
	Expt.	Calc.	Expt.	Calc.	Calc.[c]	Calc.[e]	obs'd	calc'd (O_h)[g]
Γ_7 (cm^{-1})	0	0	0	0	0	0	0	0
Γ_8	—	3649	3670	3715	3800	4386	4300	4174
Γ_7'	6801	7157	6831	7022	6794	6849	6643	6413
Γ_8'	9950, 10450 } 10190	10154	9435, 9805 } 9668	9627	10137	9808	8970, 9772 } 9371	9643
Γ_6	11470	11742	10605	10736	11520	12500	11665	11218
ζ (cm^{-1})	1913[a]	1913	2197[c]	1761(31)	2219	1770		1559(115)
Δ[h]	2936[a]		51[c]		826	3920		
θ[h]	3371[a]		5676[c]		5794	4100		
k			0.79[c]		0.78	0.90		
k'			0.32[c]		0.45	—		
B_0^4[g]		12209(710)		10953(350)				13479(1125)
B_0^6		39(776)		-1058(274)				-158.6(745)
σ[i]		266		123				370

Table 34. (Continued)

a. Edelstein et al. (1974). The Γ_8 state was assigned at 1730 cm^{-1} based on estimates from other studies.

b. Ryan (1971).

c. Eichberger and Lux (1980).

d. Selbin et al. (1968).

e. Kemmler-Sack (1968).

f. Leung and Pooni (1977), Soulie and Edelstein (1980).

g. Crystal-field parameters in O_h symmetry were computed in the present investigation. The ratios $B_4^4/B_0^4 = 5/\sqrt{70}$, $B_4^6/B_0^6 = -\sqrt{7}/2$ were fixed.

h. $\Theta = \frac{8}{33}\ [B_0^4 + \frac{35}{13}\ B_0^6]$

$\Delta = \frac{2}{33}\ [5B_0^4 - \frac{210}{13}\ B_0^6]$

i. Deviation $(\sigma) = \Sigma[\Delta i^2/n-p]^{1/2}$ where Δi is the difference between observed and calculated energies, n is the number of levels used in the fitting procedure, and p is the number of parameters freely varied.

analyzed has also been reinterpreted, Poon and Newman (1982). Unfortunately, more recent experimental studies have not been able to reproduce all aspects of the reported band structure in $CsNpF_6$, Hecht et al. (1984). Further experimental studies and theoretical analysis are clearly required. However, consistent with the approach used in discussing the spectra of other valence states, approximations can be made as a basis for extrapolation. If we use electrostatic interaction parameters of the same order of magnitude as those suggested by Poon and Newman (1982) for $CsNpF_6$, together with the D_{3d} ligand-field parameters for $CsUF_6$, and further extrapolate these results to provide values for the $CsPuF_6$ case, Table 35, the resulting energy level structures are those given in Table 36 and plotted in Figure 36. The general aspects of these predicted structures appear to be consistent with available experimental data. Aside from the structure of the ground state, we expect to observe a relatively isolated $^3F_2$ state in $CsNpF_6$. However, with the exception of this $^3F_2$-state, neither the spectrum of $CsNpF_6$ nor that of $CsPuF_6$ is expected to exhibit easily recognizable isolated band structure. A relatively high density of excited states is predicted and detailed analysis can be expected to be difficult.

6.2. Compounds of An(VI) and An(VII)

The actinide hexafluorides, UF_6, NpF_6, and PuF_6 form a unique group of volatile actinide molecular species. They are not regarded as strongly bonded since the metal-fluorine distances tend to be rather large (~1.98 Å), Claassen (1959). The combination of well-characterized spectroscopic, Goodman and Fred (1959), Steindler and Gunther (1964), and magnetic, Hutchison and Weinstock (1960), results for NpF_6 has served to establish a reasonable basis for the energy level analysis in octahedral symmetry. Sets of F^k parameters can then be combined with the results for NpF_6 to yield an estimate of the parameter sets for PuF_6 and AmF_6 as shown in Table 37. Of course, AmF_6 has not yet been characterized. The corresponding energy levels are given in Table 38. Energy level parameters similar to those given in the table were earlier shown to reproduce a number of the principal features in the absorption spectrum of PuF_6, Kugel et al. (1976), Figure 37. The detection of fluorescence in the selective excitation of NpF_6 and PuF_6 and at energies consistent with the energy gaps between the predicted ground and first excited states in both spectra, was recently reported, Beitz, et al. (1982), and further structure in PuF_6 was revealed in subsequent excitation studies, Barefield, II et al. (1983). While the estimated parameters given in Table 37 provide a starting point for the actual energy level analysis, it would not be surprising to find that the parameters for PuF_6 are modified as the experimental energy level structure is refined. The energies of some of the lower-lying states in NpF_6, PuF_6 and AmF_6 consistent with the estimated parameters are shown in Figure 38. The computed energy level scheme for AmF_6 suggests that detection of this compound via emission of characteristic fluorescence will in general be very difficult, except possibly at temperatures near 4 K, because of the narrow energy gaps between excited states.

TABLE 35

Energy Level Parameters (in cm^{-1}) for $CsAnF_6$

Based on a Consistent Predictive Model (D_{3d})[a]

	$CsUF_6$	$CsNpF_6$	$CsPuF_6$
ζ(HFR)[b]	2316	2608	2914
ζ(Est)[c]	1905	2200	2506
ΔP	411	408	408
B_o^2	426	426	426
B_o^4	-14212	-14212	-14212
B_o^6	3600	3600	3600
θ	54° 20'	54° 20'	54° 20'
F^2(HFR)		84141	86982
F^2(Est)		48920	51760
ΔP		35221	35222
F^4(HFR)		55445	57347
F^4(Est)		42300	44200
ΔP		13145	13147
F^6(HFR)		40865	42285
F^6(Est)		27700	29120
ΔP		13165	13165

[a]In addition to the parameters shown, for both the Np(V) and Pu(V) cases, α=30, β=-660, γ=1200, P^2=500, P^4=375, P^6=250; and in addition for Pu(V), T^2=200, T^3=50, T^4=100, T^6=-300, T^7=400 and T^8=350.

[b]Computed using Hartree-Fock methods and including an approximate relativistic correction, Cowan and Griffin (1976), Crosswhite (1977).

[c]Estimated parameter value used to compute the energy level structure.

TABLE 36

Energy Levels of $CsAnF_6$ (D_{3d}-Symmetry)[a]

$CsUF_6$			$CsNpF_6$		$CsPuF_6$	
State[b]	Calc.	Obs.[c]	State	Calc.	State	Calc.
E_u'	0	0	A_{1g}	0	E_u''	0
E_u'	5097	5104	A_{2g}	2550	E_u'	15
E_u''	5201	5203	E_g	2592	E_u'	1208
E_u'	7394	7396	E_g	2811	E_u'	2917
E_u'	12924	12903	E_g	4807	E_u''	2983
E_u''	13106	13098	A_{1g}	4885	E_u'	6190
E_u'	15667	15697	A_{1g}	8203	E_u'	6286
			E_g	8228	E_u''	6342
			E_g	8443	E_u'	9050
			A_{2g}	8481	E_u''	9070
			E_g	8530	E_u'	9475
			A_{1g}	9231	E_u'	10096
			A_{2g}	10012	E_u''	10112
			E_g	10092	E_u'	10392
			A_{1g}	12003	E_u''	11775
			E_g	12163[d]	E_u'	11785
					E_u''	12094[d]

[a]The parameters required for the calculated energy levels shown are given in Table 35. All values in cm^{-1}.

[b]The states are identified by labels as follows: $E_u' = \Gamma_{6u}$ and $E_u'' = \Gamma_{4u} + \Gamma_{5u}$, for odd f-electron configurations.

[c]Hecht *et al.* (1985b).

[d]At higher energies the density of states is large and given the approximate nature of the estimate, significant energy gaps between states are not expected at < 20000 cm^{-1}.

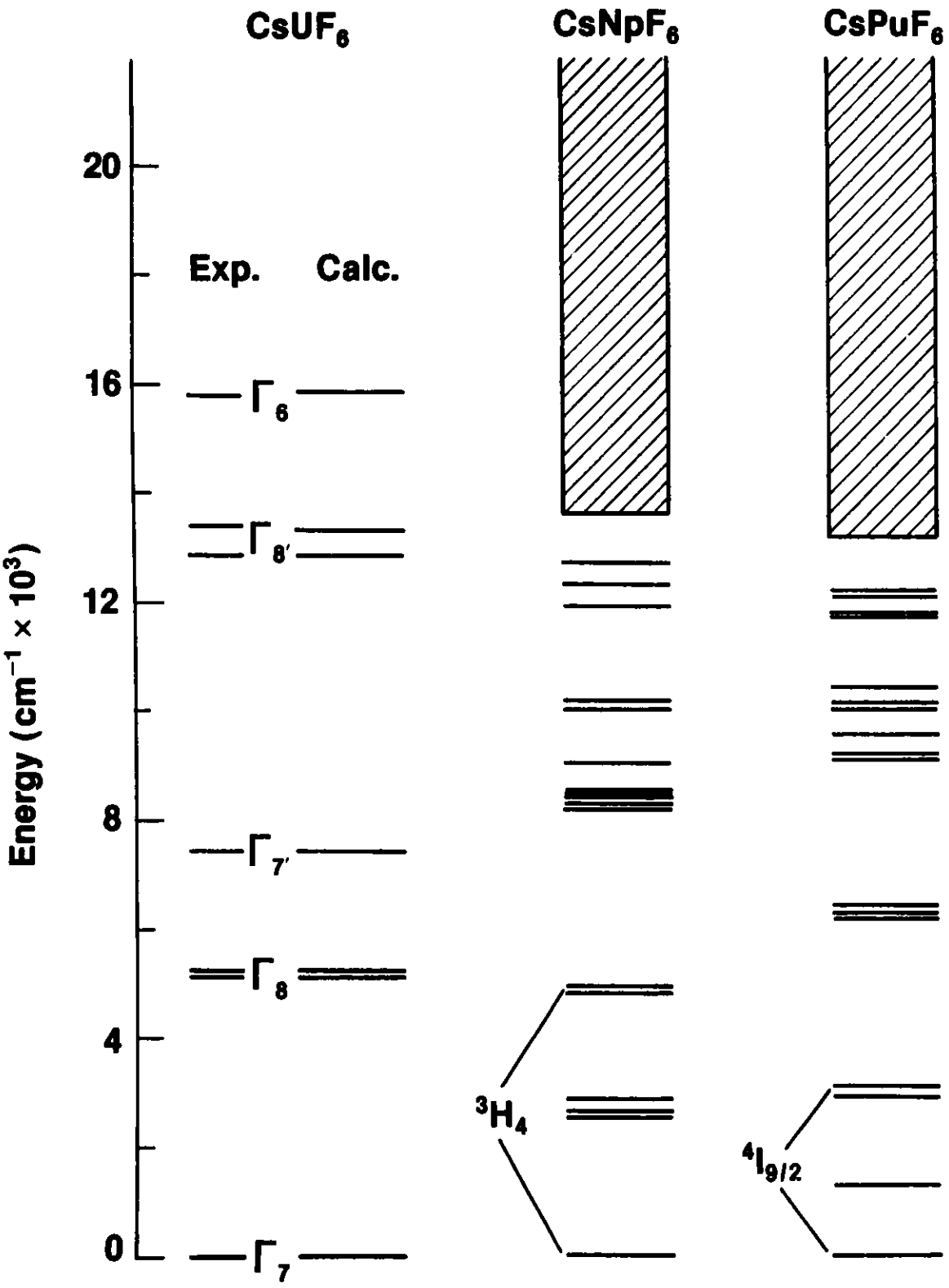

Fig. 36. Computed Energy Level Schemes for $CsUF_6$, $CsNpF_6$ and $CsPuF_6$. Experimental Results for $CsUF_6$ from Table 33. The Level Structure at > 13000 cm^{-1} for NpF_6^- and > 11000 cm^{-1} for PuF_6^- is Dense Within the Energy Range Indicated.

TABLE 37.

Energy Level Parameters (all in cm^{-1}) for AnF_6 Based on a Consistent Predictive Model.

	NpF_6	PuF_6	AmF_6
ζ(HFR)[a]	2817	3130	3459
ζ(Est)[b]	2448	2652	2800
ΔP	369	478	659
B_0^4	44553	51400[c]	49000
B_0^6	7991.7	10200[c]	10000
F^2(HFR)		90625	93280
F^2(Est)		60001	56600
ΔP		30624	36680
F^4(HFR)		60037	61810
F^4(Est)		50101	46800
ΔP		9936	15010
F^6(HFR)		44381	45702
F^6(Est)		33161	31100
ΔP		11220	14602

a. Computed using Hartree-Fock methods and including an approximate relativistic correction, Cowan and Griffin (1976), Crosswhite (1977).

b. Estimated parameter value used to compute the energy level structure.

c. Approximate crystal-field parameters for PuF_6 were based on fitting the results of Beitz et al. (1982), with in addition, $\alpha = 35$, $\beta = -700$, $\gamma = 500$.

TABLE 38.

Energy Levels of NpF_6, PuF_6, and AmF_6 (in cm^{-1})[a,b]

NpF_6			PuF_6		AmF_6	
State	Calc'	Obs'd.	State	Calc.	State	Calc.
Γ_{7u}	-18	0	Γ_{1g}	-206	Γ_{8u}	0
Γ_{8u}	7690	7711	Γ_{4g}	4505	Γ_{6u}	4139
Γ_{7u}	9563	9515	Γ_{3g}	4997	Γ_{8u}	6179
Γ_{8u}	23548	23500	Γ_{5g}	6329	Γ_{7u}	6604
Γ_{6u}	27912	28000	Γ_{4g}	10004	Γ_{8u}	8554
			Γ_{1g}	10184	Γ_{8u}	11665
			Γ_{3g}	11921	Γ_{7u}	13514
			Γ_{5g}	12103	Γ_{8u}	14998
			Γ_{4g}	16240	Γ_{8u}	15416
			Γ_{3g}	17811	Γ_{6u}	15451
			Γ_{1g}	17832	Γ_{8u}	17336
					Γ_{7u}	17690

[a]Results for NpF_6 are complete with states labelled in O_h-symmetry.

[b]Partial calculated results for PuF_6 and AmF_6. Energy level parameters given in Table 37.

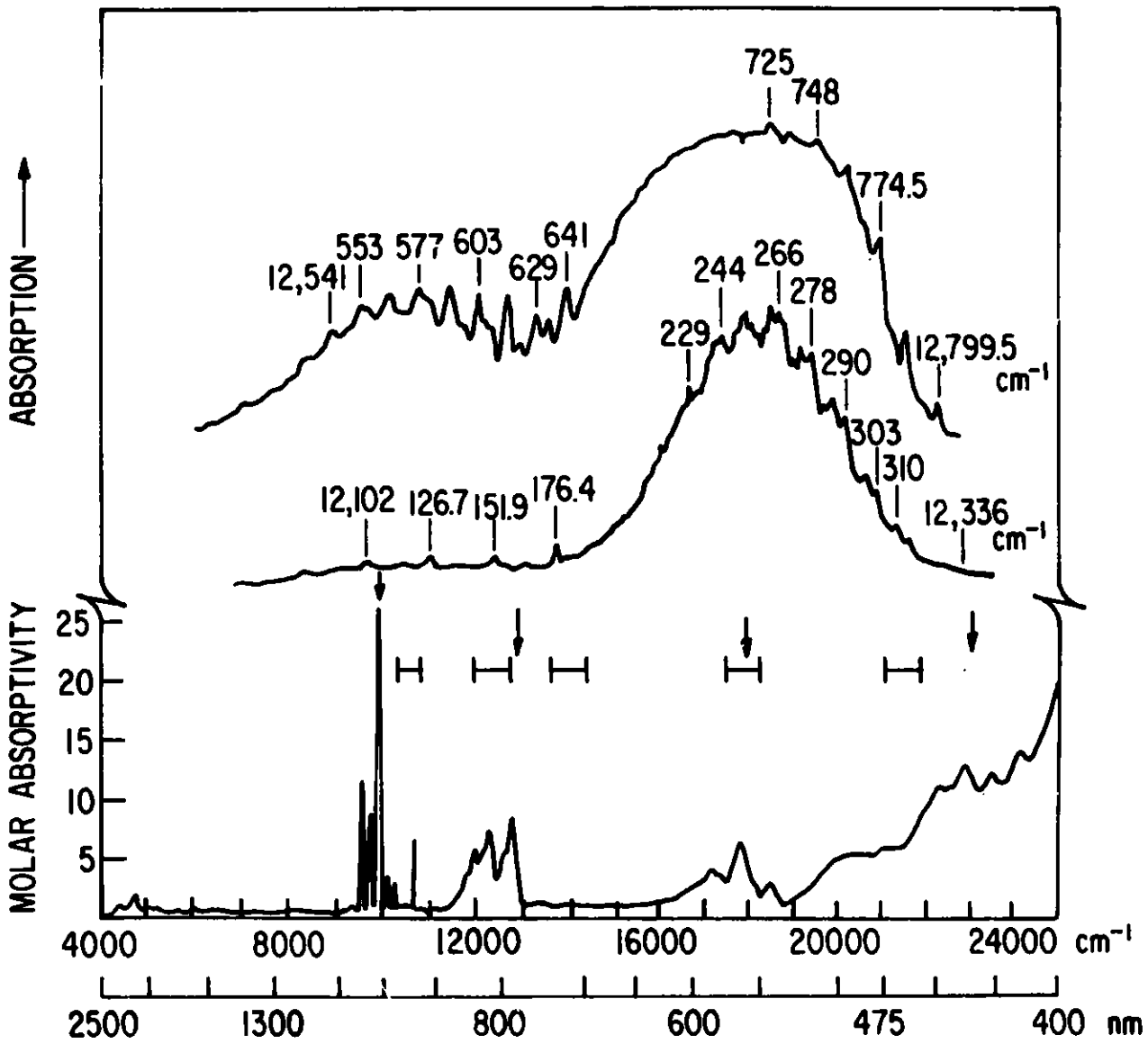

Fig. 37. Absorption Spectrum of PuF_6(g) from Kugel et al. (1976). Bottom: Spectrum from Steindler and Gunther (1964) with Arrows Indicating Regions They Reported as Showing Vibrational Structure. Bars |-| Indicate Regions Examined by Intercavity Laser Absorption; I:455-470 nm; II: 550-574 nm, III: 697-729 nm; IV: 786-845 nm; V: 918-974 nm. Top: Densitometer Tracing of the High Resolution Absorption Spectrum of PuF_6(g) in the 781-830 nm region obtained in Multipass Experiments.

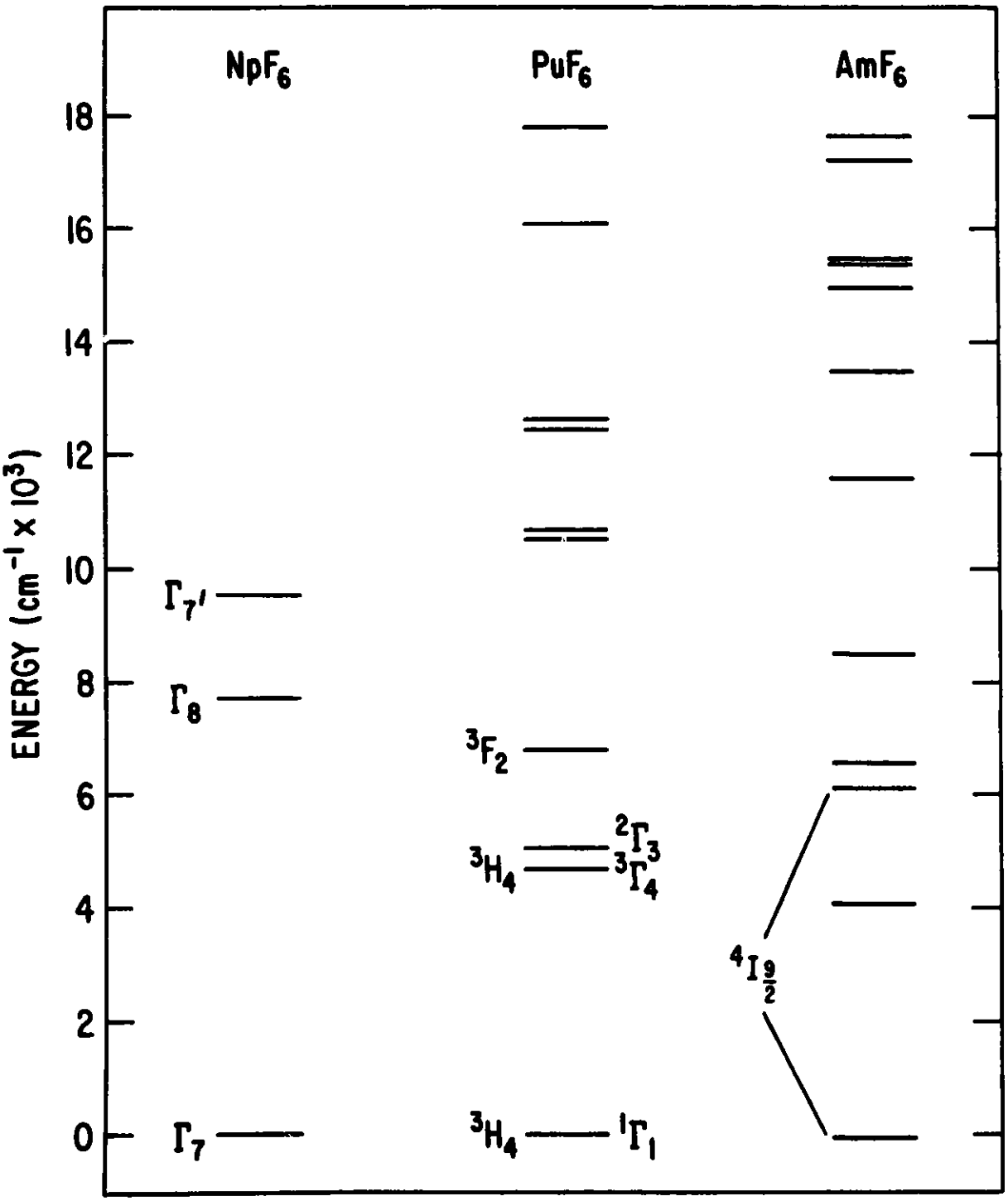

Fig. 38. Computed Energy Level Schemes for NpF_6, PuF_6, and AmF_6. Energy Level Parameters from Table 37.

The spectra of UO_2^{2+}, UF_6, UCl_6, complex fluorides or oxyfluorides containing U(VI), and of Np(VII), Spitsyn et al. (1969) are atypical of other members of the actinide series. In contrast to the transitions between states within the f^N-configuration which characterize most of the actinide spectra discussed in previous sections, the above species contain no f-electrons in open shells. Yet spectra of UF_6 and of uranyl compounds with a characteristic structure in the visible-ultraviolet range limited to the region below 400 nm, Figure 39, are probably more extensively reported and analyzed than those of any other actinide species.

While the data base is very large, and a number of ab initio calculations are available to aid the assignment of molecular orbital states, the problem of competing interpretations is not easily resolved. Important contributions to our understanding of UF_6, UO_2^{n+} (n=1,2) and related spectra continue to be made, Jørgensen (1982b), Martensson et al. (1983), DeKock et al. (1984), and new very extensive experimental analyses of crystal spectra such as those for $Cs_2UO_2Cl_4$ and $CsUO_2(NO_3)_3$, Denning et al. (1985), are proving to be a particularly valuable basis for reexamining and selecting among competing interpretations. For the closely related case of NpO_2^{2+} doped into single crystal $Cs_2UO_2Cl_4$, detailed spectroscopic studies have identified electronic transitions belonging to the $5f^1$-configuration, but also other structure similar in origin to that reported for U(VI), i.e. transitions to molecular orbital states, Stafsudd et al. (1969) and Denning et al. (1982a,b). Extensive analysis of the absorption and fluorescence spectra of UF_6 have been published and are covered in a recent review, Carnall (1982).

7.0 Concluding Remarks

As this report was being written, new developments in analysis, new insights into atomic spectra, and new condensed phase spectra were appearing. We have attempted to assemble reference data, to survey some of the growing edges of actinide spectroscopy, and to outline methods of analysis that will be of continuing value to those working in the field.

8.0 Acknowledgements

We gratefully acknowledge the large contribution of Hannah Crosswhite to the computational aspects of this effort. We would also like to thank our many colleagues for their insights and interest, particularly B. R. Judd, K. Rajnak, G. L. Goodman, and H. G. Hecht.

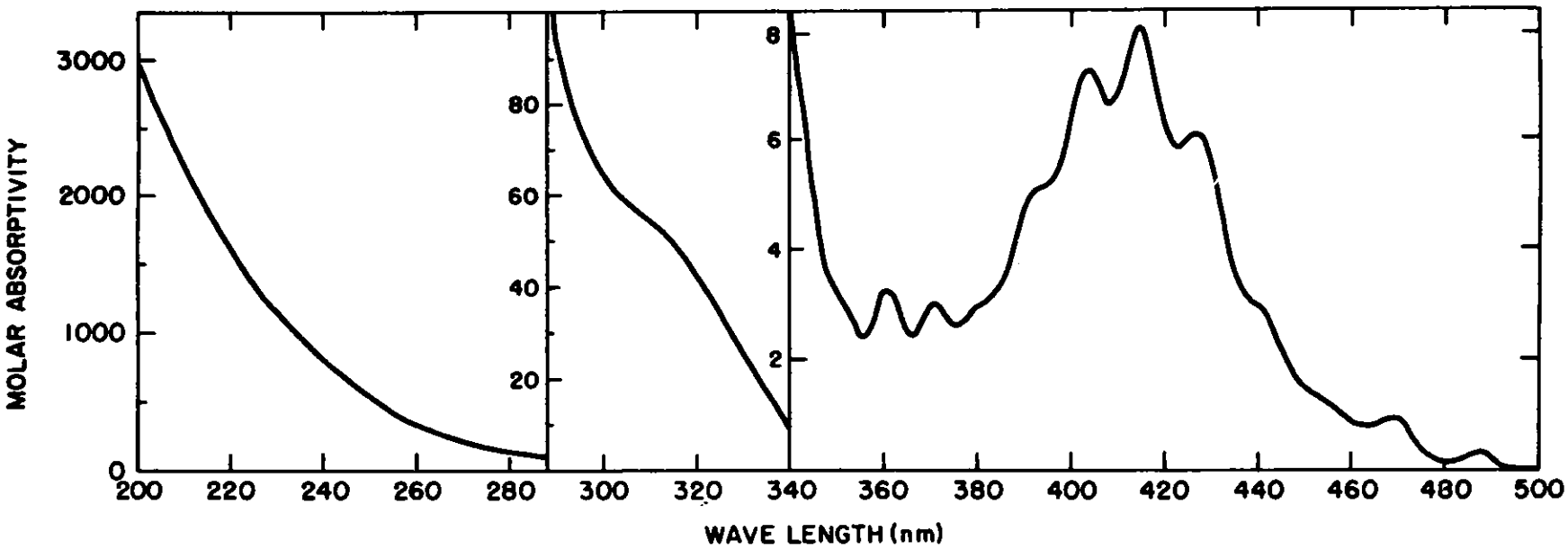

Fig. 39. Absorption Spectrum of UO_2^{++} in 1 M $HClO_4$, Cohen and Carnall (1960).

REFERENCES

Amberger, H.-D., W. Grape, and E. Stumpp, J. Less-Common Metals 95 (1983) 181.

Asprey, L. B. and R. A. Penneman, J. Am. Chem. Soc. 83 (1961) 2200.

Asprey, L. B. and T. K. Keenan, J. Inorg. Nucl. Chem. 7 (1958) 27.

Auzel, F. and O. L. Malta, J. Physique 44 (1983) 201.

Auzel, F., S. Hubert, P. Delamoye, and M. Hussonnois, J. Luminesc 26 (1982) 251.

Axe, J. D., Ph.D. Thesis - UCRL-9293 (unpublished) (1960).

Barefield, J. E., II, W. W. Rice, J. J. Tiee, and R. T. Walters, J. Chem. Phys. 79 (1983) 2621.

Baybarz, R. D., L. B. Asprey, C. E. Strouse and E. Fukushima, J. Inorg. Nucl. Chem. 34 (1972) 3427.

Beitz, J. V., C. W. Williams, and W. T. Carnall, J. Chem. Phys. 76 (1982) 2756.

Beitz, J. V., W. T. Carnall, and D. W. Wester, LBL-12441 (1981) 108.

Beitz, J. V. and Jan P. Hessler, Nuclear Technology 51 (1980) 169.

Berg, J. O., T. E. Christensen, P. W. Kidd, G. R. Neil, and J. G. Conway J. Opt. Soc. Am. 70 (1980) 716.

Bernstein, E. R. and T. A. Keiderling, J. Chem. Phys. 59 (1973) 2105.

Blaise, J., M. Fred, and R. G. Gutmacher, J. Opt. Soc. Am. B (1985), in press.

Blaise, J., M. Fred, and R. G. Gutmacher, "The Atomic Spectrum of Plutonium," Report ANL-83-95 (1984a) .

Blaise, J., J. G. Conway, and E. Worden, personal communication quoted in Crosswhite and Crosswhite, 1984a (1984b).

Blaise, J., M. S. Fred, W. T. Carnall, H. M. Crosswhite, and H. Crosswhite, ACS Symp. Series 216 (1983) 173.

Brewer, L., "Systematics and the Properties of the Lanthanides", NATO ASI Series, S. P. Sinha, ed., D. Reidel Publishing Company, Boston, (1983), 17.

Brewer L., J. Opt. Soc. Am. 61 (1971a) 1101.

Brewer, L., J. Opt. Soc. Am. 61 (1971b) 1666.

Carnall, W. T., H. Crosswhite, and K. Rajnak, Proc. Int. Symp. on Rare Earths Spectroscopy, Wroclaw, Poland (1984, in press).

Carnall, W. T., J. V. Beitz, and H. Crosswhite, J. Chem. Phys. 80 (1984) 2301.

Carnall, W. T., J. V. Beitz, H. Crosswhite, K. Rajnak, and J. B. Mann, "Systematics and the Properties of the Lanthanides", NATO ASI Series, S. P. Sinha, ed., D. Reidel Publishing Company, Boston (1983), 389.

Carnall, W. T., "Gmelin Handbuch der Anorganischen Chemie," 8th Edition, Uranium Supplement Volume A5, Springer Verlag, New York, (1982) 69.

Carnall, W. T., H. Crosswhite, H. M. Crosswhite, J. P. Hessler, N. Edelstein, J. G. Conway, G. V. Shalimoff, and R. Sarup, J. Chem. Phys. 72 (1980) 5089.

Carnall, W. T., "Handbook on the Physics and Chemistry of Rare Earths", Vol. 3, K. A. Gschneider Jr. and L. Eyring, eds., North-Holland Publishing Company, New York (1979a).

Carnall, W. T., "Organometallics of the f-Elements", T. J. Marks and R. D. Fischer, eds., D. Reidel Publishing Company, Boston (1979b).

Carnall, W. T. and K. Rajnak, J. Chem. Phys. 63 (1975) 3510.

Carnall, W. T., S. Fried, F. Wagner, Jr., J. Chem. Phys. 58 (1973a) 3614.

Carnall, W. T., S. Fried, F. Wagner, Jr., J. Chem. Phys. 58 (1973b) 1938.

Carnall, W. T., "Gmelin Handbuch der Anorganischen Chemie," 71, Gmelin Institute (1971) 120.

Carnall, W. T., P. R. Fields, and R. Sarup, J. Chem. Phys. 54 (1971) 1476.

Carnall, W. T., P. R. Fields, and R. G. Pappalardo, J. Chem. Phys. 53 (1970) 2922.

Carnall, W. T., P. R. Fields, and R. Sarup, J. Chem. Phys. 51 (1969) 2587.

Carnall, W. T., P. R. Fields, and K. Rajnak, J. Chem. Phys. 49 (1968) 4412.

Carnall, W. T. and B. G. Wybourne, J. Chem. Phys. 40 (1964) 3428.

Casimir, H., Proc. K. Akad. Wet. Amsterdam 34 (1931) 844.

Chase, L. L., Phys. Rev. B2 (1970) 2308.

Claassen, H. H., J. Chem. Phys. 30 (1959) 968.

Cohen, D. J., Inorg. Nucl. Chem. 18 (1961) 211.

Cohen, D. and W. T. Carnall, J. Chem. Phys. 64 (1960) 1933.

Condon, E. U. and G. H. Shortley, "The Theory of Atomic Spectra", Cambridge University Press, Cambridge (1963).

Conway, J. G. and K. Rajnak, J. Chem. Phys. 44 (1966) 348.

Conway, J. G., J. Chem. Phys. 41 (1964a) 904.

Conway, J. G., J. Chem. Phys. 40 (1964b) 2504.

Cordero-Montalvo, C. D. and N. Bloembergen, Phys. Rev. B 30 (1984) 438; Phys. Rev. B 31 (1985) 613.

Cowan, R. D., "The Theory of Atomic Structure and Spectra," University of California Press (1981).

Cowan, R. D. and C. D. Griffin, J. Opt. Soc. Am. 66 (1976) 1010.

Crosswhite, H. M. and H. Crosswhite, J. Opt. Soc. Am. B 1 (1984a) 246.

Crosswhite, H. M. and H. Crosswhite (1984b) (work in progress).

Crosswhite, H. and H. M. Crosswhite (1984c) (work in progress).

Crosswhite, H. and H. M. Crosswhite (1984d) (private communication).

Crosswhite, H. M., "Gmelin Handbuch der Anorganischen Chemie," 8th Edition, Uranium Supplement Volume A5, Springer Verlag, New York (1982) 1.

Crosswhite, H. M., H. Crosswhite, W. T. Carnall, and A. P. Paszek, J. Chem. Phys. 72 (1980) 5103.

Crosswhite, H. M., Colloques Internationaux du C.N.R.S., Spectroscopie des Elements de Transition et des Elements Lourds dans les Solides, 28 Juin - 3 Juillet 1976, Editions due C.N.R.S., Paris (1977) 65.

Crosswhite, H. M., H. Crosswhite, F. W. Kaseta, and R. Sarup, J. Chem. Phys. 64 (1976) 1981.

Crosswhite, H. M. Phys. Rev. A 4 (1971) 485.

Crosswhite, H. M., R. L. Schwiesow, and W. T. Carnall, J. Chem. Phys. 50 (1969) 5032.

Crosswhite, H., H. M. Crosswhite, and B. R. Judd, Phys. Rev. 174 (1968) 89.

Crosswhite, H. M, G. H. Dieke and W. J. Carter, J. Chem. Phys. 43, (1965) 2047.

Crozier, M. H., Phys. Rev. 137 (1965) 1781.

deBruin, T. L., P. F. A. Klinkenberg and Ph. Schuurmans, Z. fŭr Physik 118 (1941) 58.

DeKock, R. L., E.J. Baerends, P. M. Boerrigter, and J. G. Snijders, Chem. Phys. Lett. 105 (1984) 308.

Delamoye P., K. Rajnak, M. Genet, and N. Edelstein, Phys. Rev. B28 (1983) 4923.

Delamoye, P., S. Hubert, M. Hussonnois, J. C. Krupa, M. Genet, R. Guillaumont, C. Naud and R. Parrot, J. Luminesc. 18/19 (1979) 76.

Denning, R. G., J. O. W. Norris, and P. J. Laing, Mol. Phys. 54 (1985) 713.

Denning, R. G., J. O. W. Norris, and D. Brown, Mol. Phys. 46 (1982a) 325.

Denning, R. G., J. O. W. Norris, and D. Brown, Mol. Phys. 46 (1982b) 287.

Denning, R. G., J. O. W. Norris, I. G. Short, T. R. Snellgrove, and D. R. Woodwark, Am. Chem. Soc. Symp. Series 131 (1980) 313.

Dieke, G. H., "Spectra and Energy Levels of Rare Earth ions in Crystalls," H. M. Crosswhite and H. Crosswhite, eds., John Wiley, New York (1968).

Downer, M. C., C. D. Cordero-Montalvo, and H. Crosswhite, Phys. Rev. B28 (1983) 4931.

Drifford, M. and E. Soulie, Colloques Internat. CNRS No. 255, Paris (1977) 95.

Edelstein, N., D. Brown, and B. Whittaker, Inorg. Chem. 13 (1974) 563.

Edelstein, N., J. G. Conway, D. Fujita, W. Kolbe and R. McLaughlin, J. Chem. Phys. 52 (1970) 6425.

Edelstein, N., W. Easley and R. McLaughlin, Adv. Chem. Ser. 71 (1967) 203.

Edelstein, N., W. Easley and R. McLaughlin, J. Chem. Phys. 44 (1966) 3130.

Ehrlich, D. J., P. F. Moulton, and R. M. Osgood, Jr., Optics Letters 4 (1979) 184.

Eichberger, K. and F. Lux, Ber. Bunsenges. Phys. Chem. 84 (1980) 800.

Eisenstein, J. C. and M. H. L. Pryce, J. Res. Nat. Bureau Stds. 70A (1966) 165.

Eisenstein, J. C. and M. H. L. Pryce, Proc. Roy. Soc. A255 (1960) 181.

Ensor, D. D., J. R. Peterson, R. G. Haire, and J. P. Young, J. Inorg. Nucl. Chem. 43 (1981) 1001.

Eremin, M. V., Opt. Spektvosk. 29 (1970) 100.

Fellows, R. L., J. R. Peterson, J. P. Young, R. G. Haire, "The Rare Earths in Modern Sceince and Technology", G. J. McCarthy and J. J. Ryne, eds., Plenum Publishing Corp., New York (1978) 493.

Fischer, C. F., "The Hartree-Fock Method for Atoms," Wiley-Interscience, New York (1977).

Fischer, C. F., Comput. Phys. Commun. 1 (1969) 151.

Fred, M., "The Chemistry of the Actinide Elements," J. J. Katz, G. T. Seaborg, L. R. Morss, eds., Chapman and Hall Pub., New York, (1984) (in preparation).

Fred, M., Adv. Chem. Ser. 71 (1967) 180.

Gamp, E., N. Edelstein, C. Khan Malek, S. Hubert, and M. Genet, J. Chem. Phys. 79 (1983) 2023.

Genet, M., "Solid State Physics and Actinide Spectroscopy with $ThBr_4$ and $ThCl_4$", Report IPNO-DRE 84.02 (1984).

Goldschmidt, Z. B., "Handbook on the Physics and Chemistry of Rare Earths," Vol. 1, K. A. Gschneider Jr. and L. Eyring, eds., North-Holland Publishing Company, New York, (1978), 1.

Goodman, G. L. and M. Fred, J. Chem. Phys. 30 (1959) 849.

Gordon, S., W. A. Mulac, K. H. Schmidt, R. K. Sjoblom, and J. C. Sullivan, Inorg. Chem. 17 (1978) 294.

Gruber, J. B. and E. R. Menzel, J. Chem. Phys. 50 (1969) 3772.

Gruber, J. B., W. R. Cochran, J. G. Conway, and A. T. Nicol, J. Chem. Phys. 45 (1966) 1423.

Gruen, D. M. and R. L. McBeth, Inorg. Chem. 8 (1969) 2625.

Gruen, D. M. and C. W. DeKock, J. Inorg. Nucl. Chem. 29 (1967) 2569.

Gruen, D. M. and R. L. McBeth, J. Inorg. Nucl. Chem. 9 (1959) 290.

Hartree, D. R., "The Calculation of Atomic Structures", John Wiley and Sons, Inc., New York (1957).

Hecht, H. G., J. G. Malm, and W. T. Carnall, J. Less-Common Metals, in press (1985a).

Hecht, H. G., J. G. Malm, J. Foropoulos, and W. T. Carnall, research in progress (1985b).

Hecht, H. G., J. Malm, and W. T. Carnall, research in progress (1984).

Hecht, H. G., L. P. Varga, W. B. Lewis, and A. M. Boring, J. Chem. Phys. 70 (1979) 101.

Hessler, Jan P., private communication (1984) .

Hessler, Jan P. and W. T. Carnall, Am. Chem. Soc. Symposium Series, No. 131 (1980) 349.

Hessler, Jan P., R. T. Brundage, J. Hegarty and W. M. Yen, Optics. Lett. 5 (1980) 348.

Hessler, J. P., J. A. Caird, W. T.Carnall, H. M. Crosswhite, R. K. Sjoblom, and F. Wagner, Jr., "The Rare Earths in Modern Science and Technology," G. T. McCarthy and J. J. Rhyne, eds., Plenum Press, New York (1978) 507.

Hüfner, S., "Optical Spectra of Transport Rare Earth Compounds", Academic Press, New York (1978).

Hutchison, C. A. and B. Weinstock, J. Chem. Phys. 32 (1960) 56.

Johannson, S. and U. Litzen, Phys. Scripta 6 (1972) 139.

Johnston, D. R., R. A. Satten, C. L. Schreiber, and E. Y. Wong, J. Chem. Phys.
44 (1966a) 3141.

Johnston, D., R. A. Satten, and E. Wong, J. Chem. Phys. 44 (1966b) 687.

Jørgensen, C. K., Chem. Phys. Lett. 87 (1982a) 320.

Jørgensen, C. K., Chem. Phys. Lett. 89 (1982b) 455.

Jørgensen, C. K., Prog. Inorg. Chem. 12 (1970) 101.

Jørgensen, C. K. and J. S. Brinen, Mol. Phys. 6 (1963) 629.

Jørgensen, C. K., "Absorption Spectra and Chemical Bonding in Complexes", Pergamon Press, London (1962).

Jørgensen, C. K., Mol. Phys. 2 (1959) 96.

Judd, B. R. and H. Crosswhite, J. Opt. Soc. Am. B 1 (1984) 255.

Judd, B. R. and M. A. Suskin, J. Opt. Soc. Am. B 1 (1984) 261.

Judd, B. R., H. M. Crosswhite and H. Crosswhite, Phys. Rev. 169 (1968) 130.

Judd, B. R., Phys. Rev. 141 (1966) 4.

Judd, B. R., Phys. Rev. 127 (1962) 750.

Kaplyanskii, A. A., V. N. Medvedev, and P. P. Feofilov, Optics and Spectro. 14 (1963) 351.

Karraker, D. G., Inorg. Chem. 3 (1964) 1618.

Kaufman, V. and L. J. Radziemski, J. Opt. Soc. Am. 66 (1976) 599.

Keenan, T. K., J. Am. Chem. Soc. 83 (1961) 3719.

Kemmler-Sack, S., Z. Anorg. Allg. Chem. 363 (1968) 295.

Kim, K. C. and G. A. Laguna, Chem. Phys. Lett. 82 (1981) 292.

Krupa, J. C. and C. Khan Malek, Proc. 13 emes Journees des Actinides, April 1983, Elat, Israel (1983).

Krupa, J. C., S. Hubert, M. Foyentin, E. Gamp, and N. Edelstein, J. Chem. Phys. 78 (1983) 2175.

Kugel, R., C. Williams, M. Fred, J. G. Malm, W. T. Carnall, J. C. Hindman, W. T. Childs and L. S. Goodman, J. Chem. Phys. 65 (1976) 3486.

Lämmermann H. and J. G. Conway, J. Chem. Phys. 38 (1963) 259.

Leung, A. F., J. Phys. Chem. Solids 38 (1977) 529.

Leung, A. F. and Y-M. Poon, Can. J. Phys. 55 (1977) 937.

Lewis, W. B., J. B. Mann, D. A. Liberman and D. T. Cromer, J. Chem. Phys. 53 (1970) 809.

Loh, E., Phys. Rev. B7 (1973) 1846.

Loh, E., Phys. Rev. 184 (1969) 348.

Loh, E., Phys. Rev. 175 (1968) 533.

Loh, E., Phys. Rev. 154 (1967) 270.

Mackey, D. J., W. A. Runciman and E. R. Vance, Phys. Rev. B 11, (1975) 211.

Malm, J., L. Soderholm, C. W. Williams and W. T. Carnall, Argonne National Laboratory, work in progress, (1985).

March, N. H., "Self-Consistent Fields in Atoms", Pergamon Press, Oxford (1975).

Martensson, N., P. A. Malmquist, and S. Svensson, Chem. Phys. Letters 100 (1983) 375.

Martin, W. C., Z. Romuald, and L. Hagan, "Atomic Energy Levels - The Rare-Earth Elements", NSRDS-60, U. S. Department of Commerce (1978).

Marvin, H. H., Phys. Rev. 71 (1947) 102.

McClure, D. S. and Z. Kiss, J. Chem. Phys. 39 (1963) 3251.

Menzel, E. R., J. B. Gruber, and J. L. Ryan, J. Chem. Phys. 57 (1972) 4287.

Menzel, E. R. and J. B. Gruber, J. Chem. Phys. 54 (1971) 3857.

Morrison, C. A., G. F. de Sa, and R. P. Leavitt, J. Chem. Phys. 76 (1982) 3899.

Morrison, C. A., J. Chem. Phys. 72 (1980) 1001.

Morrison, J. C., Phys. Rev. A6, (1972) 643.

Morrison, J. C., and K. Rajnak, Phys. Rev. A 4 (1971) 536.

Morss, L. R., C. W. Williams, and W. T. Carnall, "Stability and Electronic Spectrum of $CsPuF_6$," ACS Symposium Series 216 (1983) 199.

Myasoedov, B. F., I. A. Lebedev, and V. M. Mikhailov, Dok. Akad. Nauk SSSR 211 (1973) 1351.

Naik, R. C. and J.-C. Krupa, private communication (1985).

Ofelt, G. S., J. Chem. Phys. 37 (1962) 511.

Okada, K., Y. Kaizu, and H. Kobayashi, J. Chem. Phys. 75 (1981) 1577.

Pappalardo, R. G., W. T. Carnall, and P. R. Fields, J. Chem. Phys. 51 (1969) 1182.

Paszek, A., Ph.D. thesis, The Johns Hopkins University, Baltimore, Md. (1978).

Penneman, R. A., R. R. Ryan, and A. Rosenzweig, Struct. Bonding 13 (1973) 1.

Peterson, J. R., R. L. Fellows, J. P. Young, and R. G. Haire, Radiochem. Radioanal. Letters 31 (1977) 277.

Poon, Y. M. and D. J. Newman, J. Phys. B: At. Mol. Phys. 16 (1983) 2093.

Poon, Y. M. and D. J. Newman, J. Chem. Phys. 77 (1982) 1077.

Racah, G., Phys. Rev. 76 (1949) 1352.

Rajnak, K., E. Gamp, R. Shinomoto, and N. Edelstein, J. Chem. Phys. 80 (1984a) 5942.

Rajnak, K., R. H. Banks, E. Gamp, and N. Edelstein, J. Chem. Phys. 80 (1984b) 5951.

Rajnak, K. and B. G. Wybourne, Phys. Rev. 132 (1963) 280.

Rana, R. S., C. D. Cordero-Montalvo, and N. Bloembergen, J. Chem. Phys. 81 (1984) 2951.

Rana, R. S. and F. W. Kaseta, J. Chem. Phys. 79 (1983) 5280.

Reisfeld, R. and C. K. Jørgensen, Inorg. Chem. Concepts 1 (1977) 36.

Reisfeld, M. J. and G. A. Crosby, Inorg. Chem. 4 (1965) 65.

Richardson, F. S., M. F. Reid, J. J. Dallara, and R. D. Smith, J. Chem. Phys. (1985) in press.

Richman, I., P. Kisliuk, and E. Y. Wong, Phys. Rev. 155 (1967) 262.

Ryan, J. L., J. Inorg. Nucl. Chem. 33 (1971) 153.

Satten, R. A., C. L. Schreiber, and E. Y. Wong, J. Chem. Phys. 78 (1983) 79.

Satten, R. A., C. L. Schreiber, and E. Y. Wong, J. Chem. Phys. 42 (1965) 162.

Schäffer, C. E. and C. K. Jørgensen, J. Inorg. Nucl. Chem. 8 (1958) 143.

Schlesinger, M., T. Szczurek, and M. C. K. Wiltshire, Can. J. Phys. 54 (1976) 753.

Schlesinger, M., and T. Szczurek, Phys. Rev. B 8 (1973) 2367.

Selbin, J., J. D. Ortega, G. Gritzner, Inorg. Chem. 7 (1968) 976.

Slater, J. C., "Quantum Theory of Atomic Structure," Two Volumes, McGraw-Hill, New York (1960).

Sorokin, P. P. and M. J. Stevenson, Phys. Rev. Lett. 5 (1960) 557.

Soulie, E. and N. Edelstein, Physica 102B (1980) 93.

Soulie, E. J., Phys. Chem. Solids 39 (1978) 695.

Soulie, E., Ph.D. thesis, University of Paris-Sud, Rapport CEA-R-4849 (1977).

Spitsyn, V. I., A. D. Gelman, N. N. Krot, M. P. Mefodiyeva, E. A. Zakharova, Yu. A. Komkov, V. P. Shilov, and I. V. Smirnova, J. Inorg. Nucl. Chem. 31 (1969) 2733.

Stafsudd, O. M., A. F. Leung, E. Y. Wong, Phys. Rev. 180 (1969) 339.

Steindler, M. J. and W. H. Gunther, "The Absorption Spectrum of NpF_6," ANL-6817 (1964); Spectrochim. Acta 20 (1964) 1319.

Sugar, J., Phys. Rev. Letters 14 (1965a) 731; J. Opt. Soc. Am. 55 (1965a) 1058.

Sugar, J., J. Opt. Soc. Am. 55 (1965b) 33.

Sugar, J., J. Opt. Soc. Am. 53 (1963) 831.

Svetashev, A. G. and M. P. Tsvirko, Opt. Spectrosc. (USSR) 51 (1981) 572.

Swanson, J. L., J. Phys. Chem. 68 (1964) 438.

Trees, R. E., J. Opt. Soc. Am. 54 (1964) 651.

Urland, W., Chem. Phys. 14 (1976) 393.

Van Deurzen, C. H. H., K. Rajnak, and J. G. Conway, J. Opt. Soc. Am. B1 (1984) 45.

Varga, L. P., J. D. Brown, M. J. Reisfeld and R. D. Cowan, J. Chem. Phys. 52 (1970) 4233.

Waggener, W. C., J. Phys. Chem. 62 (1958) 382.

Wagner, W., N. Edelstein, B. Whittaker, and D. Brown, Inorg. Chem. 16 (1977) 1021.

Weber, M., J. Am. Chem. Soc. Symp. Series 131 (1980) 275.

Weber, M., J. Solid State Commun. 12 (1973) 741.

Wild, J. F., E. K. Hulet, R. W. Lougheed, W. N. Hayes, J. R. Peterson, R. L. Fellows and J. P. Young, J. Inorg. Nucl. Chem. 40 (1978) 811.

Wilson, M. and M. Fred, J. Opt. Soc. Am. 59 (1969) 827.

Wyart, J. F., V. Kaufman and J. Sugar, Physica Scripta 22 (1980) 389.

Wybourne, B. G., "Spectroscopic Properties of the Rare Earths", Interscience Publishers, New York (1965).

Yanir, E., M. Givon, and Y. Marcus, Inorg. Nucl. Chem. Lett 5 (1969) 369.

Yen, W. M., C. G. Levey, Shihua Huang, and Shui T. Lai, J. Luminesc. 24/25 (1981) 6597.

Distribution for ANL-84-90

Internal

J. V. Beitz
F. A. Cafasso
W. T. Carnall (20)
W. J. Childs
H. M. Crosswhite
B. D. Dunlap
G. L. Goodman
J. P. Hessler
K. L. Kliewer
D. D. Koelling
D. J. Lam
G. H. Lander
L. R. Morss
L. C. Soderholm
E. P. Steinberg
J. C. Sullivan
C. W. Williams
ANL Patent Dept.
ANL Contract File
ANL Libraries
TIS Files (6)

External:

DOE-TIC, for distribution per UC-34A (146)
Manager, Chicago Operations Office, DOE
Chemistry Division Review Committee:
- J. L. Bolton, U. Western Ontario
- G. R. Choppin, Florida State U.
- R. E. Connick, U. California, Berkeley
- W. A. Goddard III, California Inst. Technology
- F. A. Cotton, Texas A&M
- L. Kevan, U. Houston
- J. M. Shreeve, U. Idaho
- N. Sugarman, U. Chicago
- E. Wasserman, DuPont Experimental Station, Wilmington

K. L. Andrew, Purdue U.
L. Brewer, U. California, Berkeley
J. L. Burnett, DOE, Washington
J. G. Conway, Lawrence Berkeley Lab.
R. D. Cowan, Los Alamos National Lab.
P. Cunningham, Los Alamos National Lab.
H. Dewey, Los Alamos National Lab.
P. G. Eller, Los Alamos National Lab.
R. Engleman, Los Alamos National Lab.
D. D. Ensor, Tennessee Technological U.
R. L. Hahn, Oak Ridge National Lab.
R. G. Haire, Oak Ridge National Lab.
E. K. Hulet, Lawrence Livermore Lab.
B. R. Judd, John Hopkins U.
V. Kaufman, National Bureau of Standards, Washington
O. L. Keller, Oak Ridge National Lab.
W. F. Krupke, Lawrence Livermore National Lab.

W. B. Lewis, Los Alamos National Lab.
W. C. Martin, National Bureau of Standards, Washington
J. A. Paisner, Lawrence Livermore National Lab.
R. T. Paine, U. New Mexico
J. R. Peterson, U. of Tennessee
L. J. Radziemski, New Mexico State U.
K. Rajnak, Kalamazoo College
G. L. Seaborg, U. California, Berkeley
J. L. Smith, Los Alamos National Lab.
R. W. Solarz, Lawrence Livermore National Lab.
J. S. Sugar, National Bureau of Standards, Washington
J. W. Ward, Los Alamos National Lab.
M. J. Weber, Lawrence Livermore National Lab.
E. F. Worden, Lawrence Livermore National Lab.
W. M. Yen, U. Wisconsin, Madison
J. P. Young, Oak Ridge National Lab.
F. Baumgärtner, Tech. U. München, Garching, Germany
J. Blaise, Laboratoire Aimé Cotton, Orsay, France
D. Brown, AERE Harwell, Oxfordshire, England
P. Delamoye, Inst. Physique Nucleaire, Orsay, France
J. Fuger, U. Liege, Liege, Belgium
M. Genet, Inst. Physique Nucleaire, Orsay, France
R. Guillaumont, Inst. Physique Nucleaire, Orsay, France
S. Hubert, Inst. Physique Nucleaire, Orsay, France
G. M. Kalvius, Tech. U. München, Garching, Germany
B. Kanellakopulos, Kernforschungscentrum, Karlsruhe, Germany
C. Keller, Kernforschungscentrum, Karlsruhe, Germany
J. I. Kim, Tech. U. München, Garching, Germany
J. C. Krupa, Inst. Physique Nucleaire, Orsay, France
W. Müller, Euratom, Geel, Belgium
J. R. Naegele, Euratom Inst., Karlsruhe, Germany
D. J. Newman, U. Hong Kong, Hong Kong
M. Pages, Lab. Curie, Paris, France
F. Weigel, U. München, München, Germany